A new, Early Cretaceous, small-bodied ornithopod (Ornithischia, Cerapoda) from a deep, high-energy palaeoriver of the Australian-Antarctic rift system (#17320)

First submission

Please read the **Important notes** below, the **Review guidance** on page 2 and our **Standout reviewing tips** on page 3. When ready **submit online**. The manuscript starts on page 4.

Important notes

Editor and deadline

Andrew Farke / 4 Sep 2017

Files	43 Figure file(s) 9 Table file(s) Please visit the overview page to **download and review** the files not included in this review PDF.
Declarations	**Describes a new species.**

Review guidelines

Please read in full before you begin

How to review

When ready **submit your review online**. The review form is divided into 5 sections. Please consider these when composing your review:

1. **BASIC REPORTING**
2. **EXPERIMENTAL DESIGN**
3. **VALIDITY OF THE FINDINGS**
4. General comments
5. Confidential notes to the editor

You can also annotate this PDF and upload it as part of your review

To finish, enter your editorial recommendation (accept, revise or reject) and submit.

BASIC REPORTING

- Clear, unambiguous, professional English language used throughout.
- Intro & background to show context. Literature well referenced & relevant.
- Structure conforms to **PeerJ standards**, discipline norm, or improved for clarity.
- Figures are relevant, high quality, well labelled & described.
- Raw data supplied (see **PeerJ policy**).

EXPERIMENTAL DESIGN

- Original primary research within **Scope of the journal**.
- Research question well defined, relevant & meaningful. It is stated how the research fills an identified knowledge gap.
- Rigorous investigation performed to a high technical & ethical standard.
- Methods described with sufficient detail & information to replicate.

VALIDITY OF THE FINDINGS

- Impact and novelty not assessed. Negative/inconclusive results accepted. *Meaningful* replication encouraged where rationale & benefit to literature is clearly stated.
- Data is robust, statistically sound, & controlled.
- Conclusions are well stated, linked to original research question & limited to supporting results.
- Speculation is welcome, but should be identified as such.

The above is the editorial criteria summary. To view in full visit **https://peerj.com/about/editorial-criteria/**

7 Standout reviewing tips

The best reviewers use these techniques

Tip	*Example*
Support criticisms with evidence from the text or from other sources	*Smith et al (J of Methodology, 2005, V3, pp 123) have shown that the analysis you use in Lines 241-250 is not the most appropriate for this situation. Please explain why you used this method.*
Give specific suggestions on how to improve the manuscript	*Your introduction needs more detail. I suggest that you improve the description at lines 57- 86 to provide more justification for your study (specifically, you should expand upon the knowledge gap being filled).*
Comment on language and grammar issues	*The English language should be improved to ensure that your international audience can clearly understand your text. I suggest that you have a native English speaking colleague review your manuscript. Some examples where the language could be improved include lines 23, 77, 121, 128 – the current phrasing makes comprehension difficult.*
Organize by importance of the issues, and number your points	*1. Your most important issue* *2. The next most important item* *3. …* *4. The least important points*
Give specific suggestions on how to improve the manuscript	*Line 56: Note that experimental data on sprawling animals needs to be updated. Line 66: Please consider exchanging "modern" with "cursorial".*
Please provide constructive criticism, and avoid personal opinions	*I thank you for providing the raw data, however your supplemental files need more descriptive metadata identifiers to be useful to future readers. Although your results are compelling, the data analysis should be improved in the following ways: AA, BB, CC*
Comment on strengths (as well as weaknesses) of the manuscript	*I commend the authors for their extensive data set, compiled over many years of detailed fieldwork. In addition, the manuscript is clearly written in professional, unambiguous language. If there is a weakness, it is in the statistical analysis (as I have noted above) which should be improved upon before Acceptance.*

A new, Early Cretaceous, small-bodied ornithopod (Ornithischia, Cerapoda) from a deep, high-energy palaeoriver of the Australian-Antarctic rift system

Matthew C Herne Corresp., [1, 2] , **Alan M Tait** [3] , **Vera Weisbecker** [2] , **Michael Hall** [3] , **Michael Cleeland** [4] , **Steven W Salisbury** [2]

[1] Earth, Environmental and Biological Sciences, Queensland University of Technology, Brisbane, Queensland, Australia
[2] School of Biological Sciences, University of Queensland, Brisbane, Queensland, Australia
[3] School of Earth, Atmosphere and Environment, Monash University, Melbourne, Victoria, Australia
[4] Bunurong Environment Centre, Inverloch, Victoria, Australia

Corresponding Author: Matthew C Herne
Email address: ornithomatt@gmail.com

A new, turkey-sized, small-bodied ornithopod, *Diluvicursor pickeringi*, gen. et sp. nov., is named from the lower Albian of the Eumeralla Formation in southeastern Australia. Comprising an almost complete tail and partial lower right hindlimb, the holotype (NMV P221080) was deposited as a carcass or body-part in a log-filled scour near the base of a deep, high-energy river that incised a faunally rich, substantially forested riverine floodplain within the Australian-Antarctic rift graben. The deposit is termed the 'Eric the Red West Sandstone'. The holotype is an older juvenile ~1.2 m in length that survived antemortem trauma to the pes. *Diluvicursor pickeringi* is characterized by nine potential autapomorphies, among which, dorsoventrally low neural arches and transversely broad caudal ribs on the anterior-most caudal vertebrae are visually defining features that suggest *Diluvicursor pickeringi* had robust anterior caudal musculature. A referred isolated posterior caudal vertebra (NMV P229456) from the holotype locality suggests *Diluvicursor pickeringi* grew to at least 2.3 m in length. Another isolated anterior caudal vertebra from the same deposit (NMV P228342), identified as an indeterminate ornithischian, suggests the fossil assemblage hosts at least two ornithopod taxa. *Diluvicursor pickeringi* and two stratigraphically younger, though indeterminate Eumeralla Formation ornithopods from Dinosaur Cove, NMV P185992/NMV P185993 and NMV P186047, are closely related. However, the tail of *Diluvicursor pickeringi* is far shorter than that of NMV P185992/NMV P185993 and pes more robust than that of NMV P186047. Features of the pes and possibly the tail suggest that the Eumeralla Formation ornithopods *Diluvicursor pickeringi*, NMV P185992/NMV P185993 and NMV P186047, Antarctic *Morrosaurus antarcticus* and Argentinian *Anabisetia saldiviai* and *Gasparinisaura cincosaltensis* are closely related. These Gondwanan ornithopods potentially share a close progenitor with the dryosaurids

from Africa and Laurasia.

A new, Early Cretaceous, small-bodied ornithopod (Ornithischia, Cerapoda) from a deep, high-energy palaeoriver of the Australian-Antarctic rift system

Matthew C. Herne[1,2], Alan M. Tait[3], Vera Weisbecker[2], Michael Hall[3], Michael Cleeland[4] and Steven W. Salisbury[2]

[1]School of Earth, Environmental and Biological Sciences, Queensland University of Technology, Brisbane, Queensland, Australia

[2]School of Biological Sciences, The University of Queensland, Brisbane, Queensland, Australia

[3]School of Earth, Atmosphere and Environment, Monash University, Melbourne, Victoria, Australia

[4]Bunurong Environment Centre, Inverloch, Victoria, Australia

ABSTRACT

A new, turkey-sized, small-bodied ornithopod, *Diluvicursor pickeringi*, gen. et sp. nov., is named from the lower Albian of the Eumeralla Formation in southeastern Australia. Comprising an almost complete tail and partial lower right hindlimb, the holotype (NMV P221080) was deposited as a carcass or body-part in a log-filled scour near the base of a deep, high-energy river that incised a faunally rich, substantially forested riverine floodplain within the Australian-Antarctic rift graben. The deposit is termed the 'Eric the Red West Sandstone'. The holotype is an older juvenile ~1.2 m in length that survived antemortem trauma to the pes. *Diluvicursor pickeringi* is characterized by nine potential autapomorphies, among which, dorsoventrally low neural arches and transversely broad caudal ribs on the anterior-most caudal vertebrae are visually defining features that suggest *Diluvicursor pickeringi* had robust anterior caudal musculature. A referred isolated posterior caudal vertebra (NMV P229456) from the holotype locality suggests *Diluvicursor pickeringi* grew to at least 2.3 m in length. Another isolated anterior caudal vertebra from the same deposit (NMV P228342), identified as an indeterminate ornithischian, suggests the fossil assemblage hosts at least two ornithopod taxa. *Diluvicursor pickeringi* and two stratigraphically younger, though indeterminate Eumeralla Formation ornithopods from Dinosaur Cove, NMV P185992/NMV P185993 and NMV P186047, are closely related. However, the tail of *Diluvicursor pickeringi* is far shorter than that of NMV P185992/NMV P185993 and pes more robust than that of NMV P186047. Features of the pes and possibly the tail suggest that the Eumeralla Formation ornithopods *Diluvicursor pickeringi*, NMV P185992/NMV P185993 and NMV P186047, Antarctic *Morrosaurus antarcticus* and Argentinian *Anabisetia saldiviai* and *Gasparinisaura cincosaltensis* are closely related. These

Gondwanan ornithopods potentially share a close progenitor with the dryosaurids from Africa and Laurasia.

INTRODUCTION

Lower Cretaceous fossil localities along the south coast of Victoria, southeastern Australia reveal a rich terrestrial biota that inhabited volcaniclastic river floodplains within the extensional rift system between Australia and Antarctica (Figs 1, S1) (Dettmann et al., 1992, Rich & Rich, 1989, Rich & Vickers-Rich, 2000, Rich, Vickers-Rich & Gangloff, 2002, Willcox & Stagg, 1990). Among the diverse assemblage of terrestrial and aquatic tetrapods currently recognised from this region—temnospondyls, crocodyliforms, ornithischian and theropodan dinosaurs, multituberculate, monotreme and tribosphenic mammals, plesiosaurs, pterosaurs and chelonians—small-bodied, turkey- to rhea-sized ornithopod dinosaurs were especially abundant and diverse (Barrett et al., 2011a, Barrett et al., 2010, Benson et al., 2010, Benson et al., 2012, Close et al., 2009, Currie, Vickers-Rich & Rich, 1996, Fitzgerald et al., 2012, Flannery & Rich, 1981, Herne, Nair & Salisbury, 2010, Kear, 2006, Molnar, Flannery & Rich, 1981, Rich, Gangloff & Hammer, 1997, Rich & Rich, 1989, Rich & Vickers-Rich, 1994, Rich & Vickers-Rich, 1999, Rich & Vickers-Rich, 2000, Rich & Vickers-Rich, 2004, Rich et al., 2009a, Rich et al., 2009b, Rich, Vickers-Rich & Gangloff, 2002, Smith et al., 2008, Warren, Rich & Vickers-Rich, 1997, Woodward, 1906).

Three ornithopod taxa have been named from the upper Aptian–lower Albian deposits in Victoria , including *Leaellynasaura amicagraphica* Rich & Rich, 1989 and *Atlascopcosaurus loadsi* Rich & Rich, 1989 from the Eumeralla Formation in the Otway Basin and *Qantassaurus intrepidus* Rich & Vickers-Rich, 1999, from the Wonthaggi Formation in the Strzelecki Group of the Gippsland Basin (Fig. 1B–C). The holotypes of these three Victorian taxa consist solely of fragmentary cranial remains, and of these taxa, postcranial remains have only been assigned to *Leaellynasaura amicagraphica* (Rich & Rich, 1989, Rich & Vickers-Rich, 1999).

Postcranial assignments to *Leaellynasaura amicagraphica* have included the small partial postcranium NMV P185992/NMV P185993, discovered at the *Leaellynasaura amicagraphica* holotype locality in 1987, and regarded as a scattered part of the holotype (Rich & Rich, 1989), and several isolated femora, referred to the same taxon based on features shared with NMV P185992 (Rich, Galton & Vickers-Rich, 2010, Rich & Rich, 1989, Rich & Vickers-Rich, 1999). A second partial postcranium, NMV P186047, discovered at the *Leaellynasaura amicagraphica* holotype locality in 1989, was assigned to the informal femoral taxon 'Victorian Hypsilophodontid Femur Type 1' (Gross, Rich & Vickers-Rich, 1993, Rich & Rich, 1989). However, 'Victorian Hypsilophodontid Femur Type 1' was reassessed as *Leaellynasaura amicagraphica* by Rich & Vickers-Rich (1999). More recently, Herne, Tait & Salisbury (2016) consider all postcranial materials referred to *Leaellynasaura amicagraphica* as Ornithopoda indet.

Several additional ornithopod femora from the Victorian localities were assigned to either *Fulgurotherium australe* von Huene, 1932, an ornithopod femoral taxon from the Albian Griman Creek Formation at Lightning Ridge, New South Wales (Molnar & Galton, 1986) or the informal Victorian femoral taxa, 'Victorian Hypsilophodontid Femur Type 2' (Rich & Rich, 1989). However, Rich & Vickers-Rich (1999) reconsidered the femora of 'Victorian Hypsilophodontid Femur Type 2' assignable to *Fulgurotherium australe*, and this this latter taxon was reassessed by Agnolin et al. (2010) as a *nomen dubium*, with all femora previously assigned to *F. australe* regarded as Ornithischia indet. No other significant work has been published on the postcranial remains of ornithopods from Victoria, apart from preliminary work by Herne (2009), who reported the possession of the hyperextended tail on the partial postcranium NMV P185992/NMV P185993.

Of the handful of vertebrate fossil localities in the Otway region (Fig. 1), the locality of Dinosaur Cove has been the most intensively excavated, including tunnelling into the sea-cliff (Rich & Vickers-Rich, 2000). The holotype of *Leaellynasaura amicagraphica* and the two partial postcranial skeletons NMV P185992/NMV P185993 and NMV P186047 were discovered within close proximity to each other during tunnelling at Dinosaur Cove (Herne, Tait & Salisbury, 2016, Rich & Rich, 1989, Rich & Vickers-Rich, 2000). Other vertebrate fossils from the Otway region were discovered as they eroded out of the coastal shore platforms, such as the fragmentary maxilla of the *Atlascopcosaurus loadsi* holotype, NMV P166409, discovered at the locality of Point Lewis (Fig. 1) (Flannery & Rich, 1981, Rich & Rich, 1989). In 2005, vertebrate fossils were discovered eroding out of the shore platform at a new fossil locality near Cape Otway that came to be known as the fossil locality of 'Eric the Red West' (Rich et al., 2009b) (Figs 1–2). A partial postcranium (NMV P221080) was subsequently excavated at ETRW and reported by Rich et al. (2009b) as an ornithopod. Preliminary sedimentological observations on Eric the Red West were also reported by Rich et al. (2009b), from which, the mode of fossil accumulation at the locality was postulated. According to Rich et al. (2009b), the small fragmented dinosaur carcass (NMV P221080) became entangled in a 'trap' of plant debris that accumulated around an upright tree stump in a fast flowing river and was subsequently buried.

This investigation will describe the new partial postcranium (NMV P221080) from Eric the Red West in detail, within a systematic framework. Detailed sedimentological and taphonomic interpretation of the locality will be additionally provided from which, preliminary interpretation of the palaeoecological context will extend. The relative stratigraphic range of fossil taxa important to this work will be compared, assisted by a structural geological restoration of the Eumeralla Formation in the region of interest.

PLEASE INSERT FIGURES 1–2

Abbreviations

Anatomical/technical: Ca #, caudal vertebra and designated/estimated position; *M.*, *musculus*; mpt, metatarsophalangeal; mt #, metatarsal number (may include range); NH_4Cl, ammonium chloride; and pd #, pedal digit number with phalanx position on digit (may include range). Abbreviations for vertebral laminae and fossae are provided in Table 1.

Institutional: DD, Volunteers, Monash University and Museums Victoria staff of the Dinosaur Dreaming project; MCF-PVPH, Museo Carmen Funes-Paleontología de Vertebrados, Plaza Huincul, Neuquén Province, Argentina; MCS, Museo Cinco Saltos; MU, Monash University, Melbourne, Victoria, Australia; MUCPv, Museo de Geologia y Paleontologia de la Universidad Nacional del Comahue, Paleontologia de Vertebrados, Neuquén Province, Argentina; MV, Museum Victoria, Melbourne, Victoria, Australia (formerly, National Museum of Victoria [NMV]); NHMUK, Natural History Museum, London, UK (formerly the British Museum of Natural History); QM, Queensland Museum, Brisbane, Qld, Australia; ROM, Royal Ontario Museum, Toronto, Ontario, Canada; UNPSJB, Universidad Nacional de la Patagonia 'San Juan Bosco', Argentina; USNM, National Museum of Natural History, Washington, D.C., USA; YPM, Yale Peabody Museum, New Haven, Connecticut, USA.

Geographical/Geological: az, azimuth; ETRW, 'Eric the Red West'; Ma, *mega annum* (millions of years).

PLEASE INSERT TABLE 1

MATERIALS AND METHODS

Information relevant to specimens examined in this work, either directly or indirectly, is provided in Table S1. Specimens described in this work (NMV P221080, NMV P228342 and NMV P229456) were excavated by rock sawing, plug-and-feathers, jackhammering and hammers-and-chisels (DD) and prepared using mechanical methods (L. Kool, MU and D. Pickering, MV). Computed Tomographical (CT) scan data (Siemens Sensation 64: slice thickness 400 µm, courtesy of St Vincent's Public Hospital, Melbourne) were modeled (MCH, VW) using Mimics ~~Suit~~ 14 (Materialise, Leuven, Belgium). The field site was mapped using compass, clinometer and tape (AMT, MCH). The positions of localities utilized Land Channel coordinates (Department of Environment, Land, Water and Planning, State Government of Victoria). A regional geological section was produced, upon which the vertebrate fossil localities of interest were located (MH, unpublished data). A restoration of syndepositional faulting for the Aptian-Albian was subsequently produced (MH, unpublished data), from which, the relative stratigraphic positions of the localities were determined and the stratigraphic ranges of the fossil taxa were compared. Nomenclature for vertebral laminae and fossae detailed in Table 1, follow the criteria of Wilson (1999), Wilson (2012), Tschopp (2016) and Wilson et al. (2011). Restoration of NMV P221080 was based on more complete ornithopods, such as *Hypsilophodon foxii*. An intervertebral gap of 11% was added to total caudal vertebral length using criteria in Hoffstetter & Gasc (1969) and total body length was estimated from the lengths of the anterior-most caudal vertebrae. The systematic palaeontology uses the phylogenetic framework hypothesized by Butler, Upchurch & Norman (2008) and revised by Han et al. (2012).

Nomenclatural acts

The electronic version of this article in Portable Document Format (PDF) will represent a published work according to the International Commission on Zoological Nomenclature (ICZN), and hence the new names contained in the electronic version are effectively published under that Code from the electronic edition alone. This published work and the nomenclatural acts it contains have been registered in ZooBank, the online registration system for the ICZN. The ZooBank LSIDs (Life Science Identifiers) can be resolved and the associated information viewed through any standard web browser by appending the LSID to the prefix http://zoobank.org/. The LSID for this publication is: urn:lsid:zoobank.org:pub:0ACF3BE9-8E2F-4FEA-94B9-E418BE912418. The online version of this work is archived and available from the following digital repositories: PeerJ, PubMed Central and CLOCKSS.

GEOGRAPHICAL AND GEOLOGICAL CONTEXT

Lower Cretaceous strata of the Eumeralla Formation, Otway Group, crop out in sea-cliff and shore platform exposures along the south coast of Victoria, southwest of Melbourne (Figs 1–2) and the primary vertebrate body fossil localities are located on the coastal margin between Apollo Bay and Dinosaur Cove (Felton, 1997a, Felton, 1997b, Rich & Rich, 1989, Wagstaff, Gallagher & Trainor, 2012, Wagstaff & McEwan Mason, 1989). The predominantly volcaniclastic sediments were deposited as thick multistory sheet-flood and river channel complexes within the half-graben resulting from crustal extension during rifting between Australia and Antarctica (Bryan et al., 1997, Duddy, 2003, Felton, 1997b, Norvick & Smith, 2001, Willcox & Stagg, 1990) (Fig. S1). The sediments were sourced from a contemporaneous, high-stand volcanic arc caused by subduction of the southwestern Pacific oceanic plate along the eastern continental margin of Australia (Figs 1C, S1) (see Bryan, 2007, Bryan et al., 1997, Bryan

et al., 2002, Matthews et al., 2015, Norvick et al., 2008, Tucker et al., 2016). The volcanogenic sediments discharged westward into basin systems of the Australian-Antarctic rift system and inland Australia (Figs 1C, S1). Within the Australian-Antarctic rift, minor input of quartzose grit and gravel, derived from Palaeozoic basement detritus shed from the rift margins intermixed with the volcaniclastic sediments, within the river systems (Felton, 1997b). These extrabasinal sediments are observed as thin discontinuous lenses within sand bodies cropping out between Apollo Bay and Cape Otway (Felton, 1997b)—the region within which the vertebrate fossil localities of Eric the Red West, Point Franklin and Point Lewis are located—but not at Dinosaur Cove, west of Cape Otway (Figs 1B–C, 3A–B).

PLEASE INSERT FIGURE 3

The Eumeralla Formation localities fall within the *Crybelosporites striatus* spore-pollen zone of Helby, Morgan & Partridge (1987), the base of which is at the Aptian-Albian boundary (113 Ma, following the time-scale of Gradstein, Ogg & Schmitz, 2012). The top of the *Crybelosporites striatus* spore-pollen zone is presently unresolved (following Wagstaff, Gallagher & Trainor, 2012, Wagstaff & McEwan Mason, 1989), but potentially middle Albian (~109.5 Ma) (following Korasidis et al., 2016) (Fig. S2). Palynological studies further indicate that the fossil localities northwest of Cape Otway, in particular Dinosaur Cove, are younger than the localities northeast of Cape Otway, up to Apollo Bay (following Felton, 1997a, Felton, 1997b, Korasidis et al., 2016), which includes Eric the Red West, Point Franklin and Point Lewis (Figs 1B, S2). However, more precise chronostratigraphic resolution of these localities has yet to be published.

The vertebrate fossil-bearing localities of interest to this investigation include Dinosaur Cove (38º 48' 25.2" S, 143º 27' 28.8" E), Eric the Red West (38º 51' 19.4" S, 143º 31' 53.0" E, between Cape Otway and Point Franklin), Point Franklin (38º 51' 20.9" S, 143º 33' 14.4" E) and the holotype locality of *Atlascopcosaurus loadsi* near Point Lewis (38º 50' 23.3" S, 143º 34' 28.2" E). A palaeolatitudinal reconstruction of East Gondwana for the Aptian-Albian (~113 Ma) using GPlates (Müller, Gurnis & Torsvik, 2012) (Fig. S1) places southern Victoria, in the region of Eric the Red West, at 68.0º S, 134.0º E.

Regional tectonic history and relative stratigraphic positions of the Eumeralla Formation fossil vertebrate localities

Deposition of the Eumeralla Formation coincided with north–south directed continental extension between Australia and Antarctica (see Fig S1). Northeast–southwest trending normal faults and region-wide thinning of strata towards the northwest, coincided with half-graben development and regional crustal sag through thermal subsidence (see Hall & Keetley, 2009). Following the cessation of the continental extension phase between Australia~~n~~ and Antarctica at ~95 Ma, rapid mid-Miocene to late-Pliocene oceanic plate divergence between these landmasses likely caused northwest–southeast crustal compression, resulting in folding and the inversion of normal faults from the Early Cretaceous (Felton, 1992, Hall & Keetley, 2009, Veevers, Powell & Roots, 1991). Although the fossil localities of the Eumeralla Formation are at the same relative level (i.e., shore level; Fig. 4A), their differences in age result from the complex tectonic history of compressive folding and faulting.

Structural deformation has also meant that the relative stratigraphic association of the fossil vertebrate localities has been difficult to visualise. Two northeast–southwest trending, monoclinal faults, separated by ~10 km, are apparent in the region between Dinosaur Cove and

Point Lewis (Figs 1B, 4A). These include the Castle Cove Monoclinal Fault (strike 70º) to the south of Dinosaur Cove (Duddy, 1983; see Felton 1992, fig. 2.4) and another fault north of Cape Otway (strike 45º), termed herein the 'Cape Otway Monoclinal Fault' (Duddy's, 1983, 'Cape Otway Anticline'; see Felton, 1992, fig. 2.4). A further northeast–southwest trending fault located parallel to the coast, borders the Torquay Sub-basin (e.g., Felton, 1992, Hall & Keetley, 2009, Robertson et al., 1978). These faults result in three main blocks (blocks 'A', 'B' and 'C'; Fig. 4A), with the hinges of asymmetric anticlines occurring on the hanging blocks immediately northwest of the faults (Fig. 4A). Dinosaur Cove is located on the northernmost block (hanging wall end of block 'A'), while the three localities of Point Lewis, Eric the Red West and Point Franklin, are located on the southernmost block (footwall end of block 'C'). The present-day dips at the fossil localities (Figs 1B, 4A) are attributable to their positions on the long northwest limbs of the monoclines. Dinosaur Cove (dip 11-20°, az. 357°) is located on the northwest limb of the monocline on Block 'A', while Eric the Red (dip 12°, az. 346°), Point Franklin (dip 18°, az. 307°) and Point Lewis (dip 22°, az. 316°, 150 m southwest of Point Lewis; dip 27°, az. 300°, 200 m north of Point Lewis) are located on the northwest limb of the monocline on Block 'C'. The holotype locality of *Atlascopcosaurus loadsi*, near Point Lewis, is located 4.2 km northeast of Eric the Red West and is lower than the latter (Fig. 4B) by a true stratigraphic thickness of ~180 m.

The approximate stratigraphic relationships of the Lower Albian fossil localities in the Eumeralla Formation are further assessed within a preliminary structural geological restoration (Fig. 4B; MH unpublished data). On the restored section (Fig. 4B), Neogene aged reversal of the north-south trending, Aptian–Albian aged normal faults is removed and strata pinch towards their footwall ends—a typical feature of half-graben structure (e.g., Schlische, 1991). Based on

palynological assessments (Felton, 1997b, Korasidis et al., 2016, Wagstaff, Gallagher & Trainor, 2012, Wagstaff & McEwan Mason, 1989), the restoration (Fig. 4B) shows Dinosaur Cove, on block 'A', at a stratigraphically higher/younger position than the fossil vertebrate fossil localities of Eric the Red West, Point Franklin and Point Lewis, on block 'C'. However, true stratigraphic thickness between Dinosaur Cove and the fossil vertebrate localities on block 'C' is presently unknown. In the absence of more precise chronostratigraphic data, the restoration helps visualise the stratigraphic associations of the fossil localities of interest, from which the stratigraphic range of the fossil vertebrate taxa within can be compared.

PLEASE INSERT FIGURE 4

Sedimentology and taphonomy

Locality overview

The vertebrate fossil locality of Eric the Red West is a shore platform exposure with low vertical relief (Fig. 2). However, local dip (14º) allows three distinct stratigraphic sequences to be tracked along the coast. The lowest unit observed in the region of the fossil site is termed the 'Anchor Sandstone' (Figs 2, 5), named for a ship's anchor that has been concreted onto rocks of this unit. The fossil-bearing unit of interest, termed the 'ETRW Sandstone', erosively overlies the Anchor Sandstone (Figs 2, 5). The unit overlying the ETRW Sandstone is excluded from this present work.

PLEASE INSERT FIGURE 5

Anchor Sandstone

Description: Only the top of the Anchor Sandstone is exposed at the fossil locality at low tide (Figs 2, 5). Owing to tilting, lower strata of the Anchor Sandstone are exposed on the shoreline to the southeast of the dig site. The unit fines upwards overall and is ~30 m thick. The lower strata consist of medium to coarse-grained, large-scale cross-bedded sandstone. The top beds consist of interbedded thinly laminated, silty mudstone and wave-rippled fine-grained sandstone, which pass up into a paleosol, consisting of a pale-grey, unbedded mudstone, with a purplish-brown top layer.

Interpretation: Bedding of the Anchor Sandstone is indicative of a large channel sandbody that shows decreasing depositional energy from the unit base to its top. Prior to compaction, the deposit was >25 m thick, giving an approximate depth for the river channel. The lack of three-dimensional exposure of the unit inhibits conclusive assessment of the channel pattern. However, the bedding style suggests lateral accretion in a meandering river channel (e.g., Allen, 1963, Allen, 1970, Walker, 1976). The thinly laminated, symmetrical rippled bedding at the top of the Anchor Sandstone (Figs 2, 5) formed from wind driven wave ripples in shallow water, such as in a shallow overbank lake (e.g., Nichols, 2009). A paleosol, capping the rippled beds, developed during a period of vegetation growth on the floodplain surface. Deposition of these upper beds would have been distant from the meandering channel (e.g., Kraus, 1999, p. 47).

ETRW Sandstone

Description: The base of the ETRW Sandstone is scoured into the Anchor Sandstone forming an undulating contact with a relief of ~0.5 m (Figs 2, 5). Tracking the bedding upwards from the unit base along the shoreline outcrop to the west of the fossil site indicates a total stratigraphic

thickness of ~25 m (Fig. 5A). The lower part of the ETRW Sandstone consists of overlapping, low-angled, large-scale trough cross-beds of medium- to coarse-grained sandstone (Figs 2–3, 5). Some troughs are up to 10 m wide. The large-scale trough cross-beds extend upwards to at least half of the unit thickness. Many of the troughs in the basal few metres of the unit are scoured and infilled with, or floored by, matrix-supported conglomerate, variably consisting of medium to coarse sand grains, 'grit' (very coarse sand to small pebble size quartz and feldspar) with mica flakes, rounded mudstone rip-up clasts (typically up to 10 cm, and rarer clasts up to 25 cm), coalified compacted plant fragments, charcoal, tree limbs/branches and logs (up to 1 m diameter and some up to 5 m in length) and transported tree stumps with root bases and attached soil (Fig. 3). The trough cross-beds pass up into climbing rippled beds of medium to fine-grained sandstone and interbedded, very fine-grained sandstone and siltstone layers at the unit top. Some layers show bioturbation (infilled burrows). Associated and isolated fossil vertebrate remains have been excavated from infilled scours within the basal 2 m of the ETRW Sandstone (Figs 3, 5).

Interpretation: The ETRW Sandstone is interpreted as a deep (>25 m) fluvial channel deposit with thinning-up of the bedding and fining-up of the grain-size indicating deposition by lateral accretion. However, conclusive interpretation of the channel pattern is inhibited by the lack of three-dimensional exposure. Nonetheless, unpublished data (AMT) from upstream and downstream of this locality demonstrate the width, depth and meandering channel planform of the rivers that deposited sandstones of the ETRW Sandstone type. The large-scale trough cross-beds at the unit base (Figs 3, 5) are interpreted as the preserved parts of large migrating linguoid dunes on the channel floor (e.g., Simons, Richardson & Nordin, 1965, Walker, 1976). Trough cross-bed widths of up to 10 m indicate dunes of similarly large size within the channel (Boggs,

2001, pp. 40, 41, Rubin & McCulloch, 1980, Simons, Richardson & Nordin, 1965, Southard & Boguchwal, 1990). The thickness of the ETRW Sandstone indicates a meandering channel close to 1 km in width with a meander belt, if fully developed, nearing 10 km in width (based on criteria of Collinson, 1978). The discovery of isolated fossil bones and teeth in the deposit provisionally identified as those of aquatic reptiles (see Rich, 2015), further supports the interpretation of a large permanent river.

The orientation of the troughs/scours, current-aligned logs and cross-bedding near the base of the unit indicates flow to the northwest (290º, based on present day coordinates; Fig. 5). Trough-shaped scours identified at the unit base, similar in size and orientation to those above the base, indicate scouring of the older Anchor Sandstone ahead of the migrating dune front. The flow rate of the river is suggested from two features. Firstly, flute marks identified at the unit base suggest upper regime flow of >1 m/sec (Southard & Boguchwal, 1990, Walker & Cant, 1984) and secondly, at river depths of <20 m (i.e., the depth of the river that we expect formed the ETRW Sandstone), large-sized dunes form at flow velocities of ~2.0 m/sec (Rubin & McCulloch, 1980). The grit was potentially derived from the Palaeozoic basement of the rift margin (Felton, 1997b) and the mudrock clasts derived from the older, partly consolidated overbank sediments into which the river incised. The root bases of two current-aligned logs deposited near the partial postcranium (NMV P221080) are directed downstream (Figs 3C, 5B). The current-aligned logs and tree stumps likely derive from cutbank collapse (see also Seegets-Villiers, 2012, on the Wonthaggi Formation, e.g., Wood, Thomas & Visser, 1988) and soil-derived mud retained around their root balls, suggest these debris entered the channel close to the locality.

Coarse sediment in a river, including tree debris, is typically mobilized during high stage flow (Walker, 1976). Peak migration of dunes similarly occurs during high stage flow, while peak aggradation, typically occurs during waning flow (Allen, 1984, Harms & Fahnestock, 1965). During high-stage flow in the river that formed the ETRW Sandstone, flow rate at the channel base would have been sufficient enough to mobilise a bedload mass of large waterlogged logs, tree stumps and branches. As the current slowed, movement of the logs and stumps likely halted. The grounded tree debris potentially formed obstructions, causing scouring and the entrapment of smaller plant debris as 'logjams', which in turn may have entrapped smaller objects such as isolated 'fresh' and fossil bones and carcasses/body-parts, or caused the deposition of these objects in lee-side eddies.

Fossil context and taphonomic comments

The scours near the base of the ETRW Sandstone host a rich assemblage of isolated vertebrate bones (see also, Barrett et al., 2011a, Rich et al, 2009b), among which, NMV P228342 and NMV P229456 (Fig. S3), two vertebrae of interest to this investigation, were excavated close to the position of the partial postcranium (NMV P221080; Fig. 6). These two isolated vertebrae show minor breakage and erosion of their cortical surfaces (Fig. S3), suggesting they encountered only minor hydraulic reworking prior to final deposition at this site (Behrensmeyer, 1988). The partial postcranium NMV P221080 (Fig. 6) was discovered eroding out of the shore platform, ~3.0 m north of the shore platform edge (Figs 2–3, 5B). The fossil is hosted by conglomerate extracted from a scour trough ~1.2 m above the base of the unit (Figs 3C, 5B, S4). The conglomerate additionally hosts compressed, coalified plant debris (Fig. S4), including large current-aligned logs (one immediately east of NMV P221080) and an upright tree stump (see also Rich et al., 2009b) with a partial root ball attached (1 m north of NMV P221080; Figs 3C–D, 5).

PLEASE INSERT FIGURE 6

Burial of the partial postcranium (NMV P221080) in the coarse bedload, along with tree branches, sizable logs and tree stumps is indicative of its transportation and deposition during a period of substantial in-channel hydraulic flow. NMV P221080 likely entered the river channel from the floodplain upstream of the site as a carcass or body-part: the skeleton held together by soft tissues (muscles, skin, viscera, tendons and ligaments). Transportation and burial of NMV P221080 likely occurred over a short period of time. Thus, destructive decay of the carcass/body-part and/or disarticulation by scavenging would have been prevented by rapid burial (e.g., Behrensmeyer, 1982, Behrensmeyer, 1988, Shipman, 1981, Wood, Thomas & Visser, 1988). The anterior caudal vertebrae of NMV P221080 were preserved with their ventral surfaces oriented upwards and the haemal processes were displaced from their life positions to lay flat in the bedding (Figs 6, S4A). Displacement and compaction of these haemal arches further suggests that the soft tissues were rapidly compacted by sediment. The carcass/body-part (NMV P221080) could have been deposited by eddy currents at the downstream edge of a mass of woody tree debris (‘logjam’), indicated by the current-aligned logs upstream of the fossil and the transported tree stump deposited close to the specimen (Figs 3, 5). Coalified compacted branches and finer plant fragments surround NMV P221080 in the host sediment (Fig. S4). NMV P221080 was likely to have been more complete when deposited, possibly a complete carcass, with loss of the original skeleton occurring in recent times from erosion of the shore platform (Figs 2, 5).

SYSTEMATIC PALAEONTOLOGY

ORNITHISCHIA Seeley, 1888

CERAPODA Sereno, 1986

ORNITHOPODA Marsh, 1881

Diluvicursor gen. nov. urn:lsid:zoobank.org:act:BB4925A8-A049-4569-9AF2-80B28E999279

Etymology: From the Latin *'diluvi'*, for deluge or flood, in reference to the deep high-energy palaeo-river within which the type material was deposited and the palaeo-floodplain upon which the river extended, combined with the suffix '-*cursor*', from the Latin for runner.

Diagnosis: A turkey-sized, small-bodied ornithischian differentiated from all other ornithischians by a combination of 21 features, including nine potential autapomorphies (*): (1) haemal groove on the middle and posterior caudal vertebrae deeply excavates the centrum; (2*) dorsoventrally narrowest part of the centrum on the posterior caudal vertebrae, distinctly offset posteriorly and embayed by a sulcus; (3*) triangular intervertebral process anteriorly on the centrum of the posterior-most caudal vertebrae incises a V-shaped notch at the posterior end of the adjoining centrum; (*4) spinal process on the anterior caudal vertebrae has parallel anterior and posterior margins, a proximodistal length approximately equaling anteroposterior length of the centrum and steeply reclined to 30º from the dorsal plane; (5*) dorsoventral height of the neural arch on the anterior-most caudal vertebrae approximately equal to centrum height, 20% of total vertebral height (including the haemal arch) and 22% of total transverse width across the caudal ribs; (6) transverse width across the caudal ribs at Ca 3 87% of total vertebral height; (7*) prezygapophysis on the anterior-most caudal vertebrae (up to ~Ca 5) horizontally oriented and located at base of the neural arch, lateral to the neural canal; (8*) tuberous process developed

dorsally on the spinoprezygapophyseal lamina (sprl) of the anterior-most caudal vertebrae; (9*) transprezygapophyseal lamina (tprl) extends between tuberous processes on the paired sprl, dorsal to the posterior margin of the prezygapophyses (10) tab-like prespinal lamina (prsl) developed at the base of the spinal process on the anterior caudal vertebrae; (11) spinal process on the middle caudal vertebrae is linear, proximally narrow, distally paddle-shaped and steeply reclined to 30º from the dorsal plane; (12) haemal processes on the middle caudal vertebrae with hatchet- to disc-shaped distal ends; (13) haemal processes on the posterior caudal vertebrae with boot-shaped distal ends; (14) medial malleolar ridge on the tibia, shallowly rounded; (15) transverse width of the calcaneum ~50% that of the astragalus; (16*) the lateral distal tarsal embayed anteriorly by a sulcus for the calcaneum; (17) distal condyle on metatarsal (mt) I, plantomedially positioned relative to the diaphysis of mt II; (18) dorsoplantar heights of mt I and pedal phalanx (pd) I-1, ~50% those of mt II and pd II-1, respectively; (19) pd I-1, asymmetrical with lateral flaring of the proximal cotyle; (20) plantar half of the diaphysis on mt II, transversely compressed to ~50% of the equivalent region on mt III, resulting in a lunate keyhole-shaped profile, in proximal view; and (21*) pd IV-1, strongly asymmetrical, with medial flaring of the proximal cotyle.

Diluvicursor pickeringi sp. nov. urn:lsid:zoobank.org:act:9E1765D7-756F-4CF2-A005-EC0B0BE996BA

Figures S3–S4, 6–27, 31, 33, 35; Tables 1–5

2009 Ornithopoda; Rich et al., p. 677.

2014 Ornithopoda; Herne, pp. 246–274.

Distribution: Early Cretaceous of Australia.

Holotype: NMV P221080, partial postcranium comprising an almost complete caudal vertebral series, the distal ends of the right tibia and fibula, complete right tarsus and partial right pes.

Holotype locality: Eric the Red West, ETRW Sandstone, lower Albian Eumeralla Formation, Otway Group, southern Victoria.

Derivation of name: To acknowledge the significant contribution of David A. Pickering to Australian palaeontology and in memory of his passing during the production of this work.

Diagnosis: As for genus.

Referred material: NMV P229456, partial caudal vertebra from the holotype locality.

DESCRIPTION

Axial skeleton

Preservation and overview

Only caudal vertebrae are known from the holotypic axial skeleton, with 38 caudal vertebrae preserved in articulation (Figs 6–7). The anterior-most preserved caudal vertebra (Ca) is represented by the haemal arch at a position designated ‘Ca 1’, noting that its true position within the vertebral sequence is unknown. The distal part of the neural spine is preserved at Ca 1 and the first preserved centrum at Ca 3. The ventral surfaces of Ca 3 to Ca 11 are exposed and their dorsal surfaces are within the matrix. CT imagery provided information on the neural arches from Ca 1 to Ca 11. The left and ventral surfaces of the caudal vertebrae posteriorly from Ca 13 are exposed and their right sides are within the matrix. The posterior portion of Ca 38 is missing. However, the left postzygapophyseal facet on Ca 38 indicates that additional caudal vertebrae

would have been present in life. On the referred caudal vertebra NMV P229456 (Fig. S3), the left anterior and posterior lateroventral corners of the centrum are broken and the distal portion of the left prezygapophysis is missing. The caudal series is divided into three regions. The anterior region is identified by the presence of caudal ribs from Ca 1 to Ca 13. The middle and posterior regions are differentiated by a distinct change in centrum shape. The mid-caudal vertebrae extend from Ca 14 to Ca 22 and the posterior caudal vertebrae from Ca 23 to Ca 38 (Fig. 7). Unless indicated, the following description is with respect to the holotype (NMV P221080). Nomenclature for vertebral laminae is provided in Table 1.

PLEASE INSERT FIGURE 7

Caudal vertebrae

Centra (Table 2): The neurocentral sutures are clearly defined on the anterior-most vertebrae and difficult to distinguish posterior to Ca 8. The sutures lie ventral to the transverse processes on the anterior caudal vertebrae to at least Ca 10 and at Ca 13, is dorsal to the transverse process. The centra on the anterior-most caudal vertebrae have ovoid or U-shaped anterior and posterior ends (Figs 8–10) and are elliptical in mid-transverse section. At Ca 3–6, the articulating surfaces of the centra are amphiplatyan (Figs 9–10) and posteriorly to that position, are modestly amphicoelous (Figs 11–12). The centra progressively decrease in dorsoventral height posteriorly along the tail and become anteroposteriorly longer towards the middle of the tail (Table 2). With anteroposterior lengths of ~17.5 mm, the centra from Ca 17 to Ca 18 are up to 20% longer than those of the anterior caudal vertebrae. The centra remain axially elongate on the posterior caudal vertebrae. The anteroposterior lengths of the centra are marginally longer from Ca 17 to Ca 30 (~16 mm) than the centrum at Ca 4 (15.2 mm). Posteriorly from Ca 30, the centra become progressively shorter. The transverse shape of the centrum changes from ovoid on the anterior

caudal vertebrae (i.e., Ca 3–13; Figs 8–12) to quadrangular on the middle caudals (i.e., Ca 14–22; Figs 12–15), to hexagonal on the posterior caudals (i.e., posteriorly from Ca 23; Fig. 15).

PLEASE INSERT FIGURES 8–11

The change in centrum shape between the middle and posterior caudal vertebrae results from the more ventral location of the lateral ridge on the latter vertebrae (Fig. 15). On the middle caudal vertebrae, a small protuberance is formed on the lateral ridge (Figs 12–15). Viewed laterally, a small sulcus is formed on the lateroventral fossa of the centra posterior to Ca 23 (Figs 15–17) and offset posteriorly from the mid-point on the centrum. The sulcus is most strongly developed on vertebrae posteriorly from Ca 28 (Figs 16–17). At Ca 35–38, unusual triangular processes are developed at the anterior articular ends of the centra that appear to incise corresponding notches in the posterior ends of the adjoining centra (Fig. 17). At Ca 3–11, haemal grooves are only shallowly developed (Figs 8, 11), and on vertebrae posteriorly from Ca 14, the grooves deeply excavate the centra (Figs 12–15, 17).

PLEASE INSERT FIGURES 12–15

The centrum on the referred vertebra, NMV P229456 (Fig. 18), is hexagonal in mid-transverse section. A posteriorly offset waist is present on the centrum, but is shallowly developed, while the haemal groove is deeply developed. The triangular anterior process, present on the posterior-most caudal vertebrae of the holotype, is lacking. NMV P229456 most resembles the caudal vertebrae on the holotype in the region of Ca 14–30. However, with an anteroposterior length of 26 mm, the centrum of NMV P229456 is approximately double the length of the centra in the region indicated on the holotype.

PLEASE INSERT FIGURES 16–18

Neural arches (Tables 1, 2): At Ca 3–9, the spinal processes are steeply reclined to ~30º from the dorsal plane and their anteroposterior lengths approximately equal the lengths of their centra (Ca 3–6, see Figs 9–10; note, the neural arches on Ca 7–11 are not figured herein, but observed from CT output). At Ca 3 the dorsoventral height of the neural arch (measured from the dorsal tip of the spinal process to the centre of the transverse process; distance 'a' in Fig. 9A) is 44% of the total vertebral height, excluding the haemal arch (measured from the dorsal tip of the spinal process to the ventral-most margin of the centrum; distance 'b' in Fig. 9A) and 18% of total vertebral height including the haemal arch (distance 'c' in Fig. 9A). At Ca 3–9, the anterior and posterior margins of the spinal processes are parallel (Ca 3–6, see Figs 9–10). The dorsal tips of these spinal processes are convex and their ventral tips, angular. The shape of the spinal process abruptly changes at Ca 10 (observed from CT output). Viewed laterally, the spinal processes are proximally narrow at Ca 10–19 and their distal ends expanded to form paddle-shaped ends (Ca 12–19, see Figs 12–14). At Ca 18–19, the distal ends of the processes are blunt and the degree of distal expansion of the process is greatest at Ca 18 (Figs 13–14). On vertebrae posteriorly from Ca 10, the degree of distal expansion of the spinal processes progressively reduces and the distal ends regain a rounded profile (e.g., vertebrae posteriorly from Ca 12; Figs 12–16). Spinal processes are developed up to Ca 27, after which point, a low spinal ridge is developed (Figs 16–17).

At Ca 3–5, the prespinal lamina (prsl) is prominently developed at the base of the spinal processes (Figs 9–10). On vertebrae posterior to Ca 5, the prsl could be developed, but not identified in the CT output. At Ca 1–5, a thin flange-like process projects laterally from the left sides of the spinal processes near their distal ends (Figs 9–10). The spinal processes on the

middle caudal vertebrae remain linear and reclined at ~30º relative to the dorsal plane (Figs 12–15). However, in comparison to the anterior caudal vertebrae (Figs 9–10), the spinal processes on the middle caudals are more elongate. As a result, relative to the heights of their centra, the neural arches on the middle caudal vertebrae are higher than those on the anterior caudals. At Ca 13, the dorsoventral height of the neural arch is 56% of the total vertebral height, excluding the haemal process, and at Ca 17–18, ~65%.

At Ca 3–5, the pre- and postzygapophyses are horizontally oriented and located at the base of the neural arch, lateral to the neural canal (Figs 9–10). The prezygapophyses extend only a short distance beyond the centrum. On the vertebrae posteriorly from Ca 6, the pre and postzygapophyses become more dorsally elevated, relative to the neurocentral suture, and anterodorsally oriented. At Ca 10–11 (observed from CT output), the prezygapophyses are anterodorsally oriented to ~30º from the dorsal plane and at Ca 13–15 (Fig. 16), the prezygapophyses are short, inclined to ~40º from the dorsal plane and protracted posteriorly relative to the anterior ends of their centra, as in the dryosaurids (Galton, 1981) and *Thescelosaurus neglectus* (Gilmore, 1915, fig. 7). On vertebrae posteriorly from Ca 16, the prezygapophyses extend anteriorly beyond their centra and progressively become more horizontally oriented and dorsally convex (Figs 13–17). At Ca 18–21, the prezygapophyses extend anteriorly from their centrum by ~25% of centrum length, at Ca 22–34, ~30% of centrum length and on vertebrae posteriorly from Ca 36, up to 50% of centrum length. On vertebrae posteriorly from Ca 23, the prezygapophyses are dorsoventrally expanded at their midpoint and rabbit-ear-shaped (Figs 14–17).

On the anterior caudal vertebrae, the spinoprezygapophyseal lamina (sprl) connects the prezygapophysis to the lateral surface of the spinal process and demarcates the base of the prsl

(e.g., Ca 4; Fig. 10). At Ca 3–5, a tuberous process is developed on the sprl, posterior to the prezygapophyseal articular facet (Figs 9–10). The process on the sprl is weakly developed at Ca 6 and absent posteriorly to that position. At Ca 3–5, the transprezygapophyseal lamina (tprl) extends between the tuberous processes on the paired sprl (Figs 9–10). On these vertebrae, the tprl is positioned dorsal to the prezygapophyses. The anterior margin of the tprl aligns with the posterior ends of the prezygapophyseal facets.

The transverse processes on the anterior caudal vertebrae, upon which the caudal ribs attach, are laterally reduced and dorsoventrally thickened (see Fig. 10). At Ca 3–5, the transverse processes are positioned centrally on their neural arches and at Ca 6–9, more posteriorly positioned (Figs 9–11). At Ca 10–13, the transverse processes regain a central position (Figs 11–12). The prezygodiapophyseal lamina (prdl) and postzygodiapophyseal lamina (podl) connect the pre and postzygapophyses to the transverse process (Fig. 10). On vertebrae posteriorly to Ca 13, the prdl merges with the lateral wall of the neural arch and the sprl and podl merge to form a single postzygoprezygapophyseal lamina (pprl; Figs 12–15, 16–17).

On the vertebrae posteriorly from Ca 17, a groove-like spinoprezygapophyseal fossa (sprf) is developed on the prezygapophyses, between the pprl and prdl (Figs 13, 16). The sprf is absent on the anterior caudal vertebrae and weakly developed on the anterior-most-middle caudals. On the anterior caudal vertebrae, the anterior and posterior centrodiapophyseal laminae (acdl and pcdl, respectively) connect the diapophysis to the base of the neural arch (Figs 10, 12). However, on the middle and posterior caudal vertebrae, the acdl and pcdl merge to form a continuous lateral ridge on the centrum ventral to the neurocentral suture (Figs 12–17; see also ‘centra’ above). The centroprezygapophyseal lamina (cprl) and centropostzygapophyseal lamina (cpol) connect the pre and postzygapophyses to the base of the neural arch. The centroprezygapophyseal fossa

(cprf) is formed laterally to the cprl. The cprf forms a weak depression on the anterior caudal vertebrae (Figs 9–10), is well developed on the middle caudals (Figs 12–13) and forms a narrow groove on the posterior caudals (Fig. 16). The cpol is indistinct on most of the caudal vertebrae and typically merges with the posterior margin of the pedicle.

The right prezygapophysis on the referred posterior caudal, NMV P229456 (Fig. 18), extends anteriorly beyond the centrum by 30% of the centrum length, noting that the anterior-most tip of the right prezygapophysis could be missing. The prezygapophysis on NMV P229456 is dorsoventrally expanded at its mid-point and low to the centrum, resulting in a narrow cprf (Fig. 18A–B). In lateroventral view (Fig. 18A), however, the cprf is observed undercutting the ventral surface of the prdl; a feature also apparent on the posterior caudal vertebrae of the holotype. A spinal process is not developed on NMV P229456 and the postzygapophyses merge to form a median ridge (Fig. 18). The neural arch of NMV P229456 most resembles the posterior caudal vertebrae on the holotype from Ca 28 to Ca 32.

Caudal ribs (Table 2): The caudal ribs are fused to the diapophyseal facets on the transverse processes of the neural arches (Figs 8–12). The transversely broadest distance across the caudal ribs at Ca 3 (distance ‘d’; Fig. 9B) is 87% of total vertebral height (distance ‘c’; Fig. 9A). On vertebrae posteriorly from Ca 3, the proximodistal widths of the ribs progressively decrease. In anterior and posterior views of Ca 3–6 (Fig. 9D–E), the caudal ribs are horizontally oriented and shallowly concave dorsally, as in *Hypsilophodon foxii* (Galton, 1974, figs 28-31). In dorsal and ventral views (Figs 8–11), the caudal ribs are orthogonal to the vertebral axis at Ca 3, posterolaterally oriented at Ca 4–6, and orthogonal at Ca 8. The centrodiapophyseal fossa (cdf) excavates the proximoventral surface of the transverse process and extends ventrally onto the dorsolateral surface of the centrum (Figs 8–10).

Haemal arches (Table 2): The haemal arches are transversely Y-shaped, the haemal canal is enclosed and a median groove on the anterior surface extends from the proximal base onto the shaft of the haemal process (Figs 8–9, 11). At Ca 1–4, the haemal processes are proximodistally elongate and expand to a small degree at their distal ends (Figs 8–9). On the vertebrae posteriorly from Ca 3, the proximodistal heights of the haemal arches progressively reduce. At Ca 3 (Fig. 9), the proximodistal height of the haemal arch is slightly less than three times the height of the neural arch and at Ca 15 (Fig. 12) the haemal arch is slightly shorter than neural arch height. At Ca 7–8, the haemal processes have small, paddle-shaped distal ends, at Ca 9–15, the distal ends are hatchet-shaped (Ca 14–15, see Fig. 12) and at Ca 17–19 (Figs 13–14), the processes are symmetrically disc-shaped. A displaced, boot-shaped haemal arch lying ventral to Ca 19 (Fig. 14) is likely from Ca 20. Posteriorly from Ca 20, the distal ends of the haemal processes are posteriorly expanded and thus, asymmetrical (Figs 14–15). At Ca 32–33, the haemal arches are distinctly boot-shaped (Fig. 16C). Haemal arches are developed up to the posterior-most vertebra preserved at Ca 38 (Fig. 17); however, the exact shapes of these processes are uncertain. The natural/correct orientations of the haemal arches are best observed at Ca 15–19 (Figs 12–14). At these positions, the orientation of the haemal arches range from orthogonal to ~80º. At Ca 21 and posteriorly to that position, the haemal processes are steeply reclined (Figs 14A, 16C), which is potentially attributable to postmortem contraction of the connective tissues.

PLEASE INSERT TABLE 2

Ossified tendons: From the CT imagery, elongate processes are observed on the left dorsolateral surfaces of the spinal processes at Ca 3–4 (Figs 9–10) that could be the fused remnants of ossified tendons, as in *Valdosaurus canaliculatus* (Barrett, 2016). However, other than these features, ossified tendons were not apparent.

Appendicular skeleton

Preservation and overview

From the appendicular skeleton of the holotype, only the distal right crus, complete tarsus and partial right pes are known (Figs 6–7, 19–20). The pes is preserved in a state of ~~hyperdorsoflexion~~, which likely occurred postmortem (Fig. 19). The anterior surface of the crus and the medial and plantar regions of the pes are exposed (Fig. 19). The metatarsals (mt) are imbricated (particularly mt II–III), which likely resulted from diagenetic compaction. Restoration of the right distal hind limb is shown in Figure 20, noting that imbrication of the metatarsals has not been digitally adjusted. The calcaneum appears to have been displaced laterally from the astragalus by 2 mm. Pedal digit (pd) I is almost complete; however, the distal end of the ungual, pd I-2, is eroded. Phalanges pd II-1 and pd IV-1 are preserved and of these, only pd IV-1 is complete. Of the remaining phalanges, only the proximal portion of pd IV-2 is preserved.

PLEASE INSERT FIGURES 19–20

Crus

Tibia (Table 3): Viewed distally, the tibia is reniform (Fig. 21E). The narrowest transverse width of the preserved portion of the diaphysis is 47% that of the distal tibia. The lateral malleolus is distally depressed relative to the medial malleolus (Fig. 21A–B), and 50% of the anteroposterior width of the medial malleolus. A shallow intermalleolar fossa is formed anteriorly (Fig. 21A, E). The posterior medial malleolar ridge is broad and shallowly rounded (Fig. 21B, E–G).

Fibula (Table 3): The fibula is anterolaterally positioned relative to the tibia. The diaphysis is narrow and the anteromedial edge forms a thin crista that extends to the distal condyle (Fig.

21A). The distal condyle is anteroposteriorly compressed, lunate in distal profile and flares towards its distal end where it articulates with the dorsolateral face of the calcaneum (Fig. 21A–G); noting that these two elements appear to have been slightly displaced by 5 mm on the holotype. Whether or not the fibula contacted the astragalus is uncertain. The morphology of distal fibula is typical for a small-bodied ornithopod (e.g., *Hypsilophodon foxii* (Galton, 1974) and *Mantellisaurus atherfieldensis* (Norman, 1986)).

PLEASE INSERT FIGURE 21

PLEASE INSERT TABLE 3

Tarsus

Astragalus (Table 4): The astragalus and calcaneum are unfused and cap the distal tibia and fibula forming the ginglymoid (saddle-shaped) surface of the mesotarsalian ankle joint (Fig. 21 A–B). Viewed distally (Fig. 22D), the astragalus is sub-triangular, expanding medially and truncated laterally where it adjoins the calcaneum. A low tuberosity is present on the anteromedial face (Fig. 19B, 22A) somewhat resembling the rugose feature described in *Valdosaurus canaliculatus* (Barrett et al., 2011b, fig. 8E). The anterior ascending process on the astragalus is thin, centralized and transversely broad (Fig. 22A). The distal ('dorsal') margin is obtuse. The dorsoventral height of the astragalus (measured vertically from the median point on the dorsal peak of the process to the corresponding point on the distal astragalar margin; see Figs 22A, S5; Table S3) is 58% of its transverse width. A shallow transverse fossa is formed anteriorly at the base of the process and a shallow fossa appears to border the medial margin of the anterior ascending process. The posterior ascending process (Fig. 22B–C) is thin and dorsally lower than the anterior process. In proximal and distal views, the posterior ascending process has

a shallowly rounded profile that corresponds to the convex surface of the posterior medial malleolar ridge on the tibia (Figs 21E–F–22C–D).

Calcaneum (Table 4): The calcaneum is sub-circular in distal profile (Fig. 22D) and has a transverse width slightly less than half that of the astragalus. A process on the mediodistal margin likely overlapped the adjoining lateral margin of the astragalus (Fig. 22C–D). The lateral surface forms a fossa (Fig. 21C) and the fibula likely articulated with the anteroproximal surface.

Distal tarsus (Table 4): The distal tarsus consists of the lateral and medial distal tarsals that rigidly cap the proximal end of the metatarsus (Figs 19B–20, 22E–I). The medial distal tarsal, upon which the astragalus articulates, is a thin, wavy, quadrangular-shaped bony plate that caps mt II–III. A shallow dorsoplantarly oriented groove is formed on the proximal face (Fig. 22E) between sulci on the dorsal and posterior/plantar edges. This groove, however, does not correspond to the margin between mt II–III. The convex distal surface on the medial distal tarsal is accommodated in a fossa proximally on mt II–III (Fig. 22H–I). The lateral distal tarsal is wedge-shaped, tapering both laterally and anteriorly, is thicker than the medial and caps mt IV. The entire dorsolateral region of the lateral distal tarsal is embayed by a lunate fossa for the calcaneum (Fig. 22H–I). Mt V articulates with the plantar edge of the lateral distal tarsal.

PLEASE INSERT FIGURE 22

PLEASE INSERT TABLE 4

Pes

Metatarsus and surface orientations: The metatarsus is compact, elongate and roughly cylindrical in shape (Fig**s** 19–20, 23). The proximal surface is angled to 30º relative the

transverse axis of the tarsus (Fig. 23), as in *Gasparinisaura cincosaltensis* (Cambiaso, 2007, fig. 76A, Salgado, Coria & Heredia, 1997, fig. 5.4), *Hexinlusaurus multidens* (He & Cai, 1984, Pl. 4.4) and *Orodromeus makelai* (Scheetz, 1999)**.** As a result of the cylindrical form of the metatarsus, and provisionally, diagenetically imposed imbrication of the metatarsals (Figs 19–20), typical surface orientations on mt I, II, IV and V are rotated to more plantar orientations. For example, the surface on mt I described as medial in *Hypsilophodon foxii* (Galton, 1974), is more plantomedially oriented in *Diluvicursor pickeringi*. However, to avoid confusion and to simplify the description that follows, typical surface orientations of the pedal bones are used herein.

PLEASE INSERT FIGURE 23

Pedal digit I (=hallux; Table 5): Mt I obliquely crosses the plantomedial face of mt II and is accommodated in a shallow groove on the latter (Figs 19–20B, 23–24). The proximodistal length of mt I is 58% that of mt III. The proximal end of mt I forms a transversely compressed condyle (Fig. 24C–E). The diaphysis is splint-like in its proximal half adjoining mt II and becomes sub-triangular in section distally where the bone expands to form the distal condyle (Fig. 24E–F). The distal condyle is roughly spheroidal and positioned plantomedial to mt II (Figs 20, 23C–D), Viewed distally, the condyle forms a T-shaped profile with the head of the T facing medially (Fig. 24E–F). The grooves formed are interpreted as the flexor, plantarly and the extensor, dorsolaterally. The *M. extensor hallicus longus* (e.g., White et al., 2016) that would have located within the extensor groove on the distal condyle, likely extended proximally along the medial margin of mt I and mt II. The abductor surface of the condyle is smooth and neither abductor nor adductor pits are apparent (Fig. 24A–F). The distal condyle on the metatarsal is finely proportioned, with dorsoplantar and transverse widths slightly less than 50% of those on the condyle of mt II.

Two phalanges (pd I-1 and the ungual pd I-2; Figs 19, 24G–M) are present, as in less-derived ornithopods (Moreno, Carrano & Snyder, 2007). As preserved, the proximodistal axis of pd I-1 is angled relative to the axis of the metatarsal. As a result, the phalanges of the hallux are oriented medially inwards (Figs 19–20). In dorsal and plantar views, pd I-1 is asymmetrical (Fig. 24G–H): the cotyle is flared laterally relative to the central axis of the diaphysis and the medial edge is linear. In medial and lateral views (Fig. 24I–J), pd I-1 is dorsoplantarly compressed and the diaphysis recurves dorsally; thus, the dorsal and plantar surfaces are concave and convex, respectively. Collateral ligament grooves are developed distally on the dorsolateral corners of pd I-1 (Fig. 24I–J, M). The proximodistal length of pd I-1 is 47% that of mt I and 27% that of mt III. The transverse width of pd I-1 at its proximal end is 56% that of proximal pd II-1 and the dorsoplantar depth, 50% that of proximal pd II-1. The plantar portion of the ungual is eroded. The dorsal surface of the proximally preserved portion is rounded and sub-triangular in distal view (Fig. 24L).

PLEASE INSERT FIGURE 24

Pedal digit II (Table 5): Mt II is elongate and closely articulates with mt III, which is accommodated in a lateral fossa that extends along the complete length of the bone **(**Figs 19–20B, 23, 25A–E). A fossa formed on the proximal surface of the metatarsal accommodates the medial distal tarsal and the medioproximal margin participates in the ankle joint (Figs 20B, 25A–D, F). The metatarsal forms a lunate, roughly keyhole-shaped profile in proximal view (Figs 23C, 25F). The axial length of mt II is 80% that of mt III. Viewed mediolaterally, the proximal end of the metatarsal is dorsoplantarly expanded, forming a fan-shaped profile (Fig. 25C–D). Surface bone on the proximal region of mt II is textured and rugose (Fig. 19). The plantar portion of the diaphysis on the metatarsal is transversely compressed over its length (Fig. 25B, F): the

transverse width is approximately a third that of mt III. On the plantar surface of the metatarsal, a ridge extends from the proximal end to the plantolateral corner of the distal condyle (Fig. 25B). The distal end of mt II is depressed plantarly relative to the diaphysis of mt III (Fig. 23D) and forms a quadrangular-shaped, shallowly spheroidal articular condyle (Fig. 25E). The dorsoplantar depth of the distal condyle is greater than its transverse width. The flexor, extensor and abductor (medial) grooves are shallowly developed, while the adductor (lateral) groove is continuous with the lateral fossa for mt III (Fig. 25A–E). Only the proximal portion of pd II-1 is preserved (Figs 19A, 23A–B). The cotyle is rugose and envelops the distal condyle of mt II. The proximodistal axis of pd II-1 is mediodistally directed, relative to the long axis of the metatarsal.

PLEASE INSERT FIGURE 25

Pedal digit III (Table 5): The longest of the metatarsals, mt III closely adjoins mt II and mt IV (Figs 19–20, 23). Viewed proximally, the metatarsal is roughly quadrangular in shape (Figs 23C, 25L). A fossa on the proximal surface is continuous with mt II (Fig. 23C) and accommodates the convex distal surface of the medial distal tarsal. The dorsal surface of mt III is transversely broader than the plantar (Fig. 25G–H). In mediolateral view, the proximal end of the metatarsal is dorsoplantarly expanded, forming a T-shaped flange (Fig. 25I–J). Proximally, the bone is textured and rugose (Fig. 19). In dorsal and plantar views, the metatarsal curves laterally outwards over its length (Fig 25G–H). The lateral and medial margins are modestly concave and convex, respectively and the distal condyle recurves medially at the metaphysis. Viewed medially and laterally (Fig. 25I–J), the diaphysis of the metatarsal is dorsoplantarly compressed and shallowly bowed (dorsally concave–plantarly convex). The distal end recurves plantarly at the metaphysis to form a condyle that is spheroidal on the dorsal portion and centrally grooved plantarly, suggesting a ginglymoid joint (Fig. 25G–K). The diaphysis is rectangular in transverse

section. Collateral ligament grooves on the distal condyle of the metatarsal are shallowly developed. Adductor and abductor tendons could also have located within the medial and lateral grooves. The transverse width of the diaphysis is approximately double its dorsoplantar depth. Only the proximal portion of pd III-1 is preserved (Figs 19A–20, 23A–B) and similarly to pd II-1, the cotyle forms a rugose expanded flange. The proximodistal axis of pd III-1 is aligned with the mediodistally directed distal condyle on the metatarsal.

Pedal digit IV (Table 5): The proximal end of mt IV closely abuts mt III and the diaphysis abruptly expands both plantarly and laterally near the proximal end to form a triangular proximal flange (Figs 19–20, 23, 26A–D). A fossa formed on the proximal surface of the metatarsal~~,~~ is continuous with fossae on mt II–III, and accommodates the lateral distal tarsal. The sulcus on the lateral distal tarsal for the calcaneum continues onto the proximal surface of the metatarsal and, as a result, mt IV participates in articulation with the calcaneum. Viewed dorsally and plantarly, the lateral margin of the metatarsal is concave in the proximal half and the medial margin convex where it adjoins mt III (Fig. 26A–B). A shallow fossa on the medial surface of the diaphysis accommodates mt III (Fig. 26C). A narrow fossa on the plantar surface at the proximal end of the metatarsal (Figs 19, 26B) could either be a natural feature or the result of diagenetic distortion. In transverse section, the diaphysis of the metatarsal is triangular in the region ~~of the portion~~ that adjoins mt III and becomes dorsoplantarly compressed and ovoid towards its distal end. Viewed plantarly, the proximal plantomedial edge of the metatarsal abutting mt III extends distally as an obliquely oriented ridge to connect to the prominent plantolateral process on the distal condyle (Fig. 26B, D–F). The distal end of mt IV forms spheroidal condyle that in distal view has a slanted, parallelogram-shaped profile (Fig. 26F) resulting from the prominent mediodorsal and plantolateral processes. The flexor, extensor and adductor (medial) grooves are shallowly

developed, while the abductor (lateral) groove is strongly developed. The axial length of mt IV approximately equals that of mt II.

As preserved, the axis of pd IV-1 is angled medially inwards relative to the axis of the metatarsal (Fig. 23A–B). The lateral region of the cotyle is either broken and missing or undeveloped (Figs 26G–H, J). The plantar portion of the cotyle is split in the axial direction (Figs 19A, 23B), which could be pathological. Viewed dorsally and plantarly, pd IV-1 is strongly asymmetrical (Fig. 26G–H). The cotyle flares medially relative to the diaphysis, while the lateral margin is linear and forms a deep socket (Fig. 26J, L). The distal condyle is ginglymoid and deep collateral ligament fossae are developed (Fig. 26I–J). Only the proximal portion of pd IV-2 is preserved, the cotyle of which closely fits the distal condyle on pd IV-1 (Fig. 26G–K).

PLEASE INSERT FIGURE 26

Pedal digit V (Table 5): Mt V is dorsoplantarly compressed and sickle-shaped (Fig. 27). The proximal end is thickened and rounded forming a condyle that articulates with the plantolateral edge of the lateral distal tarsal (Figs 19–20B, 22I). The axial length of mt V is 29% that of mt III, which is comparable to *Anabisetia saldiviai* (MCF-PVPH-76, Coria & Calvo, 2002), *Dryosaurus altus* (YPM 1884), *Hypsilophodon foxii* and NMV P186047. No phalanges are present.

PLEASE INSERT FIGURE 27

PLEASE INSERT TABLE 5

Systematic criteria

Placement of *Diluvicursor pickeringi* in the Ornithischia is supported by the combination of a distally tapering mt IV, sub-triangular shape of mt IV in proximal view (synapomorphic for dinosaurs Novas, 1996), a low anterior ascending process on the astragalus and lack of fusion

between the astragalus and calcaneum (following Butler et al., 2011, Novas, 1989). A laterally extended and ventrally depressed lateral malleolus on the tibia of *Diluvicursor pickeringi* is shared with more derived ornithischians (Novas, 1989). A dorsoplantarly deep distal condyle on mt II is also shared with early, small-bodied neornithischians (e.g., *Agilisaurus louderbacki* (Peng, 1992), *Lesothosaurus diagnosticus* (Thulborn, 1972)) and ornithopods, thus differing from heterodontosaurids where the depth/width ratios of the condyle are opposite (Becerra et al., 2016). Among neornithischians, transverse compression of the diaphysis on mt II of *Diluvicursor pickeringi* most closely resembles those of *Anabisetia saldiviai*, Dryosauridae and *Gasparinisaura cincosaltensis*, supporting placement of *Diluvicursor pickeringi* in the Ornithopoda (see 'Detailed comparisons', below).

Detailed comparisons

Caudal vertebrae

Increased centrum length in *Diluvicursor pickeringi* on the vertebrae towards the middle of the tail is plesiomorphic for a small-bodied ornithischian (e.g., *Jeholosaurus shangyuanensis* (Han et al., 2012), *Valdosaurus canaliculatus* (Barrett, 2016)), *Agilisaurus louderbacki* (Peng, 1992) and *Heterodontosaurus tucki* (Santa Luca, 1980)). Posterior offset of the dorsoventrally narrowest point on the lateroventral fossa of the centrum (i.e., 'waist') on the posterior caudal vertebrae of *Diluvicursor pickeringi* may be present in *Dysalotosaurus lettowvorbecki* (Janensch, 1955, table 12.26). However, the small ventral concavity on the ventrolateral fossa of the centrum on the posterior caudal vertebrae of *Diluvicursor pickeringi* (Figs 15–17) is unusual, while noting this region is poorly described in many other taxa. The strongly developed haemal grooves on the middle caudal vertebrae of *Diluvicursor pickeringi* resemble the grooves in *Gasparinisaura cincosaltensis* and *Heterodontosaurus tucki*. However, among ornithischians, well-developed

grooves persisting onto the posterior-most caudal vertebrae in *Diluvicursor pickeringi* (e.g., Figs 12, 19) are unique. The triangular intervertebral processes developed on the posterior-most caudal vertebrae of *Diluvicursor pickeringi* (Fig. 17) are similarly unique.

The dorsoventral heights of the neural arches on the anterior-most caudal vertebrae of *Diluvicursor pickeringi* are lower than in all other ornithopods (Fig. 28). This morphology results from the combination of anteroposteriorly short spinal processes and their low inclination to ~30º from the dorsal plane (Fig. 9). The spinal processes on the anterior caudal vertebrae of *Anabisetia saldiviai* (PVPH-75 Cambiaso, 2007, fig. 105) (MCH pers. obs.), *Dryosaurus altus* (Galton, 1981), *Dysalotosaurus lettowvorbecki* (Janensch, 1955, pl. 13.5–6) and *Valdosaurus canaliculatus* (Barrett, 2016) are steeply reclined (30–45º), but ~~in these taxa,~~ differ from those in *Diluvicursor pickeringi* in being comparatively lengthy. In most other ornithopods, the spinal processes on the anterior caudal vertebrae are comparatively upright and lengthy (e.g., *Haya griva* (Makovicky et al., 2011), *Hypsilophodon foxii* (Galton, 1974), *Mantellisaurus atherfieldensis* (Norman, 1986), *Othnielosaurus consors* (Galton & Jensen, 1973), *Parksosaurus warreni* (Parks, 1926, fig. 3, plate 11) (MCH pers. obs.), *Thescelosaurus neglectus* (Gilmore, 1915) and *T*. sp. (Sternberg, 1940)). While the neural arches on the anterior caudal vertebrae of *Diluvicursor pickeringi* are low, the caudal ribs are transversely broad. At Ca 3, the transverse width across the caudal ribs (distance ‘d’ in Fig. 9B) is 87% of total vertebral height (i.e., distance ‘c’; Fig. 9A). In comparison, the broadest transverse width across the caudal ribs at Ca 4 in *Hypsilophodon foxii* (~~MN~~NHUK R196, using Galton, 1974, figs 28, 29) is 55% of total vertebral height at that position.

PLEASE INSERT FIGURE 28

The steeply reclined spinal processes and dorsoventrally low neural arches on the anterior caudal vertebrae of *Diluvicursor pickeringi* are features that continue onto the middle caudals. At the anterior-most middle caudal position (i.e., Ca 14), the length centrum is 51% that of total dorsoventral vertebral height (see Fig. 29A). The dorsoventrally low proportions on the middle caudal vertebrae of *Diluvicursor pickeringi* more closely resemble those of NMV P185992/NMV P185993, *Gasparinisaura cincosaltensis* and *Valdosaurus canaliculatus* (Fig. 29B–D) than *Hypsilophodon foxii*, *Haya griva* and *Thescelosaurus* sp., where, relative to centrum length, the spinal and haemal processes are comparatively lengthy (Fig. 29E–G).

The dorsally low position of the prezygapophyses on the neural arches of the anterior-most caudal vertebrae in *Diluvicursor pickeringi* (i.e., up to Ca 5) is unusual. Typically in other ornithischians, the prezygapophyses on the anterior-most are dorsally elevated relative to the neural canal and anterodorsally projecting (e.g., *Heterodontosaurus tucki* (Santa Luca, 1980, fig. 7), *Hypsilophodon foxii* (Galton, 1974, figs 28, 30), *Lesothosaurus diagnosticus* (=Stormbergia dangershoeki, Butler, 2005, fig. 9A), *Thescelosaurus neglectus* (Gilmore, 1915, fig. 6)). The tuberous process developed dorsally on the sprl posterior to the prezygapophysis on the anterior-most caudal vertebrae of *Diluvicursor pickeringi*, is also unusual for a dinosaur, as is the position of the tprl between the paired tuberous processes on the sprl, dorsal to the level of the prezygapophyses (Figs 9–10).

A prominent, tab-like prsl on the anterior caudal vertebrae of *Diluvicursor pickeringi* (Figs 9–10) resembles the prsl on the anterior caudal vertebrae of *Camptosaurus dispar* (Gilmore, 1909, fig. 18), *Eousdryosaurus nanohallucis* (following Escaso et al., 2014), *Haya griva* (Makovicky et al., 2011, fig. 3), *Thescelosaurus neglectus* (Gilmore, 1915, fig. 6) and *Ouranosaurus nigeriensis* (Taquet, 1976). A prominent prsl on the caudal vertebrae of

theropods, such as the abelisaurid *Majungasaurus crenatissimus* (O'Connor, 2007), suggests this feature is also plesiomorphic in dinosaurs, although variably expressed among taxa.

The horizontally oriented caudal ribs in *Diluvicursor pickeringi* (Figs 9–10) resemble those of *Haya griva* (Makovicky et al., 2011) and *Hypsilophodon foxii* (Galton, 1974, figs 28, 29) and differ from the posterodorsally directed ribs in *Anabisetia saldiviai* (Cambiaso, 2007, p. 226) (MCH pers. obs.) and the dryosaurids, *Dryosaurus altus* (Galton, 1981), *Dysalotosaurus lettowvorbecki* (Janensch, 1955, pl. 13.4-11) and *Valdosaurus canaliculatus* (Barrett, 2016).

The hatchet to disc-shaped haemal processes on the middle caudal vertebrae of *Diluvicursor pickeringi* resemble those of NMV P185992/NMV P185993 and *Valdosaurus canaliculatus* (see also Barrett, 2016) (Fig. 29A–B, C). However, the distal ends of the haemal processes on the middle caudal vertebrae in NMV P185992/NMV P185993, differ from those of *Diluvicursor pickeringi* (Fig. 29A–B) in being posteriorly expanded and thus, more asymmetrical. Similarly to NMV P185992/NMV P185993 and differing from *Diluvicursor pickeringi*, the mid-caudal haemal processes of NMV P186047 are asymmetrically expanded (Fig. 29H). However, the processes in NMV P186047 differ from those of NMV P185992/NMV P185993 in being more posteriorly elongate and boot-shaped (Fig. 29B, H). The haemal processes on the middle caudal vertebrae of *Gasparinisaura cincosaltensis* (Coria et al., 2013), *Macrogryphosaurus gondwanicus* (Coria & Calvo, 2002) and *Parksosaurus warren* (Parks, 1926) (MCH pers. obs.) differ from those of *Diluvicursor pickeringi*, NMV P185992/NMV P185993 and NMV P186047, in being more greatly dorsoventrally expanded at their distal ends and thus, plate-like. It is of note that the mid-caudal haemal processes of *Gasparinisaura cincosaltensis* (Fig. 29C) and *Macrogryphosaurus gondwanicus* further differ from those of *Parksosaurus warren* in being asymmetrically expanded and in this aspect closer to NMV P185992/NMV P185993 and NMV

P186047. On the posterior caudal vertebrae of *Diluvicursor pickeringi*, the haemal processes are asymmetrically expanded and boot-shaped (Fig. 16C) and resemble those on the posterior caudal vertebrae of NMV P185992/NMV P185993 and *Camptosaurus dispar* ('C. browni' Gilmore, 1909, fig. 19). In this aspect, these boot-shaped haemal processes also resemble those on the middle caudal vertebrae of NMV P186047 (Fig. 29H).

The longitudinal protuberances developed on the spinal processes of the anterior caudal vertebrae in *Diluvicursor pickeringi* (Figs 9–10) could be the fused remnants of ossified tendons. However, apart from these protuberances, ossified tendons are lacking in the tail of *Diluvicursor pickeringi*, as in *Haya griva* (Makovicky et al., 2011), *Jeholosaurus shangyuanensis* (Han et al., 2012) and NMV P185992/NMV P185993 (Herne, 2009).

PLEASE INSERT FIGURES 29

Caudal vertebral number

The total number of caudal vertebrae in *Diluvicursor pickeringi* is unknown. However, utilising information from more complete small-bodied ornithopods (e.g., Galton, 1974, Han et al., 2012, Makovicky et al., 2011), the potential number of vertebrae can be estimated. The lengthy, spine-like haemal processes on the anterior-most vertebrae of the *Diluvicursor pickeringi* holotype (the positions designated Ca 1–4; Fig. 9) support the location of these vertebrae close to the anterior-most end of the tail. Elongate, spine-like haemal processes are typical on the anterior caudal vertebrae in ornithopods. The anteroposterior length of the first preserved centrum on the *Diluvicursor pickeringi* holotype, at the position designated Ca 3, is short relative to the anterior caudal vertebrae posteriorly to that position and the caudal ribs are transversely broader than the ribs posteriorly to Ca 3 (Fig. 9; Table 2). Similar vertebral features are apparent at Ca 3–4 in

Hypsilophodon foxii (following Galton, 1974), suggesting that the position designated Ca 3 in *Diluvicursor pickeringi* is close to correct. It is reasonable to suggest that up to four caudal vertebrae could have been present on the *Diluvicursor pickeringi* holotype anterior to that designated Ca 1. The axial lengths of the caudal centra markedly decrease between the positions designated Ca 34 and Ca 38. The anteroposterior length of Ca 38 is 66% that of Ca 34 (Table 2), suggesting Ca 38 is close to the terminal end of the tail. Although we cannot be certain, it seems unlikely that in life, any more than ten vertebrae would have been present posterior to Ca 38 in the *Diluvicursor pickeringi* holotype. The number of caudal vertebrae in *Diluvicursor pickeringi* was likely close to 50, as in *Hypsilophodon foxii*, *Thescelosaurus neglectus* and *Valdosaurus canaliculatus* (Barrett, 2016, Galton, 1974, Gilmore, 1915).

Crus

Broad transverse expansion of the distal tibia in *Diluvicursor pickeringi* (Figs 21A–B, 30A) is symplesiomorphic for a neornithischian (e.g., *Agilisaurus louderbacki* (Peng, 1992), *Lesothosaurus diagnosticus* (Thulborn, 1972) and ornithopods (e.g., Galton, 1974, Galton, 1981, Han et al., 2012)) and notably lacking in the heterodontosaurid *Heterodontosaurus tucki* (Galton, 2014, Sereno, 2012, fig. 70). Differing from *Diluvicursor pickeringi*, the distal ends on both the left and right tibiae of NMV P186047 are weakly expanded (Fig. 30C) and in this context, comparable to *Heterodontosaurus tucki*. Shallow posterior expression of the medial malleolar ridge on the tibia of *Diluvicursor pickeringi* (Fig. 21E) is unusual, with the ridge typically more pronounced in other ornithopods (e.g., *Dysalotosaurus lettowvorbecki* (Janensch, 1955, pl. 14.5b), *Jeholosaurus* shangyuanensis (Han et al., 2012) and *Mantellisaurus atherfieldensis* (Norman, 1986)).

PLEASE INSERT FIGURE 30

Proximal tarsus

The proportions of the astragalus in *Diluvicursor pickeringi* (i.e., proximodistal height at the middle of the anterior ascending process versus transverse width; see Fig. S5; Table S3) resemble those of small-bodied ornithopods such as *Hypsilophodon foxii* and *Dryosaurus altus*. The astragali in these ornithopods are proportionately taller than in large-bodied taxa, such as *Mantellisaurus atherfieldensis* (Norman, 1986) and *Muttaburrasaurus langdoni* (QM F6140). However, astragalar height is quite variable among smaller ornithopod taxa. For example, similarly to large-bodied taxa, astragalar height is low in *Parksosaurus warreni* (Fig. S5; Table S3).

The transversely broad, proximally obtuse, centrally positioned anterior ascending process on the astragalus of *Diluvicursor pickeringi* (Fig. 22A), resembles the processes in *Gasparinisaura cincosaltensis* (Salgado, Coria & Heredia, 1997, fig. 4.12), *Dysalotosaurus lettowvorbecki* (Janensch, 1955, pl. 14.5a), *Talenkauen santacrucensis* (Cambiaso, 2007, fig. 36A) and possibly *Notohypsilophodon comodorensis* (Ibiricu et al., 2014, fig. 9G) and *Valdosaurus canaliculatus* (Barrett et al., 2011b, fig. 8E). The shape of the process is similar in *Anabisetia saldiviai*, *Dryosaurus altus* and *Muttaburrasaurus langdoni* (Fig. S6). However, in these taxa, the process differs from that of *Diluvicursor pickeringi* by having a well-developed fossa that borders the lateral margin of the process (Fig. S6). The lateral margin on the process of *Diluvicursor pickeringi* only forms a weak fossa (Fig. 22A). The anterior ascending process on the right astragalus of NMV P186047 (Fig. 30C) differs from that of *Diluvicursor pickeringi* in being hook-shaped, as in *Drinker nisti* (Bakker et al., 1990, fig. 13) and *Orodromeus makelai* (see Scheetz, 1999). The process in *Jeholosaurus shangyuanensis* (Han et al., 2012) differs from

that of *Diluvicursor pickeringi* in being transversely narrow and tab-shaped and the process in *Hypsilophodon foxii* differs by forming a sharp cusp on the dorsal margin (following Galton, 1974). Unlike *Diluvicursor pickeringi*, the anterior ascending processes on the astragali of *Iguanodon bernissartensis* (Norman, 1980, fig. 69a) and the rhabdodontids, *Zalmoxes robustus* and *Z. shqiperorum* (Weishampel et al., 2003) are medially offset.

The thin rounded posterior margin on the astragalus of *Diluvicursor pickeringi*, attributable to the shallowly developed medial malleolar ridge (Figs 21F, 22C–D), contrasts with other ornithopods where the posterior margin is typically more protrusive (e.g., *Anabisetia saldiviai*, *Dryosaurus altus* (Galton, 1981, fig. 18f), *Dysalotosaurus lettowvorbecki* (Janensch, 1955, table 14: figs 5a, b), *Hypsilophodon foxii* (Hulke, 1882, pl. 80, figs 5, 7), *Muttaburrasaurus langdoni* (Bartholomai & Molnar, 1981, fig. 10) and *Tenontosaurus tilletti* (Forster, 1990)).

Distal tarsus

The presence of two distal tarsals in *Diluvicursor pickeringi* is typical for an ornithopod, although differing from *Jeholosaurus shangyuanensis* and *Orodromeus makelai* that possess three distal tarsals (Han et al., 2012). The thin, plate-like, approximately quadrangular-shaped medial distal tarsal of *Diluvicursor pickeringi*, closely resembles that of NMV P186047, including the presence of a central, dorsoplantarly oriented groove on the proximal surface that extends between sulci on the dorsal and plantar margins (Fig. 30). In contrast, the medial distal tarsals of other ornithopods (e.g., *Hypsilophodon foxii* (Galton, 1974, fig. 57) and *Jeholosaurus shangyuanensis* (Han et al., 2012)) are comparatively blocky. The medial distal tarsals of *Anabisetia saldiviai* and *Gasparinisaura cincosaltensis* (Cambiaso, 2007, figs 75, 119, Salgado, Coria & Heredia, 1997, fig. 5) differ from that of *Diluvicursor pickeringi* in being thicker and

sub-circular in shape. The lateral distal tarsal of *Diluvicursor pickeringi* differs from those of all other ornithopods in being embayed dorsally by a fossa for the calcaneum (Fig. 22E–H). The lateral distal tarsals of *Anabisetia saldiviai* (MCF-PVPH-75), *Gasparinisaura cincosaltensis* (Cambiaso, 2007, fig. 75, Salgado, Coria & Heredia, 1997, fig. 5), *Hypsilophodon foxii* (Galton, 1974, fig. 57) and *Jeholosaurus shangyuanensis* (Han et al., 2012, fig. 12) also differ from that of *Diluvicursor pickeringi* in having a reniform shape. The concave medial edges on the lateral distal tarsals of the former taxa, closely articulate with concave lateral margins on their medial distal tarsals. In *Diluvicursor pickeringi* and possibly NMV P186047 the adjoining margin between the distal tarsals is linear (Fig 30).

Pes

The compact, elongate, cylindrically shaped metatarsus in *Diluvicursor pickeringi*, where the pes retains five metatarsals and phalanges on pedal digits I–IV, is plesiomorphic for an ornithopod (e.g., Becerra et al., 2016). Among ornithopods, a finely proportioned pedal hallux, where the distal condyle on mt I is located plantar to mt II, is most closely shared between *Diluvicursor pickeringi*, *Anabisetia saldiviai* (MCF-PVPH-75; Fig S6F), NMV P18599/NMV P186047 and NMV P186047 (Figs 19–20, 31, S6D–F, S7; Table S4). Among these taxa, the hallux of *Anabisetia saldiviai* is most reduced (Figs S6D–F, S7; Table S4). Similar features of the hallux in the early ornithischian *Lesothosaurus diagnosticus* (Thulborn, 1972), suggests this condition may be plesiomorphic for ornithopods. However, the halluces of the early ornithischians *Agilisaurus louderbacki* (Peng, 1992) and *Heterodontosaurus tucki* (Santa Luca, 1980, fig. 20) are comparatively robust (Fig. S7; Table S4) and the distal condyles on mt I in these taxa are located medially to mt II, indicating that the plesiomorphic condition of the hallux in ornithischians is presently not understood. Similarly to *Agilisaurus louderbacki* and

Heterodontosaurus tucki and differing from *Diluvicursor pickeringi*, the halluces of ornithopods such as *Changchunsaurus parvus* (Butler et al., 2011, figs 7–8), *Hypsilophodon foxii* (Galton, 1974, figs 57–58), *Jeholosaurus shangyuanensis* (Han et al., 2012, table A5), *Thescelosaurus assiniboiensis* (Brown, Boyd & Russell, 2011, fig. 22) and *Parksosaurus warreni* (Parks, 1926, figs 15–16, table pp. 39–41) are comparatively robust (Fig. S7; Table S4) and in these taxa, with the possible exception of *Jeholosaurus shangyuanensis*, the distal condyle on mt I is located medially to mt II.

The T-shaped distal condyle on mt I of *Diluvicursor pickeringi*, where the head of the 'T' faces medially, closely resembles those of NMV P185992/NMV P185993 and NMV P186047 (Fig. 31A, B)..An isolated fragment of mt I from the left pes of *Anabisetia saldiviai* (MCF-PVPH-74) glued onto the medial groove at the proximal end of mt II (following Cambiaso, 2007, p. 253, fig. 120), is provisionally considered as the distal condyle, rather than the proximal head of the metatarsal (see Fig S6D–E), and resembles the T-shaped distal condyle on mt I of *Diluvicursor pickeringi* (Figs 24, S6F). The distal condyles of mt I in *Changchunsaurus parvus* (Butler et al., 2011), *Hypsilophodon foxii* (following Galton, 1974, fig. 57J), *Othnielosaurus consors* (ROM 46240) and *Parksosaurus warreni* (ROM 804) are sub-triangular in distal view, and thus, lack the T-shaped distal profile evident in *Diluvicursor pickeringi*. Furthermore, the surface for the extensor tendon (*M. extensor hallicus longus*; e.g., White et al., 2016) on the distal condyle of mt I in taxa such as *Changchunsaurus parvus* (Butler et al., 2011) and *Parksosaurus warreni* (ROM 804), is dorsomedially oriented. This orientation differs from the likely location of this tendon in *Diluvicursor pickeringi*, NMV P185992/NMV P185993, NMV P186047 and provisionally *Anabisetia saldiviai*, within a dorsolaterally oriented extensor groove (Figs 31A–B, S6E–F).

The proximodistal axis of the phalanges on the right pedal hallux of the *Diluvicursor pickeringi* holotype is preserved orthogonal to the long axis of the metatarsal (Fig. 19). However, preservation of mt I and pd I-1 in correct alignment on the right pes of NMV P185992/NMV P185993 (Fig. 31B) reveals the misalignment of these bones in the *Diluvicursor pickeringi* holotype (see restoration, Fig 31A), as well as on the left pes of NMV P186047 (Fig. 31C). The asymmetrical shape of pd I-1 in *Diluvicursor pickeringi* and its dorsoplantar compression, are a combination of features uniquely shared with NMV P185992/NMV P185993 (Figs 24, 31A–B). The asymmetrical form of pd I-1 likely allowed the ungual (pd I-1) to clear the medial edge of mt II. Lateral flaring of the cotyle is lacking on pd I-1 of NMV P186047.

PLEASE INSERT FIGURE 31

Transverse compression of mt II in *Diluvicursor pickeringi* resembles the condition in *Anabisetia saldiviai* (MCF-PVPH-74, Cambiaso, 2007, fig. 120B) (Fig. S6D), *Gasparinisaura cincosaltensis* (MUCPv-214, Salgado, Coria & Heredia, 1997, fig 5.6) (MCS-3), *Morrosaurus antarcticus* (Cambiaso, 2007, Novas, 2009, p. 352, Rozadilla et al., 2016, fig. 5A), NMV P186047 and the dryosaurids, *Dryosaurus altus* (YPM 1884), *Dysalotosaurus lettowvorbecki* (MB.R. 1398) and possibly *Valdosaurus canaliculatus* (following Barrett, 2016, fig. 9D, E) (Fig. 32). In these taxa, the transverse width of the diaphysis in the plantar portion of mt II is <50% that of the equivalent region on mt III. In *Diluvicursor pickeringi* the width of the diaphysis is ~33% (Fig. 25). In proximal view, the profile of mt II in *Diluvicursor pickeringi* (Figs 23, 32) is keyhole-shaped and lunate. This shape proximally on mt II more closely resembles the shape in *Anabisetia saldiviai* and *Gasparinisaura cincosaltensis*, *Morrosaurus antarcticus* and the dryosaurids, *Dryosaurus altus* and *Dysalotosaurus lettowvorbecki* and possibly *Kangnasaurus*

coerzeei than other ornithopods where the profile is typically more uniform or blocky (see Fig. 32).

PLEASE INSERT FIGURE 32

Pedal pathologies

Features on the right pes suggest the holotype endured antemortem injury to the second and fourth digits (Fig. 33). Subluxation, the angulation or partial dislocation of two articulating bones at their joint resulting from trauma or disease (following Burgener, Kormano & Tomi, 2006), is suggested at the metatarsophalangeal ~~(mpt)~~ joint of pedal digit II. The proximodistal axis of the first phalanx is deflected medially relative to the proximodistal axis of mt II. Anti-mortem angulation of this joint, rather than postmortem preservation is further supported by the identification of bone overgrowth, osteophytosis (e.g., Burgener, Kormano & Tomi, 2006 p.166, Resnick, 1983), proximally on pd II-1. Osteophytosis at the ~~mpt~~ joint of pedal digit II is evident as rugosely textured bone overgrowth on the proximal margin of pd II-1 (Figs 21A, 33). Bone overgrowth on the cotyle of pd II-1 conforms to the shape of the distal condyle on mt II (Figs 21A, 33), suggesting osteophytosis in the form of intramembranous ossification at the joint (following Resnick, 1983). Pd II-1 was likely to have had limited mobility or immobile. Osteophytosis may have helped to stabilize the ~~mpt~~ joint of pedal digit II following trauma (e.g., Lieben, 2016). Bone of similar appearance to that proximally on pd II-1 is also apparent on pd III-1 (Figs 21A, 33), also suggesting osteophytosis at the joint. However, unlike pedal digit II, subluxation of the mpt joint on pedal digit III is not evident. Subluxation is apparent at the ~~mpt~~ joint of pedal digit IV (Figs 26, 33). However, osteophytosis is not evident (Figs 21A, 33). Bone on the proximal margin of the cotyle on pd IV-1 is unevenly developed (Figs 21A, 26, 33), which may also have resulted from subluxation.

PLEASE INSERT FIGURE 33

Ornithischia indet.

Figures S3, 34

Distribution: Early Cretaceous Australia.

Material: MV P228342: almost complete isolated caudal vertebra lacking caudal ribs.

Locality: ETRW Sandstone, Eric the Red West, Eumeralla Formation (lower Albian), Otway Group, southern Victoria.

PLEASE INSERT FIGURE 34

Description

Preservation: NMV P228342 is prepared out and missing the distal-most tip of the spinal process and the caudal ribs (Fig. S3). The spinal process is bent to the left towards the distal end, the distal ends of the transverse processes are eroded or broken and the anterior and posterior margins of the centrum are only slightly eroded (Fig. S3).

Morphology: The centrum is amphiplatyan, the anterior and posterior faces round in profile and the laterocentral fossa is shallow. The centrum lacks anterior and posterior haemal facets and a haemal groove is undeveloped. The neurocentral suture is fused and the transverse processes located on the neural arch. The prezygapophyses are anterodorsally oriented and project only a short distance anteriorly beyond the centrum. The spinal process is shallowly inclined at 32º from the dorsal plane. The process expands towards its distal end and has a proximodistal length approximately equaling centrum length. The dorsoventral height of the neural arch is 50% of total vertebral height (‘a/b’; see Figs 28, 34). Elliptically shaped postzygapophyses protrude

posteriorly from the base of the spinal process. A thin and tab-like prespinal lamina (prsl) is developed anteriorly at the base of spinal process. On the right side, the spinoprezygapophyseal lamina (sprl) connects the prezygapophysis and the base of the spinal process. However, on the left side, the sprl merges with the postzygodiapophyseal lamina (podl) to form a prezgopostzygapophyseal lamina (pprl), which fails to contact to the spinal process. The podl/pprl forms a thin crista that connects the dorsal margin of the postzygapophysis and the anterior margin of the transverse process and constitutes the lateral margin of the spinodiapophyseal fossa (sdf) (Fig. 34A, C–D). A small dorsally oriented protuberance is developed on the podl/pprl, lateral to the sdf. The transprezygapophyseal lamina (tprl) extends between the left and right sprl and its anterior edge coincides with the posterior margin of the prezygapophyses (Fig. 34D–E). The medial-spinopostzygapophyseal lamina (m-spol) connects the postzygapophysis to the posterior margin of the spinal process (Fig. 34B, C'–D'). The paired m-spol remain separated by a groove-like postspinal fossa (psf). The prezygodiapophyseal lamina (prdl) connects the prezygapophysis and the dorsal surface of the transverse process (Fig. 34C'–D'), and the centroprezygapophyseal lamina (cprl) extends as a bony sheet from the prdl to the centrum. As a result, the centroprezygapophyseal fossa (cprf) is undeveloped.

Vertebral position

Typically in ornithischians, the spinal processes on the thoracic vertebrae are vertically oriented, anteroposteriorly broad and roughly rectangular in profile (e.g., *Heterodontosaurus tucki* and *Hypsilophodon foxii* (Galton, 1974, fig. 22B, Santa Luca, 1980, fig. 5B)). On the thoracic vertebrae of ornithopods, a broadly striated margin developed at both the anterior and posterior ends of the centrum, border the centrolateral fossa (e.g., *Dryosaurus altus* (Galton, 1981), *Jeholosaurus shangyuanensis* (Han et al., 2012) and *Thescelosaurus neglectus* (Gilmore, 1915,

fig. 4)). This margin is not typically developed on the caudal vertebrae. The highly reclined spinal process and the lack of striated anterior and posterior margins on the centrum identify NMV P228342 as a caudal vertebra. The lack of facets for haemal processes suggests a caudal position of Ca 1. However, a position of Ca 2 is possible (e.g., Han et al., 2012).

Comparisons

Steeply reclined spinal processes of short proximodistal length (approximately equaling centrum length) and a thin, tab-like prsl are features shared between NMV P228342 and the anterior-most preserved caudal vertebrae of *Diluvicursor pickeringi* (Figs 9–11, 34). The dorsoventral height of the neural arch in NMV P228342 is higher relative to centrum height than at the designated vertebral position Ca 3 on the *Diluvicursor pickeringi* holotype (i.e., distance 'a' relative to distance 'b'; Figs 9, 34). However, neural arch heights in NMV P228342 and at Ca 3 in *Diluvicursor pickeringi* are lower than other ornithopods (Fig. 28). The crista-like podl/pprl on NMV P228342 with its dorsally protrusive process (Fig. 34) may be unique for an ornithischian and possibly among dinosaurs. However, these features could be developed in *Diluvicursor pickeringi*, but are unclear from the CT ~~imigery~~ (Figs 9B–10A–B). Where a crista-like podl/pprl is developed in NMV P228342, a shallow ridge or bulge is formed in other ornithopods (e.g., *Hypsilophodon foxii* (Galton, 1974, Hulke, 1882), and *Ouranosaurus nigeriensis* (Taquet, 1976)), if formed at all.

The transversely round profile of the centrum in NMV P228342 (Fig. 34) contrasts with the transversely narrower, elliptical profile on the centrum of the anterior-most caudal vertebrae in *Diluvicursor pickeringi* (Figs 8–10). However, at the provisional position of Ca 1, the centrum of NMV P228342 is not directly comparable to the anterior-most centra preserved on the

Diluvicursor pickeringi holotype, from Ca 3. It is of note that the centra of the anterior caudal vertebrae in ornithopods progressively become transversely narrower posteriorly from Ca 1 and the transverse profile of the centrum changes from a fuller, cylindrical outline to elliptical (e.g., *Hypsilophodon foxii* (Galton, 1974, figs 29B, 31B) and *Jeholosaurus shangyuanensis* (Han et al., 2012, fig. 6A)). Therefore, the difference in centrum shape between NMV P228342 and the anterior-most vertebrae in the *Diluvicursor pickeringi* holotype could signify different positions in the vertebral series rather than taxonomic variation.

The neural arch on NMV P228342 differs from those on the anterior-most caudal vertebrae of *Diluvicursor pickeringi* in several aspects. Where the dorsal and ventral margins of the spinal processes on the anterior-most caudal vertebrae of *Diluvicursor pickeringi* are parallel, the margins on NMV P228342 expand distally. Unlike *Diluvicursor pickeringi*, where the prezygapophyses are horizontal and attach at the base of neural arch (Figs 9–10), the prezygapophyses on NMV P228342 are dorsally elevated and anterodorsally directed (Fig. 34). The tuberous process on the sprl of the anterior caudal vertebrae in *Diluvicursor pickeringi* is lacking in NMV P228342. Unlike *Diluvicursor pickeringi*, the tprl in NMV P228342 aligns with the ventral margin of the paired prezygapophyses, as opposed to the dorsal margin (Figs 9–10, 34). The differing morphology of the prezygapophyses and sprl between NMV P228342 and *Diluvicursor pickeringi* support their taxonomic separation. We cannot confidently assign NMV P228342 to Ornithopoda, but consider this assignment likely.

DISCUSSION

Diluvicursor pickeringi nov. gen. et sp., a new small-bodied ornithopod from the locality of Eric the Red West, near Cape Otway, in the lower Albian of the Eumeralla Formation, southeastern

Australia, provides new insight on the diversity of the small-bodied ornithischian dinosaurs from the Lower Cretaceous of the Australian-Antarctic rift system. The holotype (NMV P221080) consists of an almost complete tail, distal portion of the right crus, the complete right tarsus and partial right pes of a turkey-sized juvenile. These remains were buried in coarse sediments along with substantially sized tree debris that filled scours formed between sand dunes that were migrating downstream in a deep, broad, high-energy river. This deposit is called the 'ETRW Sandstone'. An isolated posterior caudal vertebra (NMV P229456) from the same deposit is referred to *Diluvicursor pickeringi* and pertains to a larger individual than the holotype. A further isolated caudal vertebra (NMV P228342) from the same deposit is identified as ~Ca 1 of an indeterminate ornithischian, but most likely an ornithopod closely related to *Diluvicursor pickeringi*.

Unusual characteristics of *Diluvicursor pickeringi*

Diluvicursor pickeringi is characterized by nine potential autapomorphies, among which, dorsoventrally low neural arches and transversely broad caudal ribs on the anterior caudal vertebrae are a visually defining combination of features. Typically in ornithischians and theropods, the prezygapophyses on the anterior caudal vertebrae are, to some extent, elevated dorsally on the neural arch and, thus, located above the level of the neurocentral suture and dorsal to the neural canal. However, on the anterior-most caudal vertebrae of the *Diluvicursor pickeringi* holotype (i.e., Ca 3–5), the prezygapophyses attach at the base of the neural arches, laterally to the neural canal (Figs 9–10). This morphology appears integral to the dorsoventrally low character of the neural arches. Unusually on these vertebrae of *Diluvicursor pickeringi*, a protuberance is also developed on each of the paired spinoprezygapophyseal lamina (sprl), between which, the transprezygapophyseal lamina (tprl) extends dorsally to both the neural canal

and the prezygapophyses (Figs 9–10). The protuberance on the sprl of the anterior caudal vertebrae of *Diluvicursor pickeringi* and the location of the tprl, dorsally to the level of the prezygapophyses, superficially resemble zygosphene-zygantrum morphology in lepidosauromorhans (e.g., Benton, 2005, p. 150, Rieppel & Hagdorn, 1997, p. 125, Romer, 1956, p. 256, Tschopp, 2016). We postulate this morphology may have provided strengthened surfaces for the attachment of musculature and ligaments between the neural arches of the adjoining vertebrae (Fig. 9).

In *Diluvicursor pickeringi*, triangular intervertebral processes developed on the anterior articular faces of the posterior-most caudal centra incise V-shaped notches on the posterior faces of the adjoining centra (Fig. 17). These features have not been previously reported in an ornithopod, and whether or not they are surficial on the centra or developed more deeply on the articular surfaces, is presently unknown. Similarly to the function of ossified caudal tendons in ornithischians, such as *Hypsilophodon foxii* (Galton, 1974) and the hyper-extended prezygapophyses and haemal processes in the maniraptoran *Deinonychus antirrhopus* (Ostrom, 1969), the intervertebral processes on the posterior caudal vertebrae of *Diluvicursor pickeringi* potentially stiffened the posterior end of the tail. The herringbone form of the interlocking centra and the prezygapophyses on the posterior-most caudal vertebrae of *Diluvicursor pickeringi* (Fig. 17) resembles the structure in the ankylosaur *Euoplocephalus tutus* (Coombs, 1978a, fig. 7).

The lateral distal tarsal of *Diluvicursor pickeringi* is embayed by a sulcus that allowed partial direct articulation between the calcaneum and mt IV (Fig. 22). With the exception of stegosaurs (Galton & Upchurch, 2004), direct articulation between the calcaneum and mt IV is unusual for an ornithischian and unknown in other ornithopods. The asymmetrical form of pd

IV-1 in *Diluvicursor pickeringi*, where the proximal cotyle is strongly flared medially (Fig. 26G–H), is also unusual in an ornithopod, and possibly for a dinosaur (e.g., Coombs, 1978b, fig. 12).

Differentiation of *Diluvicursor pickeringi* among Victorian ornithopods

The three previously named ornithopods from Victoria, *Atlascopcosaurus loadsi*, *Leaellynasaura amicagraphica* and *Qantassaurus intrepidus* are known only from cranial remains (Herne, Tait & Salisbury, 2016, Rich & Vickers-Rich, 1999) and whether or not *Diluvicursor pickeringi* is synonymous with any of these taxa can only be determined from future discoveries of associated skeletal remains. The only Victorian associated ornithopod fossils that can be readily compared with *Diluvicursor pickeringi* are those of the two indeterminate partial postcranial skeletons NMV P185992/NMV P185993 and NMV P186047 from Dinosaur Cove.

The similarities between the partial postcrania from Dinosaur Cove (NMV P185992/NMV P185993 and NMV P186047) and *Diluvicursor pickeringi* will be discussed in 'phylogenetic affinities of *Diluvicursor pickeringi*' (below). However, *Diluvicursor pickeringi* clearly differs from NMV P185992/NMV P185993 by having a far shorter tail. Where NMV P185992/NMV P185993 has >71 caudal vertebrae (Herne, 2009), *Diluvicursor pickeringi* has ~50. The metatarsus of *Diluvicursor pickeringi* differs from that of NMV P186047 in being relatively shorter and transversely broader, indicating that the pes of *Diluvicursor pickeringi* was more robust. The spinal processes on the middle caudal vertebrae of *Diluvicursor pickeringi* differ from those of NMV P185992/NMV P185993 in being linear along their length, whereas those of the latter recurve dorsally towards their distal ends (Fig. 29A–B). Where the haemal processes on the middle caudal vertebrae of *Diluvicursor pickeringi* are symmetrically expanded, those of NMV P185992/NMV P185993 are posteriorly expanded (Fig. 29A–B). The haemal processes on

the middle caudal vertebrae of NMV P186047 further differ from those of both *Diluvicursor pickeringi* and NMV P185992/NMV P185993 in being more posteriorly extended and boot-shaped (Fig. 29H). Unfortunately, the neural arches anterior to Ca 13 on the caudal vertebrae of NMV P185992/NMV P185993 are not preserved and thus, cannot be compared with those of *Diluvicursor pickeringi*. Although more detailed body-form comparisons between the Eumeralla Formation ornithopods require more complete specimens, caudal and pedal morphologies presently suggest that the two Dinosaur Cove ornithopods NMV P185992/NMV P185993 and NMV P186047 were more gracile ornithopods than *Diluvicursor pickeringi*.

Stratigraphic associations of the Eumeralla Formation ornithopods

The holotype locality of *Atlascopcosaurus loadsi* near Point Lewis (Figs 1, 4), is stratigraphically older than the ETRW Sandstone hosting *Diluvicursor pickeringi*. These two horizons are separated by a true stratigraphic thickness of ~180 m (Figs 1, 4). Strata at Dinosaur Cove, which hosts the holotype of *Leaellynasaura amicagraphica*, NMV P185992/NMV P185993 and NMV P186047 (see Felton, 1997b, Herne, Tait & Salisbury, 2016), are stratigraphically younger than both the ETRW Sandstone and Point Lewis (Figs 1, 4). However, apart from palynological work that currently indicates that the Eumeralla Formation fossil vertebrate localities fall within ~3.5 Ma, from the beginning of the Albian (following Korasidis et al., 2016), more precise chronostratigraphic data for these localities has yet to be published.

Diluvicursor pickeringi and the Dinosaur Cove ornithopods *Leaellynasaura amicagraphica*, NMV P185992/NMV P185993 and NMV P186047 are not currently known to be coeval. However, the stratigraphically older taxon *Atlascopcosaurus loadsi* is also known from Dinosaur Cove (Rich & Rich, 1989), including from the Tunnel Sandstone assemblage (Herne, Tait &

Salisbury, 2016). Thus, as the stratigraphic range of *Atlascopcosaurus loadsi* extends through the ETRW Sandstone *A. loadsi* and *Diluvicursor pickeringi* are coeval. However, whether or not *Diluvicursor pickeringi* and *Atlascopcosaurus loadsi* are synonymous can only be determined from new fossil discoveries that can demonstrate anatomical congruence. Importantly, the presence of the isolated caudal vertebra NMV P228342 (Figs S3, 34) in the fossil assemblage of the ETRW Sandstone, identified as an indeterminate ornithischian and with morphology clearly differing from *Diluvicursor pickeringi*, also suggests the ETRW Sandstone hosts more small-bodied ornithischians than *Diluvicursor pickeringi*. NMV P228342 is potentially attributable to *Atlascopcosaurus loadsi* or another, presently unknown, taxon

Phylogenetic affinities of *Diluvicursor pickeringi*

The phylogenetic relationships of *Diluvicursor pickeringi* have yet to be analyzed within a cladistics analysis. However, several features from comparisons of *Diluvicursor pickeringi* are potentially phylogenetically informative. The dorsoventrally low height of the middle caudal vertebrae, in NMV P185992/NMV P185993, *Gasparinisaura cincosaltensis* and *Valdosaurus canaliculatus* and distally expanded, hatchet-shaped haemal processes in NMV P185992/NMV P185993 and *Valdosaurus canaliculatus* (see also Barrett, 2016) (Fig. 29), suggests a close relationship between these taxa and *Diluvicursor pickeringi*. However, no specific feature on the caudal vertebrae of *Diluvicursor pickeringi* is currently identified as strongly synapomorphic and among ornithopods, the shapes, sizes and angles of the vertebral processes presents a continuous range of variation.

The asymmetrical form of the first phalanx on the hallux (i.e., pd I-1) of *Diluvicursor pickeringi* is uniquely shared with the Dinosaur Cove ornithopod NMV P185992/NMV P185993

(Fig. 31), suggesting these two taxa share a close ~~ancestral~~ relationship. The morphology of the medial distal tarsal in *Diluvicursor pickeringi* closely resembles that of NMV P186047 (Fig. 30B, D). However, we cannot determine to what extent this morphology is shared with other taxa. A finely proportioned hallux, relative to the equivalent bones in pedal digit II, and consisting of two reduced phalanges and a T-shaped distal condyle on mt I, positioned plantar to mt II are a combination of features most closely shared between *Diluvicursor pickeringi*, NMV P185992/NMV P185993, NMV P186047 and Argentinean *Anabisetia saldiviai* (Figs 19–20, 24F, 31, S6G–S7; Table S4). However, the hallux in *Anabisetia saldiviai* is more reduced than those of the Eumeralla Formation ornithopods (Figs S6–S7; Table S4).

An mt I of reduced proportions is described in the dryosaurids *Dysalotosaurus lettowvorbecki* (HMN dy V Galton, 1981, figs 8V–Z, 19A–B, Janensch, 1955) and *Eousdryosaurus nanohallucis* (Escaso et al., 2014, figs 6, 7A) and unusually in the latter taxon, a small ungual is described as pd I-1. It is of note that the elements described as mt I in *Dysalotosaurus lettowvorbecki* and *Eousdryosaurus nanohallucis* more closely resemble the shape and proportions of pd I-1 in ornithopods such as *Diluvicursor pickeringi*, NMV P186047 and particularly *Anabisetia saldiviai* (Figs S6G; Fig S8; Table S4) (see also Cambiaso, 2007, fig. 121). We posit that the bones identified as mt I in the two aforementioned dryosaurids could be pd I-1 and if confirmed from future investigations, would indicate halluces most resembling *Anabisetia saldiviai* and to some extent, the Eumeralla Formation ornithopods.

Transverse compression of the diaphysis of mt II, where the proximal profile has a lunate keyhole shape (Figs 23C, 25B, F, 32) is shared between *Diluvicursor pickeringi*, NMV P186047, *Anabisetia saldiviai*, *Gasparinisaura cincosaltensis*, *Morrosaurus antarcticus* (Cambiaso, 2007, Rozadilla et al., 2016, Salgado, Coria & Heredia, 1997) (Figs 32, S6D), and the dryosaurids~~,~~

Dryosaurus altus, *Dysalotosaurus lettowvorbecki*, *Eousdryosaurus nanohallucis*, *Valdosaurus canaliculatus* (Barrett, 2016, Coria & Calvo, 2002, Escaso et al., 2014, Galton, 1981, Janensch, 1955) and possibly *Kangnasaurus coerzeei* (Fig. 32). Mt II in other ornithopods is relatively uniform, but may be transversely narrow and/or blocky (Fig. 32). The proximal end of mt II in NMV P185992/NMV P185993 is not preserved and cannot be compared.

A finely proportioned hallux and transversely compressed mt II provisionally suggest that the Eumeralla Formation ornithopods (*Diluvicursor pickeringi*, NMV P185992/NMV P185993, NMV P186047), Argentinean *Anabisetia saldiviai* and *Gasparinisaura cincosaltensis*, Antarctic *Morrosaurus antarcticus* and African to Laurasian dryosaurids share closer phylogenetic relationships than with Laurasian 'basal' ornithopods, such as *Hypsilophodon foxii*, *Jeholosaurus shangyuanensis* and *Thescelosaurus neglectus*.

Pathologies among ornithopods of the Eumeralla Formation

The *Diluvicursor pickeringi* holotype (NMV P221080) presents trauma to the right pes and is the second ornithopod individual from the Eumeralla Formation to present pathologies of the hind limb. The first occurrence of a pathological condition reported in any dinosaur from Australia was in the Dinosaur Cove ornithopod NMV P186047. This individual endured antemortem disease to the left hind limb, interpreted as a chronic osteomyelitis of the tibia caused by inflammatory infection (Gross, Rich & Vickers-Rich, 1993). According to Gross, Rich & Vickers-Rich (1993), NMV P186047 survived for several years before succumbing to disease. Pedal digits II and IV on the *Diluvicursor pickeringi* holotype appear to have endured medially directed subluxation (angulation) at the metatarsophalangeal (mpt) joint. Following subluxation, osteophytosis (bone overgrowth) on pd II-1 potentially acted in stabilizing the mpt joint (Fig.

33). Minor osteophytosis is also apparent at the mpt joint of pedal digit III. The pathologies on the pes of the *Diluvicursor pickeringi* holotype could have limited movement of the weight-bearing toes. Whether or not these pathologies contributed to the death of the *Diluvicursor pickeringi* holotype cannot be known. However, the condition endured likely resulted in less than normal functionality of the right pes.

Ontogeny and body-size of *Diluvicursor pickeringi*

Restoration of the *Diluvicursor pickeringi* holotype (Fig. 7) suggests that the total anteroposterior length of this individual was ~1.2 m. Unfused anterior caudal vertebrae on the *Diluvicursor pickeringi* holotype further suggest this individual was a juvenile (e.g., Hone, Farke & Wedel, 2016). However, antemortem osteophytosis on the right pes also suggests that the *Diluvicursor pickeringi* holotype was of sufficient age to have recovered from traumatic subluxation of the pedal digits. The size of the isolated posterior caudal vertebra, NMV P229456, referred to *Diluvicursor pickeringi* (Fig**.** 21) further suggests the taxon grew to at least 2.3 m in length. However, whether or not NMV P229456 pertains to an adult is unknown.

Anterior caudal myology of *Diluvicursor pickeringi*

In the anterior caudal region of non-avian dinosaurs, the epaxial and hypaxial musculature are located dorsally and ventrally to the caudal ribs, respectively (Fig. 35) (e.g., Mallison, Pittman & Schwarz, 2015). The epaxial musculature likely comprised the *musculus* (*M.*) *dorsalis caudae* (see Galton, 1974, Mallison, Pittman & Schwarz, 2015, Norman, 1986, in crocodilians, the *M. transversospinalis* and *M. longisimus caudalae/dorsi*, following Organ, 2003, Persons & Currie, 2014, see also Persons, Currie & Norell, 2014), while the hypaxial musculature likely comprised the *M. rectus abdominus, M. ilio-ischiocaudalis*, *M. transversus perinei* and *M. caudofemoralis*

longus; the latter integral to locomotion of the hind limb (Maidment & Barrett, 2011, Maidment et al., 2014, Mallison, Pittman & Schwarz, 2015, Persons & Currie, 2014, Persons, Currie & Norell, 2014). Relative to the neural arches, the caudal ribs on the anterior-most caudal vertebrae in *Diluvicursor pickeringi* are transversely broad (e.g., Ca 3; Fig. 35), indicating that the musculature in this region was transversely broad. The dorsoventral proportions of the vertebrae in this region of the tail further indicate that the epaxial musculature was dorsoventrally shallow, while the hypaxial musculature was dorsoventrally deep.

PLEASE INSERT FIGURE 35

In comparison to the proportionately deep hypaxial locomotory musculature in the tail of *Diluvicursor pickeringi*, the epaxial and hypaxial musculature in the tail in *Hypsilophodon foxii* would have been roughly equal in dorsoventral depth (e.g., Ca 4, based on Galton (Galton, 1974); Fig. 35). Furthermore the width across the caudal ribs in this region of *Hypsilophodon foxii*, suggests that the musculature was transversely narrower than in *Diluvicursor pickeringi* (Fig. 35). The differences between the anterior caudal musculature of *Diluvicursor pickeringi* and *Hypsilophodon foxii* potentially signify differing locomotor abilities between these taxa and provide an area for future investigations on ornithopod locomotion

It is interesting to note that the proportions of the epaxial and hypaxial musculature in the anterior caudal region of *Diluvicursor pickeringi* resemble those in the oviraptorosaur *Ajancingenia yanshini*. In *Ajancingenia yanshini*, the neural arch is 22% of total vertebral height and the transverse width across the caudal ribs is 75% of total vertebral height (following Persons, Currie & Norell, 2014). These vertebral proportions in *Ajancingenia yanshini* have been considered unusual in a theropod (Persons, Currie & Norell, 2014). Calculation of relative

femoral adductor muscle mass (*M. caudofemoralis longus*) in *Ajancingenia yanshini*, against body weight, suggested to Persons, Currie & Norell (2014), a taxon with substantial running ability. Although we cannot estimate the body mass of the *Diluvicursor pickeringi* holotype (e.g., the femur, from which body-mass can be calculated (Anderson, Hall-Martin & Russell, 1985), is unknown), similarity in the proportions of the caudal hypaxial musculature between *Diluvicursor pickeringi* and *Ajancingenia yanshini* suggests *D. pickeringi* could have shared similarly strong locomotory abilities.

Palaeoecological context of *Diluvicursor pickeringi*

A rich assemblage of isolated vertebrate fossils has been reported from the locality of Eric the Red West, including fishes, chelonians, plesiosaurs, pterosaurs, small ornithischians, theropods and mammals (e.g., Rich, 2015). However, apart from the new ornithischians described in this present work, an indeterminate spinosaurid cervical vertebra (NMV P221081, Barrett et al., 2011a) (Fig. 5B) and a mandible fragment (NMV P228848) referred to the ausktribosphenid, cf. *Bishops whitmorei* (Rich et al., 2009b), much of the fossil material from this locality has yet to be published. The description of *Diluvicursor pickeringi* now adds to the growing body of information on the tetrapods from this site, and importantly also, interpretation of the ETRW Sandstone helps shed light on the palaeoecosystem ~~within~~ the rift graben, within which *Diluvicursor pickeringi* and the other biota coexisted.

Scours in the ETRW Sandstone filled with coarse bedload containing mudstone rip-up clasts, medium and coarse sand, quartzose gravel/grit and sizable woody plant debris, including transported logs and tree stumps (Figs 3, 5). Fossil plant material in the ETRW Sandstone suggests that the channel ~~in~~ which the deposit represents, incised a substantially forested

floodplain. Previous macrofloral and palynological investigations indicate that conifers, principally Araucariaceae (*Agathis* and *Araucaria*), Podocarpaceae and Cupressaceae, were the dominant forest tree types in the Eumeralla Formation during the late Aptian-early Albian (Dettmann, 1994, Dettmann et al., 1992, Douglas, 1969, Douglas & Williams, 1982, Korasidis et al., 2016, Wagstaff & McEwan Mason, 1989). Ginkgos, although present, were rare. The logs and tree stumps potentially pertain to these tree types. The sizes of some of the logs in the deposit at Eric the Red West further suggest old-growth forests had been established, with trees that were potentially several hundreds of years in age (see also Seegets-Villiers, 2012).

Lower story plants (understory, groundcover and shallow aquatic plants) in the region of Eric the Red West~~,~~ potentially included terrestrial and aquatic pteridophytes (ferns), hepatics, lycopods, cycadophytes, bennettitaleans, seed-bearing fern- or cycad-like taeniopterids and non-magnoliid dicotyledonous angiosperms, as data for other Eumeralla Formation localities have indicated (Dettmann, 1994, Dettmann et al., 1992, Douglas, 1969, Douglas, 1973, Douglas & Williams, 1982). Recent investigations by Korasidis et al. (2016) further indicate that in the Eumeralla Formation during the later Early Cretaceous, early Australian angiosperms also become established.

The Lower Cretaceous floodplain forests within the rift graben would have been interspersed by large, deep rivers with broad inner banks and shallow floodplain lakes. These hydrological features, evident from the ETRW and Anchor sandstones, would have supported varied vegetation zones and complex faunal habitat opportunities. The migrating banks of the meandering rivers would have provided ideal conditions for vegetation successions, as in modern systems (Hickin, 1974) and periodic disturbance of the forests by overbank flooding would have created local physiographic differences. Similarly to present-day floodplain ecosystems (e.g.,

Baker & Barnes, 1998, Junk, Bayley & Sparks, 1989, Tockner et al., 2008), a mosaic of vegetation zones likely characterised the Lower Cretaceous floodplain in the region of Eric the Red West. We speculate that periodic disturbance of older forests through flooding and the migration of high-energy river channels, such as that represented by the ETRW Sandstone, potentially favoured opportunistic pteridophytes, cycadophytes and angiosperms. The dynamics of change in physiography and vegetation on the rift floodplain would have provided varied niche opportunities for dinosaurian herbivores, such as *Diluvicursor pickeringi*, and predators alike.

Investigations on disparity in dental and cranial features between both co-occurring dinosaurian and ancient mammalian herbivores have addressed questions of habitat preferences within these groups (Barrett & Rayfield, 2006, Barrett & Willis, 2001, Feranec & MacFadden, 2006, Fricke & Pearson, 2008, Henderson, 2010, MacFadden & Shockey, 1997, MacLaren et al., 2017, Mallon & Anderson, 2013). However, the palaeoecological implications of cranial, dental and postcranial disparity between small-bodied ornithopods have yet to be investigated. Morphological disparity between the associated postcranial skeletons of *Diluvicursor pickeringi* and the ornithopods from Dinosaur Cove (NMV P185992/NMV P185993 and NMV P186047) provisionally signify differing niche selection preferences between ornithopod taxa. These Victorian ornithopods provide significant materials for future research on the palaeoecology of dinosaurs in Gondwana.

CONCLUSIONS

Diluvicursor pickeringi nov. gen. et sp. is a new small-bodied ornithopod from the lower Albian of the Eumeralla Formation in the Otway Basin, rocks of which crop out along the coast of

Victoria, southeastern Australia. The taxon is known from an almost complete tail and lower partial right limb of the holotype (NMV P221080) and an isolated posterior caudal vertebra (NMV P229456), all of which were discovered at the fossil locality of Eric the Red West. The deposit, termed the ETRW Sandstone, is interpreted to have been a broad (~600 m), deep (~25 m), high-energy meandering river. Sediments and fossils from the ETRW Sandstone indicate that *Diluvicursor pickeringi* inhabited a faunally rich, substantially forested riverine floodplain in the Australian-Antarctic rift half-graben. A further isolated caudal vertebra from the deposit (NMV P228342), interpreted as that of an indeterminate ornithischian, suggests the locality may have hosted at least two small-bodied ornithischians. *Diluvicursor pickeringi* grew to at least 2.3 m in length and is characterized by nine potential autapomorphies, among which, the combination of dorsoventrally low neural arches and transversely broad caudal ribs on the anterior-most caudal vertebrae is a visually defining combination of features.

Features of the tail and pes suggest that *Diluvicursor pickeringi* is closely related to the two stratigraphically younger indeterminate ornithopods from Dinosaur Cove, NMV P185992/NMV P185993 and NMV P186047. However, *Diluvicursor pickeringi* differs from NMV P185992/NMV P185993, by having a far shorter tail (50 vertebrae compared to >71) and from NMV P186047 by having a comparatively shorter and more robust pes. Features of the pes provisionally suggest that the Eumeralla Formation ornithopods *Diluvicursor pickeringi*, NMV P185992/NMV P185993 and NMV P186047 are more closely related to the Argentinean ornithopods *Anabisetia saldiviai* and *Gasparinisaura cincosaltensis*, the Antarctic ornithopod *Morrosaurus antarcticus* and possibly African and Laurasian dryosaurids, than all other ornithopods. A common progenitor of these taxa is suggested.

The discovery of *Diluvicursor pickeringi* in the ETRW Sandstone suggests that future prospecting efforts in the Eumeralla Formation where coarse sediments crop-out at the base of deep palaeoriver channels, could lead to significant new discoveries (see also Rich et al., 2009). The articulated postcrania of similarly sized, but anatomically diverse, small-bodied ornithopods from the Eumeralla Formation provide excellent potential for future comparative investigations into dinosaur biomechanics, and how differing locomotor abilities may relate to differing palaeoecosystems.

ACKNOWLEDGEMENTS

The authors gratefully thank George Caspar for the discovery of the *Diluvicursor pickeringi* holotype and the field volunteers of Dinosaur Dreaming who participated in the excavations at Eric the Red West. We gratefully thank L. Kool (MU) and D. Pickering (MV) for preparation of the fossils in this work. We further thank Geological Sciences staff of Museums Victoria for their assistance and resources. For access to specimens in their care, we thank R. Coria (MCF-PVPH), J. Calvo, J. Porfiri and R. Juérez Valieri (Centro Paleontológico Lago Barreales), I. Cerda (MCS), L. Salgado (MUCPv), P. Barrett, S. Chapman (NHMUK), K. Spring (QM), palaeontological collections staff at the ROM and R. Martinez (UNPSJB). We are extremely grateful to S. O'Hara and St Vincent's Hospital Melbourne for the CT scanning of NMV P221080. We thank S. Bryan, J. Nair, T. Page, T. Rich, P. Vickers-Rich, P. Trusler and W. White for useful discussions and/or editing advice that greatly helped improve this paper, and C. Coronel, E. Fitzgerald, D. E. Herne, V. Korasidis, M. Lamanna, M. Lyon, A. Maguire, F. Novas, K. Poole, J. Rosine, D. Seegets-Villiers, M. Walters, D. Wings-Schwartz for additional assistance, discussion, images, advice or support that made this work possible. MCH thanks P.

Currie and L. Salgado for suggestions stemming from examination of his unpublished PhD thesis that preceded this work.

REFERENCES

Agnolin FL, Ezcurra MnD, Pais DF, Salisbury SW. 2010. A reappraisal of the Cretaceous non-avian dinosaur faunas from Australia and New Zealand: evidence for their Gondwanan affinities. *Journal of Systematic Palaeontology* 8:257–300.

Allen JRL. 1963. The classification of cross-stratified units, with notes on their origin. *Sedimentology* 2:93–114.

Allen JRL. 1970. Studies in fluviatile sedimentation; a comparison of fining-upwards cyclothems, with special reference to coarse-member composition and interpretation. *Journal of Sedimentary Research* 40:298–323.

Allen JRL. 1984. *Sedimentary structures, their character and physical basis*. Amsterdam, New York: Elsevier Scientific Pub. Co.

Anderson JF, Hall-Martin A, Russell DA. 1985. Long-bone circumference and weight in mammals, birds and dinosaurs. *Journal of Zoology* 207:53–61.

Baker ME, Barnes BV. 1998. Landscape ecosystem diversity of river floodplains in northwestern Lower Michigan, U.S.A. *Canadian Journal of Forest Research* 28:1405–1418.

Bakker RT, Galton P, Siegwarth J, Filla J. 1990. A new latest Jurassic vertebrate fauna, from the highest levels of the Morrison Formation at Como Bluff, Wyoming. Part IV. The dinosaurs: a new *Othnielia*-like hypsilophodontid. *Hunteria* 2:8–19.

Barrett PM. 2016. A new specimen of *Valdosaurus canaliculatus* (Ornithopoda: Dryosauridae) from the Lower Cretaceous of the Isle of Wight, England *Memoirs of Museum Victoria* 74:29–48.

Barrett PM, Benson RBJ, Rich TH, Vickers-Rich P. 2011a. First spinosaurid dinosaur from Australia and the cosmopolitanism of Cretaceous dinosaur faunas. *Biology Letters* 7:933–936.

Barrett PM, Butler RJ, Twitchett RJ, Hutt S. 2011b. New material of *Valdosaurus canaliculatus* (Ornithischia: Ornithopoda) from the Lower Cretaceous of southern England. *Special Papers in Palaeontology* 86:131–163.

Barrett PM, Rayfield EJ. 2006. Ecological and evolutionary implications of dinosaur feeding behaviour. *Trends in Ecology and Evolution* 21:217–224.

Barrett PM, Rich TH, Vickers-Rich P, Tumanova TA, Inglis M, Pickering D, Kool L, Kear BP. 2010. Ankylosaurian dinosaur remains from the Lower Cretaceous of southeastern Australia. *Alcheringa* 34:205–217.

Barrett PM, Willis KJ. 2001. Did dinosaurs invent flowers? Dinosaur-angiosperm coevolution revisited. *Biological Reviews* 76:411–447.

Bartholomai A, Molnar RE. 1981. *Muttaburrasaurus*, a new iguanodontid (Ornithischia: Ornithopoda) dinosaur from the Lower Cretaceous of Queensland. *Memoirs of the Queensland Museum* 20:319–349.

Becerra MG, Pol D, Rauhut OWM, Cerda IA. 2016. New heterodontosaurid remains from the Cañadón Asfalto Formation: cursoriality and the functional importance of the pes in small heterodontosaurids. *Journal of Paleontology* 90:555–577.

Behrensmeyer AK. 1982. Time resolution in fluvial vertebrate assemblages. *Paleobiology* 8:211–227.

Behrensmeyer AK. 1988. Vertebrate preservation in fluvial channels. *Palaeogeography, Palaeoclimatology, Palaeoecology* 63:183–199.

Benson RBJ, Barrett PM, Rich TH, Vickers-Rich P. 2010. A southern tyrant reptile. *Science* 327:1613.

Benson RBJ, Rich TH, Vickers-Rich P, Hall M. 2012. Theropod fauna from southern Australia indicates high polar diversity and climate-driven dinosaur provinciality. PLoS ONE: Public Library of Science. p 29 pp.

Benton MJ. 2005. *Vertebrate palaeontology (3rd edition)*. London: Blackwell Publishing.

Boggs JS. 2001. *Principals of Sedimentology and Stratigraphy*. New Jersey: Prentice Hall.

Brown CM, Boyd CA, Russell AP. 2011. A new basal ornithopod dinosaur (Frenchman Formation, Saskatchewan, Canada), and implications for late Maastrichtian ornithischian diversity in North America. *Zoological Journal of the Linnean Society* 163:1157–1198.

Bryan SE. 2007. Silicic large igneous provinces. *Episodes* 30:20–31.

Bryan SE, Constantine AE, Stephens CJ, Ewart A, Schon RW, Parianos J. 1997. Lower Cretaceous volcano-sedimentary successions along the eastern Australian continental margin: Implications for the break-up of eastern Gondwana. *Earth and Planetary Science Letters* 153:85–102.

Bryan SE, Riley TR, Jerram DA, Stephens CJ, Leat PT. 2002. Silicic volcanism: An undervalued component of large igneous provinces and volcanic rifted margins. *Geological Society of America Special Papers* 362:97–118.

Burgener FA, Kormano M, Tomi P. 2006. *Joint and bone disorders: differential diagnosis in conventional radiology*. Stuttgart, New York: Thieme.

Butler RJ. 2005. The 'fabrosaurid' ornithischian dinosaurs of the Upper Elliot Formation (Lower Jurassic) of South Africa and Lesotho. *Zoological Journal of the Linnean Society* 145:175–218.

Butler RJ, Jin L, Jun C, Godefroit P. 2011. The postcranial osteology and phylogenetic position of the small ornithischian dinosaur *Changchunsaurus parvus* from the Quantou Formation (Cretaceous: Aptian–Cenomanian) of Jilin Province, north-eastern China. *Palaeontology* 54:667–683.

Butler RJ, Upchurch P, Norman DB. 2008. The phylogeny of the ornithischian dinosaurs. *Journal of Systematic Palaeontology* 6:1–40.

Cambiaso AV. 2007. Los ornitópodos e iguanodontes basales (Dinosauria, Ornithischia) del Cretácico de Argentina y Antártida. Unpublished PhD thesis. Universidad de Buenos Aires.

Close RA, Vickers-Rich P, Trusler P, Chiappe LM, O'Connor JK, Rich TH, Kool L, Komarower P. 2009. Earliest Gondwanan bird from the Cretaceous of southeastern Australia. *Journal of Vertebrate Paleontology* 29:616–619.

Collinson JD. 1978. Vertical sequence and sand body shape in alluvial sequences. In: Miall AD, ed. *Fluvial Sedimentology*. Calgary: Memoirs of the Canadian Society of petroleum Geologists, 576–586.

Coombs WP, Jr. 1978a. The families of ornithischian dinosaur order Ankylosauria. *Palaeontology* 21:143–170.

Coombs WP, Jr. 1978b. Theoretical aspects of cursorial adaptations in dinosaurs. *Quarterly Review of Biology* 53:393–418.

Coria RA, Calvo JO. 2002. A new iguanodontian ornithopod from Neuquén Basin, Patagonia, Argentina. *Journal of Vertebrate Paleontology* 22:503–509.

Coria RA, Moly 32, Reguero M, Santillana S, Marenssi S. 2013. A new ornithopod (Dinosauria; Ornithischia) from Antarctica. *Cretaceous Research* 41:186–193.

Coria RA, Salgado L. 1996. A basal iguanodontian (Ornithischia: Ornithopoda) from the Late Cretaceous of South America. *Journal of Vertebrate Paleontology* 16:445–457.

Currie PJ, Vickers-Rich P, Rich TH. 1996. Possible oviraptorosaur (Theropoda, Dinosauria) specimens from the Early Cretaceous Otway Group of Dinosaur Cove, Australia. *Alcheringa* 20:73–79.

Dettmann ME. 1994. Cretaceous vegetation: the microfossil record. In: Hill RS, ed. *History of the Australian Vegetation*. Cambridge: Cambridge University Press, 143–188.

Dettmann ME, Molnar RE, Douglas JG, Burger D, Fielding C, Clifford HT, Francis J, Jell P, Rich T, Wade M, Vickers-Rich P, Pledge N, Kemp A, Rozefeld A. 1992. Australian Cretaceous terrestrial faunas and floras: biostratigraphic and biogeographic implications. *Cretaceous Research* 13:207–262.

Douglas JG. 1969. *The Mesozoic Floras of Victoria, Parts 1 and 2*. Melbourne: Mines Department.

Douglas JG. 1973. *The Mesozoic Floras of Victoria, Part 3*. Melbourne: Mines Department.

Douglas JG, Williams GE. 1982. Southern polar forests: The Early Cretaceous floras of Victoria and their palaeoclimatic significance. *Palaeogeography, Palaeoclimatology, Palaeoecology* 39:171–185.

Duddy IR. 1983. The Geology, Petrology and Geochemistry of the Otway Formation Volcanogenic Sediments. Unpublished PhD Thesis. University of Melbourne.

Duddy IR. 2003. Mesozoic: a time of change in tectonic regime. In: Birch WD, ed. *Geology of Victoria*. 1st ed. Sydney: Geological Society of Australia, 239–287.

Escaso F, Ortega F, Dantas P, Malafaia E, Silva B, Gasulla JM, Mocho P, Narváez I, Sanz JL. 2014. A new dryosaurid ornithopod (Dinosauria, Ornithischia) from the Late Jurassic of Portugal. *Journal of Vertebrate Paleontology* 34:1102–1112.

Felton EA. 1992. Sedimentary History of the Early Cretaceous Otway Group, Otway Basin, Australia. Unpublished PhD thesis. University of Wollongong.

Felton EA. 1997a. A non-marine Lower Cretaceous rift-related epiclastic volcanic unit in southern Australia: the Eumeralla Formation in the Otway Basin. Part I: lithostratigraphy and depositional environments. *ASGO Journal of Australian Geology and Geophysics* 16:717–730.

Felton EA. 1997b. A non-marine Lower Cretaceous rift-related epiclastic volcanic unit in southern Australia: the Eumeralla Formation in the Otway Basin. Part II: fluvial systems. *ASGO Journal of Australian Geology and Geophysics* 16:731–757.

Feranec RS, MacFadden BJ. 2006. Isotopic discrimination of resource partitioning among ungulates in C3-dominated communities from the miocene of Florida and California. *Paleobiology* 32:191–205.

Fitzgerald EMG, Carrano MT, Holland T, Wagstaff BE, Pickering D, Rich TH, Vickers-Rich P. 2012. First ceratosaurian dinosaur from Australia. *Naturwissenschaften* 99:397–405.

Flannery TF, Rich TH. 1981. Dinosaur Digging in Victoria. *Australian Natural History* 20:195–198.

Forster CA. 1990. The postcranial skeleton of the ornithopod dinosaur *Tenontosaurus tilletti*. *Journal of Vertebrate Paleontology* 10:273–294.

Fricke HC, Pearson DA. 2008. Stable isotope evidence for changes in dietary niche partitioning among hadrosaurian and ceratopsian dinosaurs of the Hell Creek Formation, North Dakota. *Paleobiology* 34:534–552.

Galton PM. 1974. The ornithischian dinosaur *Hypsilophodon* from the Wealden of the Isle of Wight. *Bulletin of the British Museum (Natural History) Geology* 25:1–152.

Galton PM. 1981. *Dryosaurus*, a hypsilophodontid dinosaur from the Upper Jurassic of North America and Africa. Postcranial skeleton. *Paläontologische Zeitschrift* 55:271–312.

Galton PM. 2014. Notes on the postcranial anatomy of the heterodontosaurid dinosaur *Heterodontosaurus tucki*, a basal ornithischian from the Lower Jurassic of South Africa. *Revue de Paleobiologie* 33:97–141.

Galton PM, Jensen JA. 1973. Skeleton of a hypsilophodontid Dinosaur (*Nanosaurus* (?) *rex*) from the Upper Jurassic of Utah. *Brigham Young University, Geology Studies* 20:137–157.

Galton PM, Upchurch P. 2004. Stegosauria. In: Weishampel DB, Dodson P, Osmólska H, eds. *The Dinosauria (2nd ed)*. Berkeley: University of California Press, 343–362.

Gilmore CW. 1909. Osteology of the Jurassic reptile *Camptosaurus*, with a revision of the species of the genus, and descriptions of two new species. *Proceedings of the United States National Museum* 36:197–332.

Gilmore CW. 1915. Osteology of *Thescelosaurus*, an orthopodous dinosaur from the Lance Formation of Wyoming. *Proceedings of the United States National Museum* 49:591–616.

Gradstein FM, Ogg G, Schmitz M. 2012. *The Geologic Time Scale 2012, 2-Volume Set*: Elsevier.

Gross JD, Rich TH, Vickers-Rich P. 1993. Dinosaur bone infection: chronic osteomyelitis in a hypsilophodontid dinosaur in Early Cretaceous, polar Australia. *National Geographic Research and Exploration* 9:286–293.

Hall M, Keetley J. 2009. *Geoscience Victoria 3D Victoria, Report 2*. Melbourne: Department of Primary Industries.

Han F-L, Barrett PM, Butler RJ, Xu X. 2012. Postcranial anatomy of *Jeholosaurus shangyuanensis* (Dinosauria, Ornithischia) from the Lower Cretaceous Yixian Formation of China. *Journal of Vertebrate Paleontology* 32:1370–1395.

Harms JC, Fahnestock RK. 1965. Stratification, bed forms, and flow phenomena (with an example from the rio grande). In: Middleton GV, ed. *Primary Sedimentary Structures and Their Hydrodynamic Interpretation*. Tulsa: Society of Economic Paleontologists and Mineralogists, 84–115.

He X, Cai K. 1984. *The Middle Jurassic dinosaurian fauna from Dashanpu, Zigong, Sichuan, Volume 1*. Chengdu, Sichuan: Sichuan Scientific and Technological Publishing House.

Helby R, Morgan R, Partridge AD. 1987. A palynological zonation of the Australian Mesozoic. *Memoirs of the Association of Australasian Palaeontologists* 4:1–94.

Henderson DM. 2010. Skull shapes as indicators of niche partitioning by sympatric chasmosaurine and centrosaurine dinosaurs. In: Ryan MJ, Chinnery-Allgeier BJ, Eberth DA,

eds. *New Perspectives on Horned Dinosaurs: The Royal Tyrrell Museum Ceratopsian Symposium*. Bloomington and Indianapolis: Indiana University Press, 293–307.

Herne MC. 2009. Postcranial osteology of *Leaellynasaura amicagraphica* (Dinosauria; Ornithischia) from the Early Cretaceous of southeastern Australia. *Sixty-ninth Annual Meeting Society Of Vertebrate Paleontology* 29:77A.

Herne MC. 2014. Anatomy, Systematics and Phylogenetic Relationships of the Early Cretaceous Ornithopod Dinosaurs of the Australian-Antarctic Rift System PhD dissertation. The University of Queensland.

Herne MC, Nair JP, Salisbury SW. 2010. Comment on "A Southern Tyrant Reptile". *Science* 329:1013.

Herne MC, Tait AM, Salisbury SW. 2016. Sedimentological reappraisal of the *Leaellynasaura amicagraphica* (Dinosauria, Ornithopoda) holotype locality in the Lower Cretaceous of Victoria, Australia with taphonomic implications for the taxon. *New Mexico Museum of Natural History and Science Bulletin* 71:121–148.

Hickin EJ. 1974. The development of meanders in natural river-channels. *Am J Sci* 274:414–442.

Hoffstetter R, Gasc J-P. 1969. Vertebrae and ribs of modern reptiles. In: Gans C, d'A. Bellairs A, Parsons TS, eds. *Biology of the Reptilia*. London, New York: Academic Press, 201–310.

Hone DWE, Farke AA, Wedel MJ. 2016 Ontogeny and the fossil record: what, if anything, is an adult dinosaur? *Biology Letters* 12:1–9.

Huene FFv. 1932. Die fossile reptie-ordung Saurischia, ihre entwicklung und geschichte. *Monographien zur Geologie und Palaeontologie (Serie I)* 4:1–361.

Hulke JW. 1882. An attempt at a complete osteology of *Hypsilophodon foxii*: a British Wealden dinosaur. *Philosophical Transactions of the Royal Society of London* 172:1035–1062.

Ibiricu LM, Martínez RD, Luna M, Casal GA. 2014. A reappraisal of *Notohypshilophodon comodorensis* (Ornithischia: Ornithopoda) from the Late Cretaceous of Patagonia, Argentina. *Zootaxa* 3786:401–422.

Janensch H. 1955. Der ornithopode *Dysaltosaurus* der Tendaguruschichten. *Palaeontographica (Supplement 7)* 3:105–176.

Junk WJ, Bayley PB, Sparks RE. 1989. The flood-pulse concept in river-floodplain systems. In: Dodge DP, editor. Proceedings of the International Large River Symposium. Canada: Special Publication of Fish and Aquatic Science. p 110–127.

Kear BP. 2006. Plesiosaur remains from Cretaceous high-latitude non-marine deposits in southeastern Australia. *Journal of Vertebrate Paleontology* 26:196–199.

Korasidis VA, Wagstaff BE, Gallagher SJ, Duddy IR, Tosolini AMP, Cantrill DJ, Norvick MS. 2016. Early angiosperm diversification in the Albian of southeast Australia: implications for flowering plant radiation across eastern Gondwana. *Review of Palaeobotany and Palynology* 232:61–80.

Kraus MJ. 1999. Paleosols in clastic sedimentary rocks: their geologic applications. *Earth-Science Reviews* 47:41–70.

Lieben L. 2016. Osteoarthritis: Osteophyte formation involves PAR2. *Nat Rev Rheumatol* advance online publication.

MacFadden BJ, Shockey BJ. 1997. Ancient feeding ecology and niche differentiation of Pleistocene mammalian herbivores from Tarija, Bolivia: morphological and isotopic evidence. *Paleobiology* 23:77–100.

MacLaren JA, Anderson PSL, Barrett PM, Rayfield EJ. 2017. Herbivorous dinosaur jaw disparity and its relationship to extrinsic evolutionary drivers. *Paleobiology* 43:15–33.

Maidment SCR, Barrett PM. 2011. The locomotor musculature of basal ornithischian dinosaurs. *Journal of Vertebrate Paleontology* 31:1265–1291.

Maidment SCR, Bates KT, Falkingham PL, VanBuren CS, Arbour VM, Barrett PM. 2014. Locomotion in ornithischian dinosaurs: an assessment using three-dimensional computational modelling. *Biological Reviews* 89:588–617.

Makovicky PJ, Kilbourne BM, Sadleir RW, Norell MA. 2011. A new basal ornithopod (Dinosauria, Ornithischia) from the Late Cretaceous of Mongolia. *Journal of Vertebrate Paleontology* 31:626–640.

Mallison H, Pittman M, Schwarz D. 2015. Using crocodilian tails as models for dinosaur tails. PeerJ PrePrints. p 3:e1653v1651.

Mallon JC, Anderson JS. 2013. Skull ecomorphology of megaherbivorous dinosaurs from the Dinosaur Park Formation (Upper Campanian) of Alberta, Canada. PLoS ONE: Public Library of Science. p e67182.

Marsh OC. 1881. Principal characters of American Jurassic dinosaurs. Part V. *American Journal of Science (Series 3)* 21:417–423.

Matthews KJ, Williams SE, Whittaker JM, Müller RD, Seton M, Clarke GL. 2015. Geologic and kinematic constraints on Late Cretaceous to mid Eocene plate boundaries in the southwest Pacific. *Earth-Science Reviews* 140:72–107.

Molnar RE, Flannery TF, Rich TH. 1981. An allosaurid theropod dinosaur from the Early Cretaceous of Victoria, Australia. *Alcheringa* 5:141–146.

Molnar RE, Galton PM. 1986. Hypsilophodontid dinosaurs from Lightning Ridge, New South Wales, Australia. *Geobios* 19:231–239.

Moreno K, Carrano MT, Snyder R. 2007. Morphological changes in pedal phalanges through ornithopod dinosaur evolution: a biomechanical approach. *Journal of Morphology* 268:50–63.

Müller RD, Gurnis M, Torsvik T. 2012. GPlates 1.2.0. *Available at* http://www.gplates.org/index.html.

Nichols G. 2009. *Sedimentology and Stratigraphy*. Hoboken: Wiley-Blackwell.

Norman DB. 1980. On the ornithischian dinosaur *Iguanodon bernissartensis* from the Lower Cretaceous of Bernissart (Belgium). *Instiut Royal des Sciences Naturelles de Belgique, Memoire* 178:1–105.

Norman DB. 1986. On the anatomy of *Iguanodon atherfieldensis* (Ornithischia: Ornithopoda). *Bulletin de l'Institut Royal des Sciences Naturelles de Belgique: Sciences de la Terre* 56:281–372.

Norvick MS, Langford RP, Rollet N, Hashimoto T, Higgins KL, Morse MP. 2008. New insights into the evolution of the Lord Howe Rise (Capel and Faust basins), offshore eastern Australia, from terrane and geophysical data analysis. In: Blevin JE, Bradshaw BE, Uruski C, eds.

Eastern Australasian Basins Symposium III: Energy security for the 21st century: Petroleum Exploration Society of Australia Special Publications, 291–310.

Norvick MS, Smith MA. 2001. Mapping the plate tectonic reconstructions of southern and southeastern Australia and implications for petroleum systems. *AS6EA journal* 41:15–35.

Novas FE. 1989. The tibia and tarsus in Herrerasauridae (Dinosauria, incertae sedis) and the origin and evolution of the dinosaurian tarsus. *Journal of Paleontology* 63:677–690.

Novas FE. 1996. Dinosaur monophyly. *Journal of Vertebrate Paleontology* 16:723–741.

Novas FE. 2009. *The Age of Dinosaurs in South America*. Bloomington: Indiana University Press.

O'Connor PM. 2007. The postcranial axial skeleton of *Majungasaurus crenatissimus* (Theropoda: Abelisauridae) from the Late Cretaceous of Madagascar. *Journal of Vertebrate Paleontology* 27:127–163.

Organ CL. 2003. Epaxial muscles and ossified tendons in dinosaurs: anatomy, development, histology, and biomechanics Doctor of Philosophy dissertation. Montana State University.

Ostrom JH. 1969. Osteology of *Deinonychus antirrhopus*, an unusual theropod from the Lower Cretaceous of Montana. *Bulletin of the Peabody Museum of Natural History* 30:1–165.

Parks WA. 1926. *Thescelosaurus warreni*, a new species of orthopodous dinosaur from the Edmonton Formation of Alberta. *University of Toronto Studies, Geological Series* 21:1–42.

Peng G. 1992. Jurassic ornithopod *Agilisaurus louderbacki* (Ornithopoda: Fabrosauridae) from Zigong, Sichuan, China. *Vertebrata PalAsiatica* 30:39–53.

Persons WS, IV, Currie PJ. 2014. Duckbills on the run: the cursorial abilities of hadrosaurs and implications for tyrannosaur-avoidance strategies. In: Eberth DA, Evans D, eds. *Hadrosaurs*. Bloomington: Indiana University Press, 449-458.

Persons WS, IV, Currie PJ, Norell MA. 2014. Oviraptorosaur tail forms and functions. *Acta Palaeontologica Polonica* 59:553–567.

Resnick D. 1983. Osteophytosis of the femoral head and neck. *Arthritis & Rheumatism* 26:908-913.

Rich TH. 2015. Research report. In: White W, ed. *Dinosaur Dreaming 2015 Field Report*. Melbourne: Monash University, 16–21.

Rich TH, Galton PM, Vickers-Rich P. 2010. The holotype individual of the ornithopod dinosaur *Leaellynasaura amicagraphica* Rich & Rich, 1989 (late Early Cretaceous, Victoria, Australia). *Alcheringa* 34:385–396.

Rich TH, Gangloff RA, Hammer WR. 1997. Polar dinosaurs. In: Currie PJ, Padian K, eds. *Encyclopedia of Dinosaurs*. San Diego: Academic Press, 562–573.

Rich TH, Rich PV. 1989. Polar dinosaurs and biotas of the Early Cretaceous of southeastern Australia. *National Geographic Society Research Reports* 5:15–53.

Rich TH, Vickers-Rich P. 1994. Neoceratopsians and ornithomimosaurs; dinosaurs of Gondwana origin? *National Geographic Research and Exploration* 10:129–131.

Rich TH, Vickers-Rich P. 1999. The Hypsilophodontidae from southeastern Australia. In: Tomida Y, Rich TH, Vickers-Rich P, eds. *Proceedings of the Second Gondwanan Dinosaur Symposium*. Tokyo: National Science Museum, 167–180.

Rich TH, Vickers-Rich P. 2000. *Dinosaurs of Darkness*. Sydney: Allen & Unwin.

Rich TH, Vickers-Rich P. 2004. Diversity of Early Cretaceous Mammals from Victoria. *Bulletin of the American Museum of Natural History* 285:36–53.

Rich TH, Vickers-Rich P, Flannery T, Kear BP, Cantrill DJ, Komarower P, Kool L, Pickering D, Trusler P, van Klaveren NA, Fitzgerald EMG. 2009a. An Australian multituberculate and its palaeobiogeographic implications. *Acta Palaeontologica Polonica* 54:1–6.

Rich TH, Vickers-Rich P, Flannery TF, Pickering D, Kool L, Tait AM, Fitzgerald EMG. 2009b. A fourth Australian Mesozoic mammal locality. *Museum of Northern Arizona, Bulletin* 65:677–681.

Rich TH, Vickers-Rich P, Gangloff RA. 2002. Polar dinosaurs. *Science* 295:979–980.

Rieppel O, Hagdorn H. 1997. Paleobiogeography of Middle Triassic Sauropterygia in central and western Europe. In: Callaway JM, Nicholls EL, eds. *Ancient Marine Reptiles*. San Diego: Academic Press, 121–144.

Robertson CS, Cronk DK, Mayne SJ, Townsend DG. 1978. A Review of Petroleum Exploration and Prospects in the Otway Basin Region. Canberra: Geoscience Australia. p 49.

Romer AS. 1956. *Osteology of the Reptiles*. Chicago, Illinois: University of Chicago Press.

Rozadilla S, Agnolin FL, Novas FE, Aranciaga Rolando AM, Motta MJ, Lirio JM, Isasi MP. 2016. A new ornithopod (Dinosauria, Ornithischia) from the Upper Cretaceous of Antarctica and its palaeobiogeographical implications. *Cretaceous Research* 57:311–324.

Rubin DM, McCulloch DS. 1980. Single and superimposed bedforms: a synthesis of San Francisco Bay and flume observations. *Sedimentary Geology* 26:207–231.

Salgado L, Coria RA, Heredia SE. 1997. New materials of *Gasparinisaura cincosaltensis* (Ornithischia, Ornithopoda) from the Upper Cretaceous of Argentina. *Journal of Paleontology* 71:933–940.

Santa Luca AP. 1980. The postcranial skeleton of *Heterodontosaurus tucki* (Reptilia, Ornithischia) from the Stormberg of South Africa. *Annals of the South African Museum* 79:159–211.

Scheetz RD. 1999. Osteology of *Orodromeus makelai* and the phylogeny of basal ornithopod dinosaurs Doctor of Philosophy Unpublished PhD dissertation. Montana State University.

Schlische RW. 1991. Half-graben basin filling models: new constraints on continental extensional basin development. *Basin Research* 3:123–141.

Seegets-Villiers D. 2012. Taphonomy, palynology, dendrology and sedimentology of the Inverloch fossil site, Victoria, Australia PhD Unpublished PhD thesis. Monash University.

Seeley HG. 1888. On the classification of the fossil animals commonly named Dinosauria. *Proceedings of the Royal Society of London* 43:165–171.

Sereno P. 2012. Taxonomy, morphology, masticatory function and phylogeny of heterodontosaurid dinosaurs. *ZooKeys* 226:1–225.

Sereno PC. 1986. Phylogeny of the bird-hipped dinosaurs (Order Ornithischia). *National Geographic Research* 2:234–256.

Shipman P. 1981. *Life History of a Fossil*. Cambridge, Massachusetts, London: Harvard University Press.

Simons DB, Richardson EV, Nordin CF. 1965. Sedimentary structures generated by flow in alluvial channels. In: Middleton GV, ed. *Primary Sedimentary Structures and their*

Hydrodynamic Interpretation. Tulsa: Society of Economic Paleontologists and Mineralogists, 34–52.

Smith ND, Makovicky PJ, Agnolín FL, Ezcurra MD, Pais DF, Salisbury SW. 2008. A *Megaraptor*-like theropod (Dinosauria: Tetanurae) in Australia: support for faunal exchange across eastern and western Gondwana in the mid-Cretaceous. *Proceedings of the Royal Society of London B* 275:2085–2093.

Southard JB, Boguchwal LA. 1990. Bed configuration in steady unidirectional water flows; Part 2, Synthesis of flume data. *Journal of Sedimentary Research* 60:658–679.

Sternberg CM. 1940. *Thescelosaurus edmontonensis*, n. sp., and classification of the hypsilophodontidae. *Journal of Paleontology* 14:481–494.

Taquet P. 1976. *Geologie et paleontologie du gisement de Gadoufaoua (Aptien du Niger)*. Paris: Editions du Centre National de la Recherche Scientifique.

Thulborn RA. 1972. The post cranial skeleton of the Triassic ornithischian dinosaur *Fabrosaurus australis*. *Palaeontology* 15:29–60.

Tockner K, Bunn SE, Gordon C, Naiman RJ, Quinn GP, Stanford JA. 2008. Flood plains: critically threatened ecosystems. In: Polunin N, ed. *Aquatic Ecosystems*. Cambridge: Cambridge University Press, 45–61.

Tschopp E. 2016. Nomenclature of vertebral laminae in lizards, with comments on ontogenetic and serial variation in Lacertini (Squamata, Lacertidae). PLoS ONE: Public Library of Science. p 21 pp.

Tucker RT, Roberts EM, Henderson RA, Kemp AIS. 2016. Large igneous province or long-lived magmatic arc along the eastern margin of Australia during the Cretaceous? Insights from the sedimentary record. *Geological Society of America Bulletin* 128:1461–1480.

Veevers 32, Powell CM, Roots SR. 1991. Review of seafloor spreading around Australia. I. synthesis of the patterns of spreading. *Australian Journal of Earth Sciences* 38:337–389.

Wagstaff BE, Gallagher SJ, Trainor JK. 2012. A new subdivision of the Albian spore-pollen zonation of Australia. *Review of Palaeobotany and Palynology* 171:57–72.

Wagstaff BE, McEwan Mason J. 1989. Palynological dating of Lower Cretaceous coastal vertebrate localities, Victoria, Australia. *National Geographic Research* 5:54–63.

Walker RG. 1976. Facies models 3. sandy fluvial systems. *Geoscience Canada* 3:101–109.

Walker RG, Cant DJ. 1984. Sandy fluvial systems. In: Walker RG, ed. *Facies Models*. 2 ed. Toronto: Geological Society of Canada, 71–89.

Warren A, Rich TH, Vickers-Rich P. 1997. The last last labyrinthodonts. *Palaeontographica Abteilungen A* 247:1–24.

Weishampel DW, Jianu C-M, Csiki Z, B. ND. 2003. Osteology and phylogeny of *Zalmoxes* (n. g.), an unusual Euornithopod dinosaur from the latest Cretaceous of Romania. *Journal of Systematic Palaeontology* 1:65–123.

White MA, Cook AG, Klinkhamer AJ, Elliott DA. 2016. The pes of Australovenator wintonensis (Theropoda: Megaraptoridae): analysis of the pedal range of motion and biological restoration. *PeerJ* 4:e2312.

Willcox JB, Stagg HMJ. 1990. Australia's southern margin: a product of oblique extension. *tectonophysics* 173:269–281.

Wilson JA. 1999. A nomenclature for vertebral laminae in sauropods and other saurischian dinosaurs. *Journal of Vertebrate Paleontology* 19:639–653.

Wilson JA. 2012. New vertebral laminae and patterns of serial variation in vertebral laminae of sauropod dinosaurs. *Contributions from the Museum of Paleontology, University of Michigan* 32:91–110.

Wilson JA, D'Emic MD, Ikejiri T, Moacdieh EM, Whitlock JA. 2011. A nomenclature for vertebral fossae in sauropods and other saurischian dinosaurs. PLoS ONE: Public Library of Science. p 19 pp.

Wood JM, Thomas RG, Visser J. 1988. Fluvial processes and vertebrate taphonomy: the Upper Cretaceous Judith River Formation, south-central Dinosaur Provincial Park, Alberta, Canada. *Palaeogeography, Palaeoclimatology, Palaeoecology* 66:127–143.

Woodward AS. 1906. On a tooth of *Ceratodus* and a dinosaurian claw from the Lower Jurassic of Victoria, Australia. *Annals and Magazine of Natural History (Series 7)* 18:1–3.

Figure 1

Maps showing positions of localities and regional geological features, relative to the city of Melbourne.

(A) Australia, indicating Otway region (box). (B) Positions of coastal vertebrate body fossil localities in the Eumeralla Formation, faulting and location of section 'A-A' (see Fig 4). (C) Southern Victoria showing subsurface extent of basin systems (dashed lines), outcrop (dark shaded areas) and vertebrate fossil localities (following Bryan et al., 1997). Dashed arrows in C indicate the direction of palaeo-flow from contemporaneous volcanism on the eastern Australian plate margin (see Fig. S1). Abbreviations: EF, Eumeralla Formation; Lat., latitude; Lon., longitude; TSg, Tyers Subgroup; WF, Wonthaggi Formation.

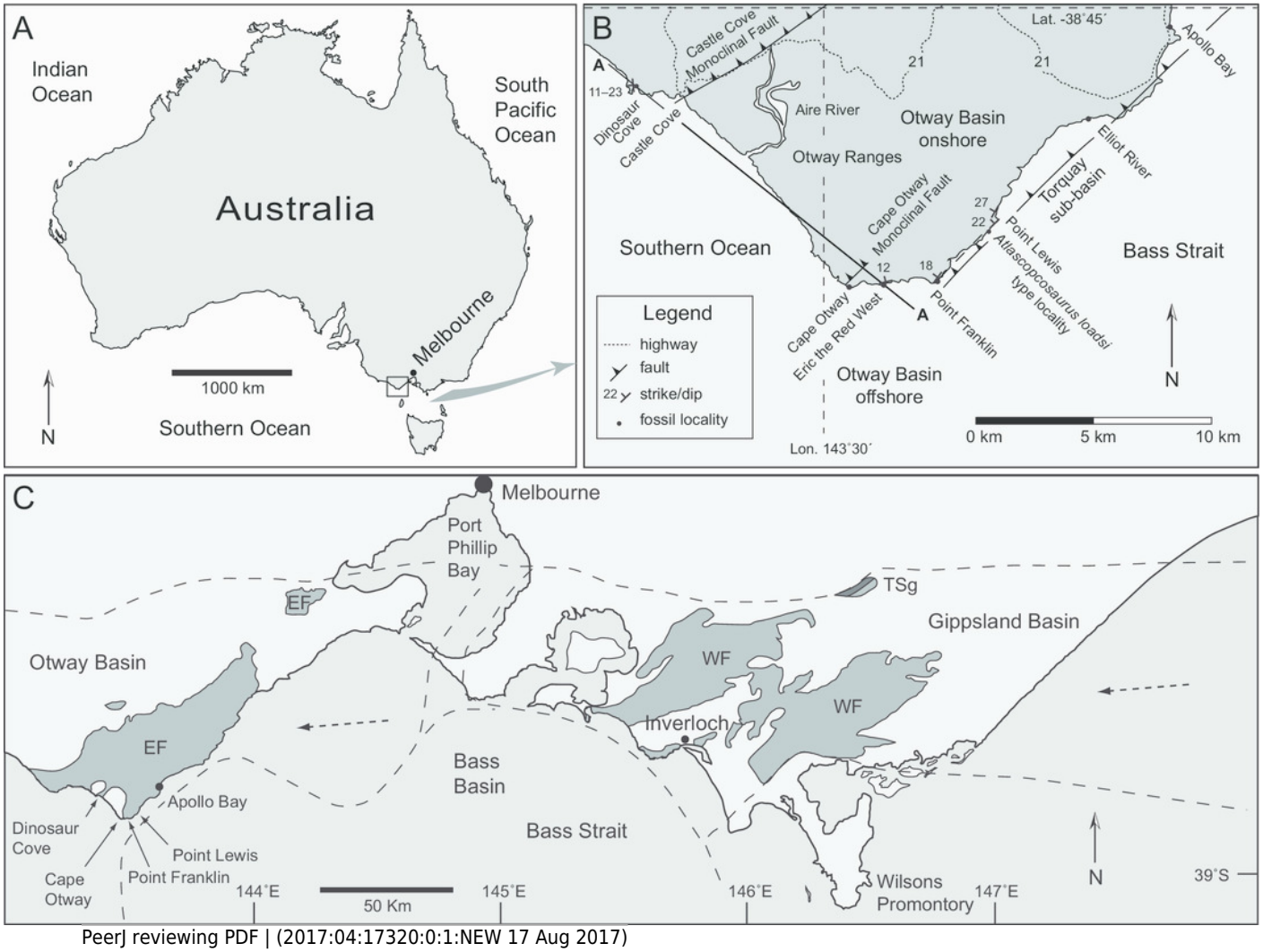

Figure 2

Fossil vertebrate locality of Eric the Red West.

Shore platform looking west, showing undulating erosive boundary (solid white line) between the top of the Anchor Sandstone (AS) and the base of the ETRW Sandstone (ES). White dashed lines indicate selected bedding surfaces. White scale in mid-ground (indicated by arrow), 1 m.

Figure 3

Depositional features of the ETRW Sandstone.

(A) Gritty conglomerate trough cross-bed comprising coarse sand, quartzose/metamorphic gravel/grit matrix, mudrock rip-up clasts, coalified/carbonized wood fragments and vertebrate fossils. (B) Stacked, large-scale, medium- to coarse-grained sandstone and matrix supported conglomerate trough cross-beds. (C) Westernmost section of excavation looking northwest, showing compacted coalified/carbonised woody debris (the partial postcranium NMV P221080 was excavated in the region immediately to the left of the log indicated). (D) Upright coalified tree stump and root-ball (dark bluish-grey mudstone) within conglomerate trough base overlain by large-scale trough cross-beds of a clearer medium- to coarse-grained sandstone (lighter greenish-grey sandstone), which have buried the top of the coalified stump. Abbreviations: ctf, conglomerate trough fill; g, gravel/grit; mc, mudrock clast; rb, root-ball; tcb, trough cross-bed; tm, trough margin; ts, tree stump.

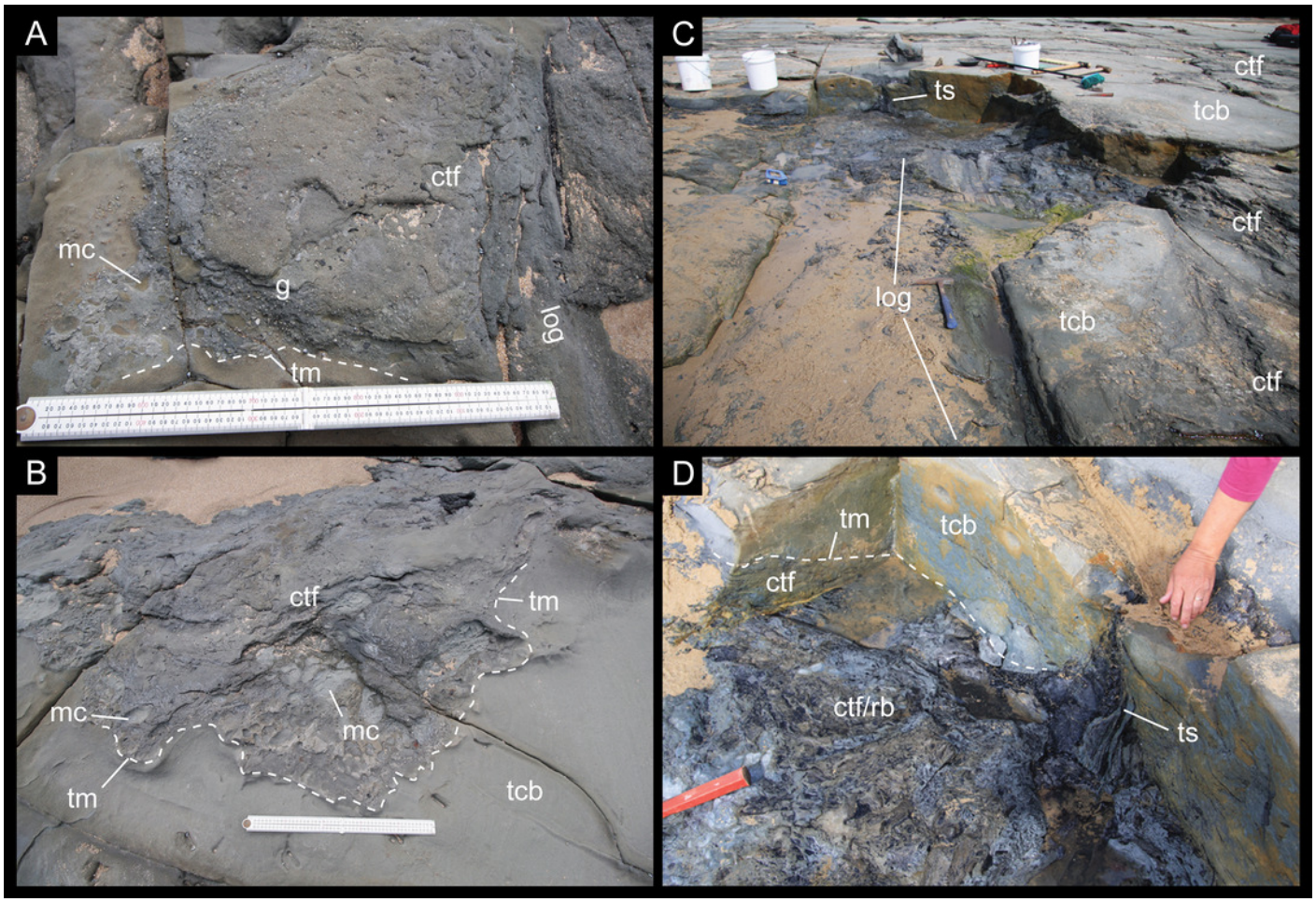
A
ctf
mc
g
log
tm
C
ctf
ts
tcb
ctf
log
tcb
ctf
B
ctf
tm
mc
mc
tm
tcb
D
tm
tcb
ctf
ctf/rb
ts

Figure 4

Schematic stratigraphic relationships of the Eumeralla Formation fossil vertebrate localities looking northeast along section 'A–A (Fig. 1B).

(A) Present-day structural geological features. (B) Restored section for the early Albian (stratigraphic age estimates following Helby et al., 1987; Gradstein et al., 2012; Wagstaff et al.,2012; Korasidis et al., 2016). Stratigraphic zones '1' and '2' in B are arbitrary surfaces for reference between faulted blocks. Dashed line in B indicates present day coastal margin. Abbreviations: *C. paradoxa*, *Coptospora paradoxa*; *C. striatus*, *Crybelosporites striatus*; *C. hughesii*, *Cyclosporites hughesii*; **F, footwall; H, hanging wall;** *P. pannosus*, *Phimopollenites pannosus*. Horizontal scale approximate and vertical scale exaggerated.

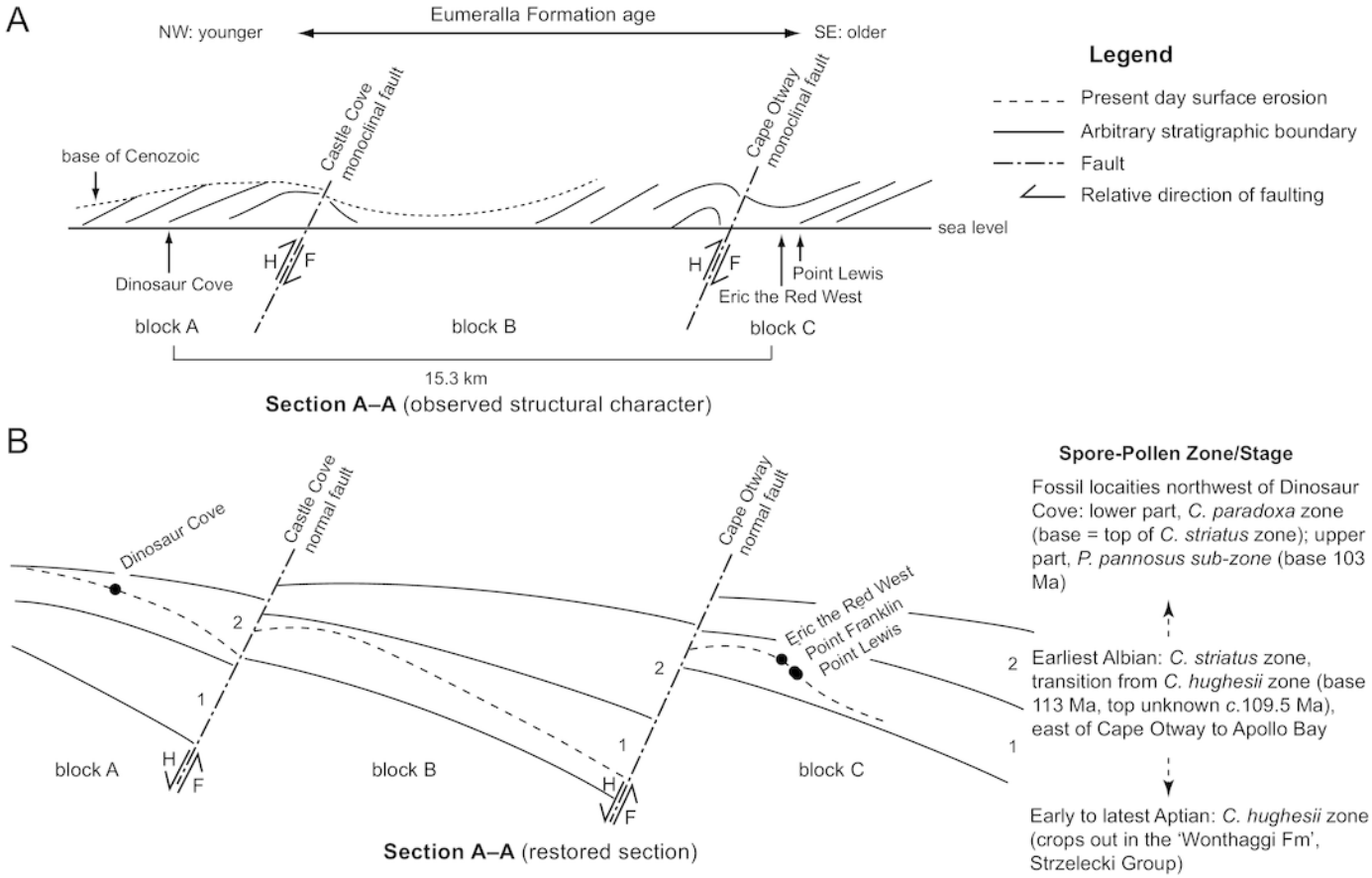

Figure 5

Stratigraphic features of the Eumeralla Formation at the fossil locality of Eric the Red West.

(A) Stratigraphic profile. (B) Depositional features in the region of the westernmost excavation. Abbreviations: c, conglomerate; m, mudstone; s, sandstone.

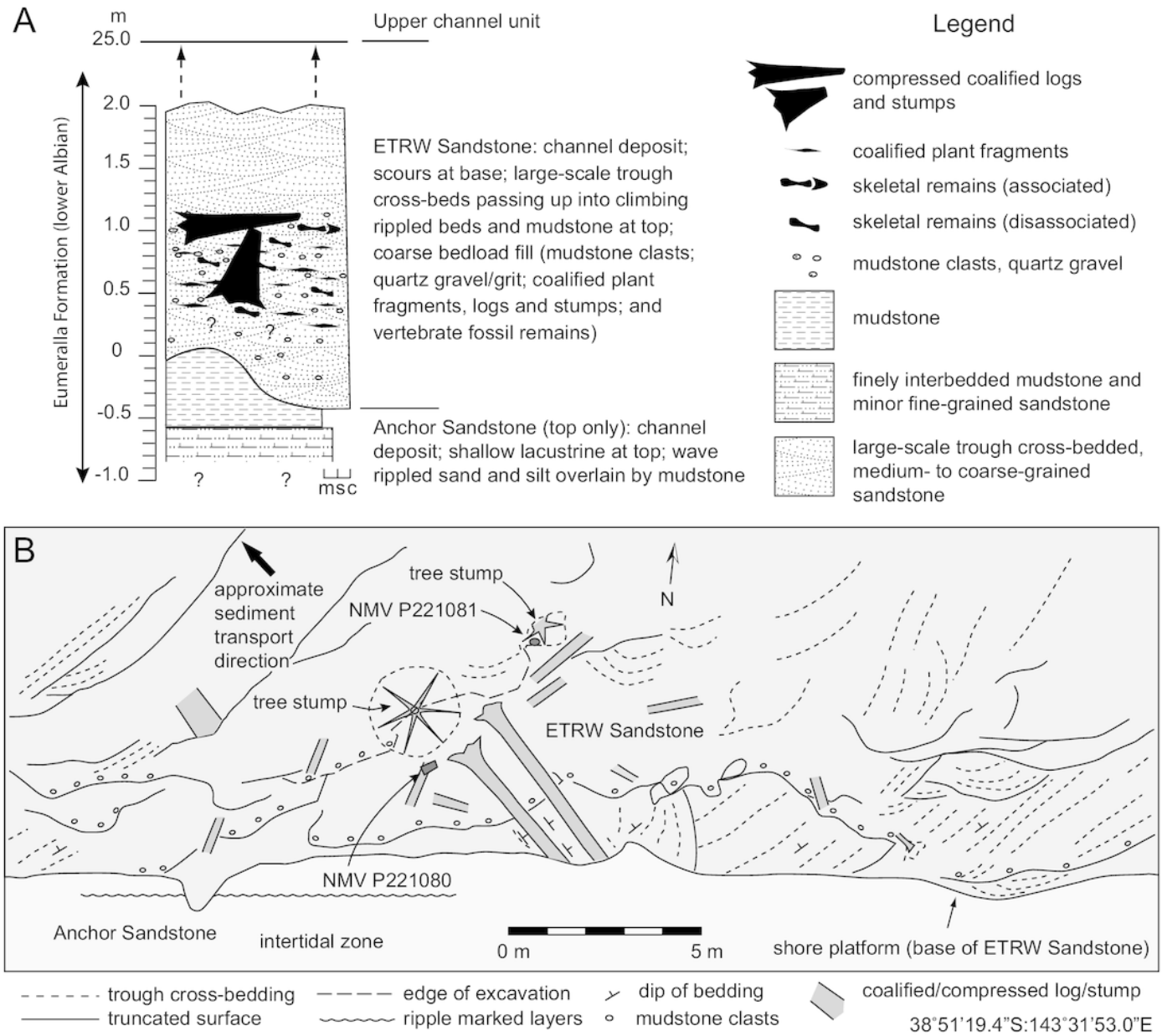

Figure 6

Photograph and schematic of partial postcranium NMV P221080, as prepared on five blocks of ETRW Sandstone.

Specimen NH_4Cl coated. Abbreviations: as, astragalus; B #, host block number; Ca #, designated caudal vertebra and position; cal, calcaneum; fib, fibula; ha #, haemal arch/process and position; pd #, pedal digit number; tib, tibia.

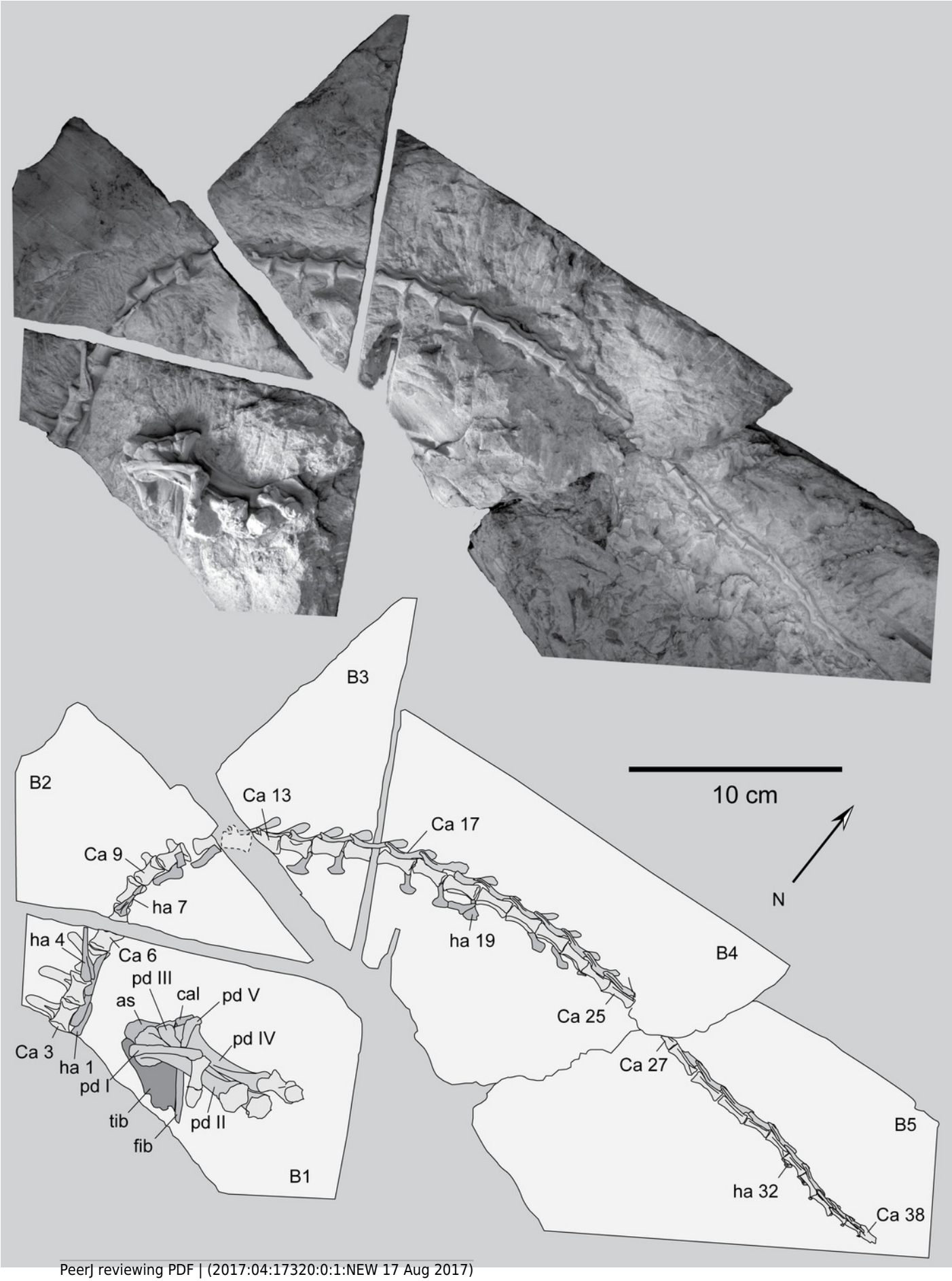
B3
B2
Ca 13
Ca 17
10 cm
Ca 9
ha 7
N
ha 19
B4
ha 4
Ca 6
pd III
as
cal
pd V
Ca 25
pd IV
Ca 3
ha 1
pd I
Ca 27
tib
pd II
B5
fib
B1
ha 32
Ca 38

Figure 7

Schematic restoration of the *Diluvicursor pickeringi* gen. et sp. nov. holotype (NMV P221080), showing preserved bones (light shading) and incomplete caudal vertebrae (outlined), in left lateral view.

Abbreviations: as, astragalus; Ca #, designated caudal vertebral position; pd #, pedal digit number; tib, tibia.

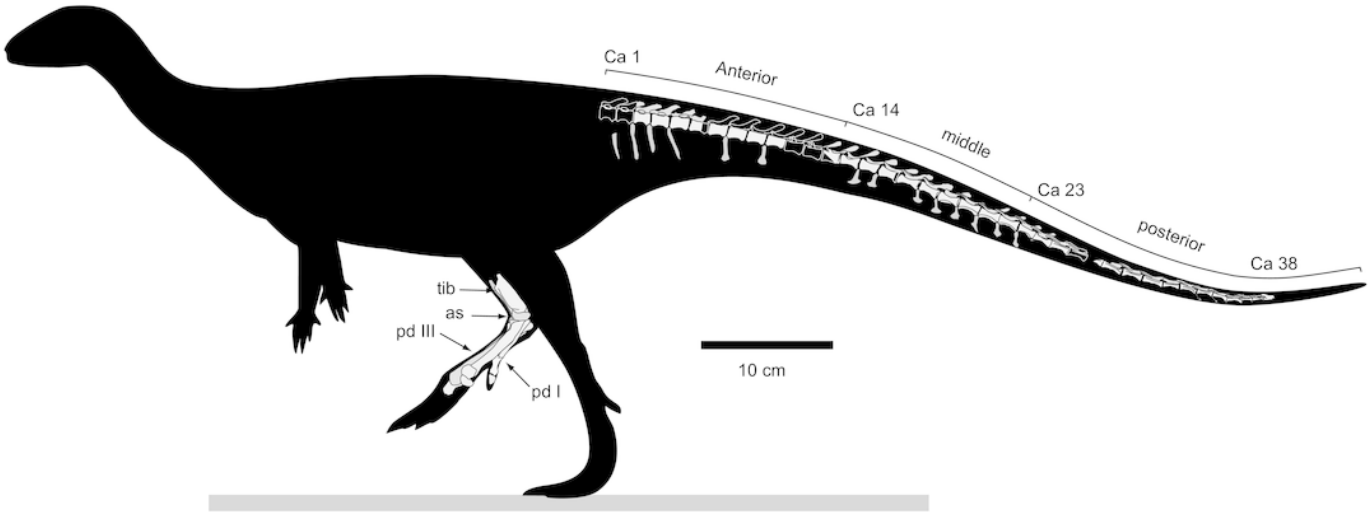

Figure 8

Anterior caudal vertebrae Ca 3–6 of the *Diluvicursor pickeringi* gen. et sp. nov. holotype (NMV P221080) in ventral view.

Specimen in lower image NH_4Cl coated. Abbreviations: Ca #, caudal vertebra and position; cdf, centrodiapophyseal fossa; cr, caudal rib; ha #, haemal arch/process and position; hg, haemal groove; gv, groove. Scale increments, 1 cm.

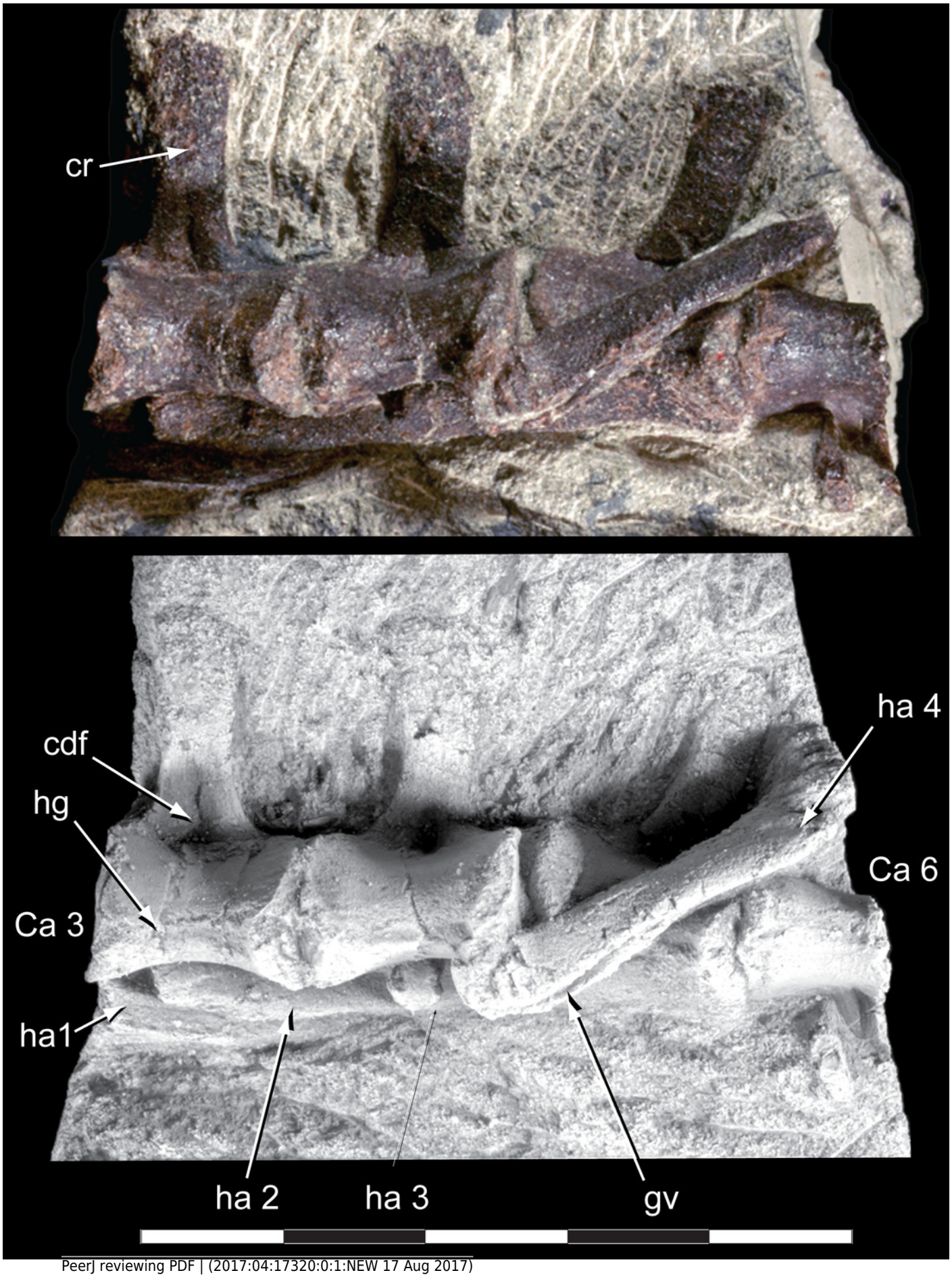
cr
cdf
hg
Ca 3
ha1
ha 2
ha 3
gv
ha 4
Ca 6

Figure 9

Virtual anterior caudal vertebrae, Ca 1–6, of the *Diluvicursor pickeringi* gen. et sp. nov. holotype (NMV P221080).

A–E: (A) left lateral; (B) dorsal; (C) ventral; (D) cranial; and (E) terminal views. Short dashed lines are estimated bone margins. Abbreviations: Ca #, caudal vertebra and position; cr, caudal rib; dap, diapophysis; ha #, haemal arch/process and position; nc, neural canal; pprl?, uncertain postzygoprezygapophyseal lamina; pro?, uncertain processes/protuberance; prsl(p), prespinal lamina (and process); sp, spinal process; sprl(p), spinoprezygapophyseal lamina (and protuberance). Distances: ‘a’, neural arch (=dorsal tip of spinal process to top of centrum or centre of the transverse process base); ‘b’, vertebral height without haemal arch; ‘c’ vertebral height including haemal arch; ‘d’, transverse width across caudal ribs. Scale increments, 1 cm.

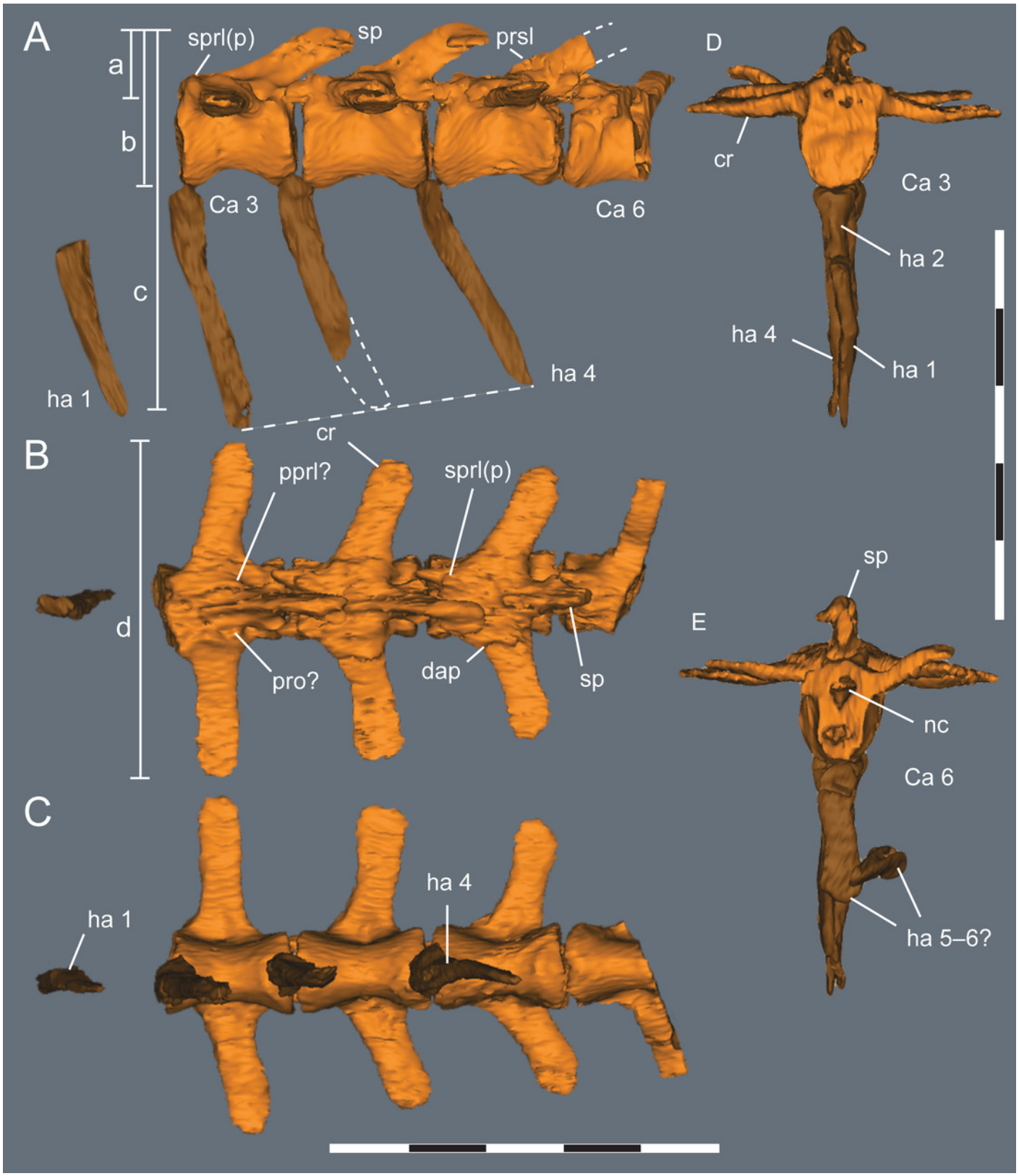
A
a
b
c
sprl(p)
sp
prsl
Ca 3
Ca 6
ha 1
ha 4
cr
B
d
pprl?
sprl(p)
pro?
dap
sp
C
ha 1
ha 4
D
cr
Ca 3
ha 2
ha 4
ha 1
E
sp
nc
Ca 6
ha 5–6?

Figure 10

Virtual anterior caudal vertebra, Ca 4, of the *Diluvicursor pickeringi* gen. et sp. nov. holotype (NMV P221080).

A–F: (A) left lateral; (B) right lateral; (C) ventral; (D) dorsal; (E) cranial; and (F) terminal views. Abbreviations: acdl, anterior centrodiapophseal lamina;cdf, centrodiapophseal fossa; cen, centrum; cprl, centroprezygapophyseal lamina; cr, caudal rib; fac, facet; lcf, laterocentral fossa; m-spol, medial-spinopostzygapophyseal lamina; nc, neural canal; pcdl, posterior centrodiapophyseal lamina; poz, postzygapophysis; pro, protuberance/process; prsl, prespinal lamina; prz, prezygapophysis; sp, spinal process; sprl(p), spinoprezygapophyseal lamina (and protuberance); tp, transverse process; tprl, intraprezygapophyseal lamina. Scale increments, 1 cm.

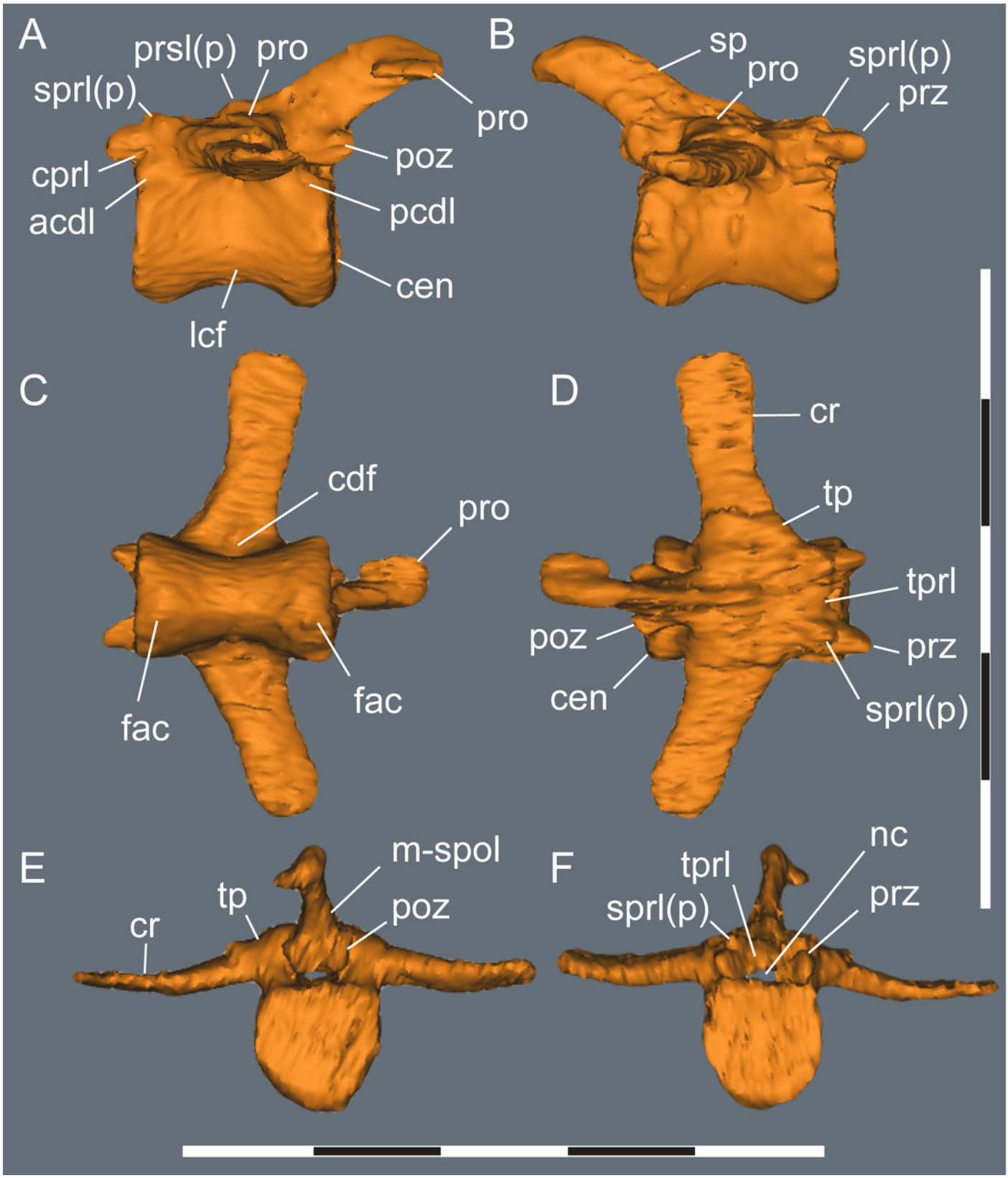
A
prsl(p)
pro
sprl(p)
pro
cprl
poz
acdl
pcdl
cen
lcf
B
sp
pro
sprl(p)
prz
C
cdf
pro
fac
fac
D
cr
tp
tprl
poz
prz
cen
sprl(p)
E
m-spol
tp
poz
cr
F
tprl
nc
sprl(p)
prz

Figure 11

Anterior caudal vertebrae, Ca 7–11, of the *Diluvicursor pickeringi* gen. et sp. nov. holotype (NMV P221080), in ventral view.

Abbreviations: Ca #, caudal vertebra and position; cr, caudal rib; gv, groove; ha #, haemal arch and position; ha ?, haemal arch with uncertain position; hg, haemal groove. Specimen NH_4Cl coated. Scale increments, 1 cm.

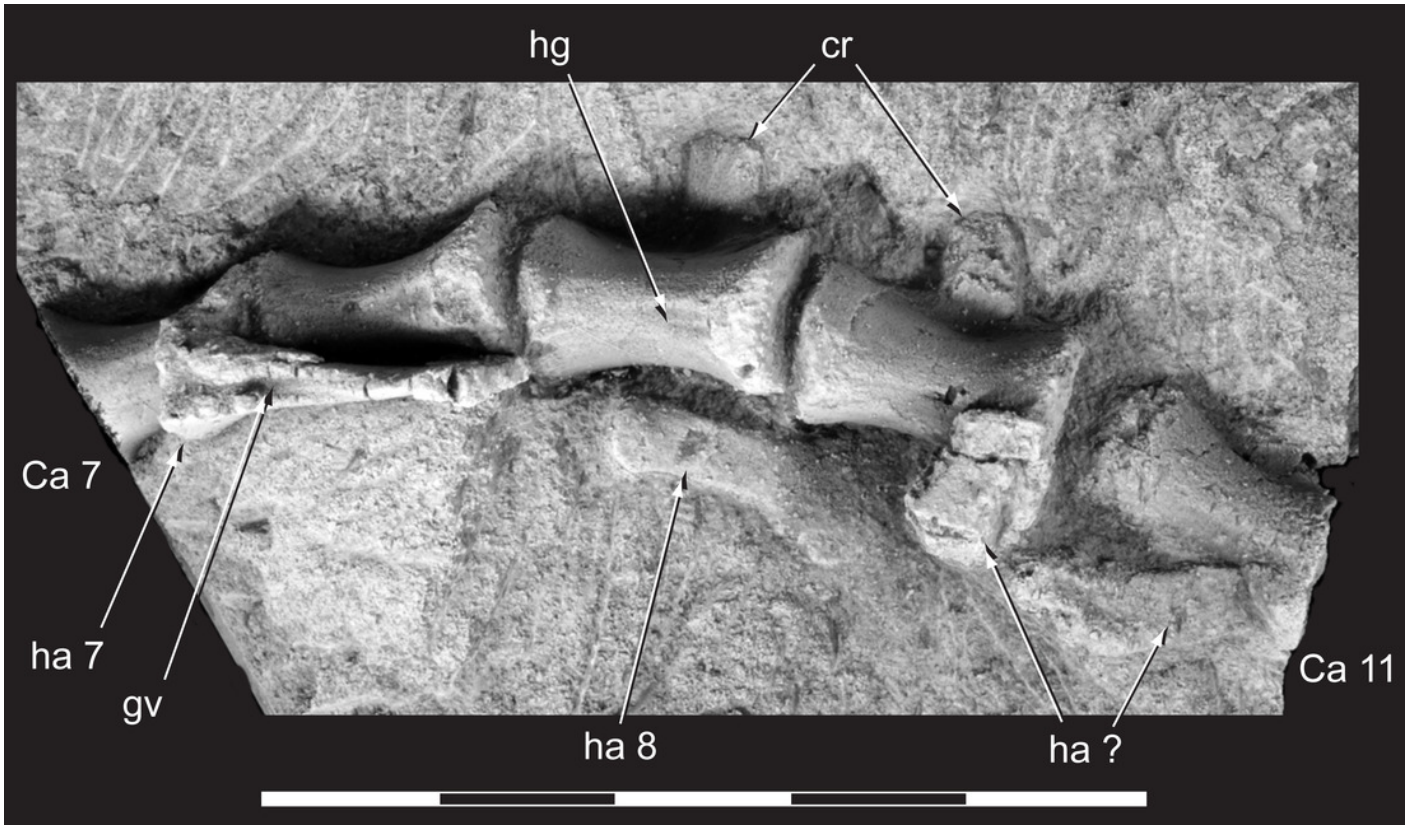

Figure 12

Anterior to middle caudal vertebrae, Ca 12–16, of the *Diluvicursor pickeringi* gen. et sp. nov. holotype (NMV P221080), in left lateral view.

Abbreviations: Ca #, caudal vertebra and position; acdl, anterior centrodiapophyseal lamina; cr, caudal rib; ha, haemal arch/process; hg, haemal groove; lr(p), lateral ridge (and protuberance); pcdl, posterior centrodiapophyseal lamina; poz, postzygapophysis; prdl, prezygodiapophyseal lamina; prz, prezygapophysis; sp, spinal process. Specimen in lower image NH_4Cl coated. Scale increments: top image, 1 mm; lower image, 1 cm.

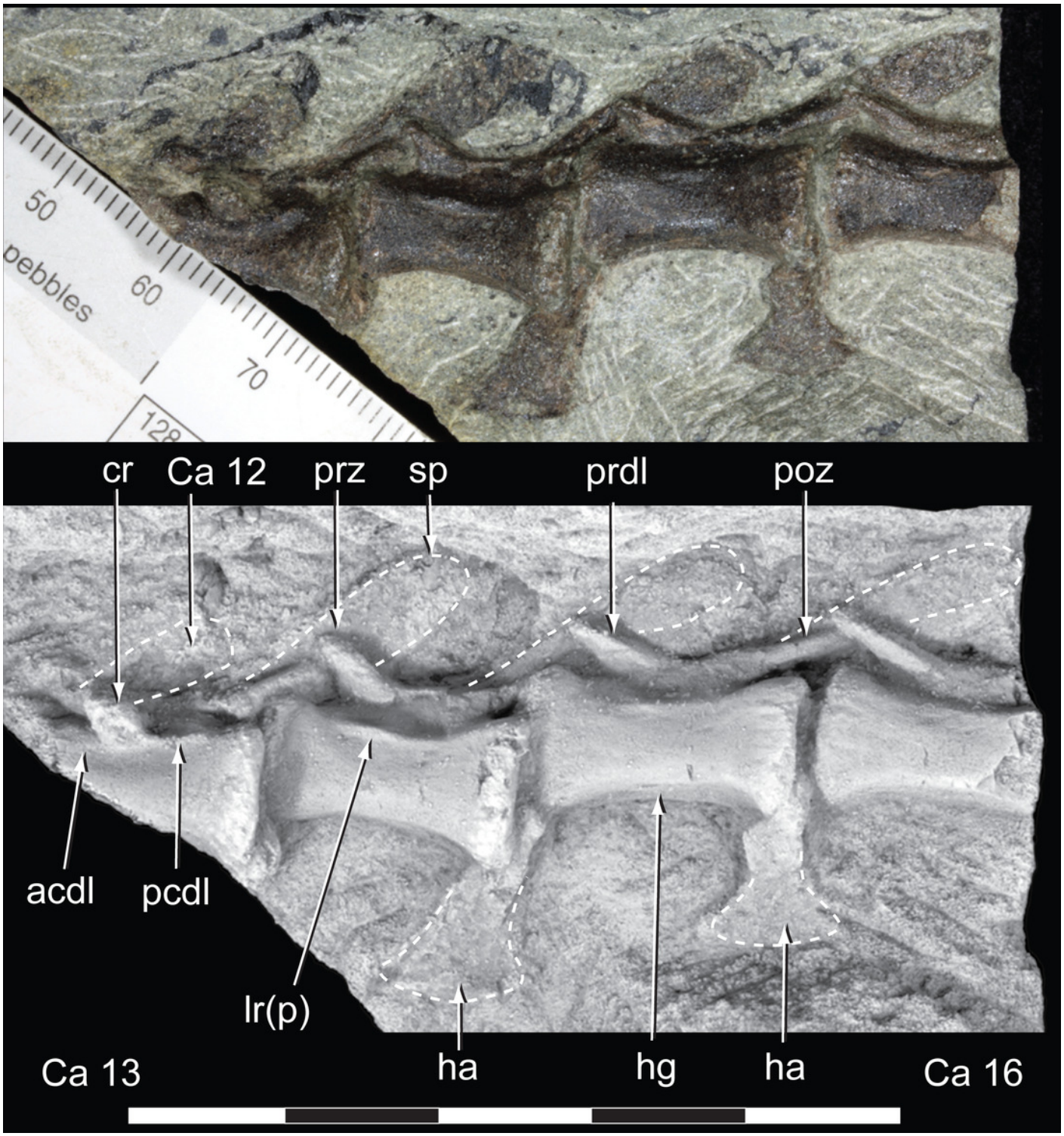
50
pebbles
60
70
cr
Ca 12
prz
sp
prdl
poz
acdl
pcdl
lr(p)
ha
hg
ha
Ca 13
Ca 16

Figure 13

Middle caudal vertebrae, 16–20, of the *Diluvicursor pickeringi* gen. et sp. nov. holotype (NMV P221080), in left lateral view.

Abbreviations: Ca #, caudal vertebra and position; cpol,centropostzygapophyseal lamina; cprl, centroprezygapophyseal lamina; ha, haemal arch/process; hg, haemal groove; lr(p), lateral ridge (and protuberance); poz, postzygapophysis; pprl, postzygoprezygapophyseal lamina; prdl, prezygodiapophyseal lamina; prz, prezygapophysis; sdf, spinodiapophyseal fossa; sp, spinal process; sprf, spinoprezygapophyseal fossa. Specimen in lower image NH_4Cl coated. Scale increments: top image, 1 mm; lower image, 1 cm.

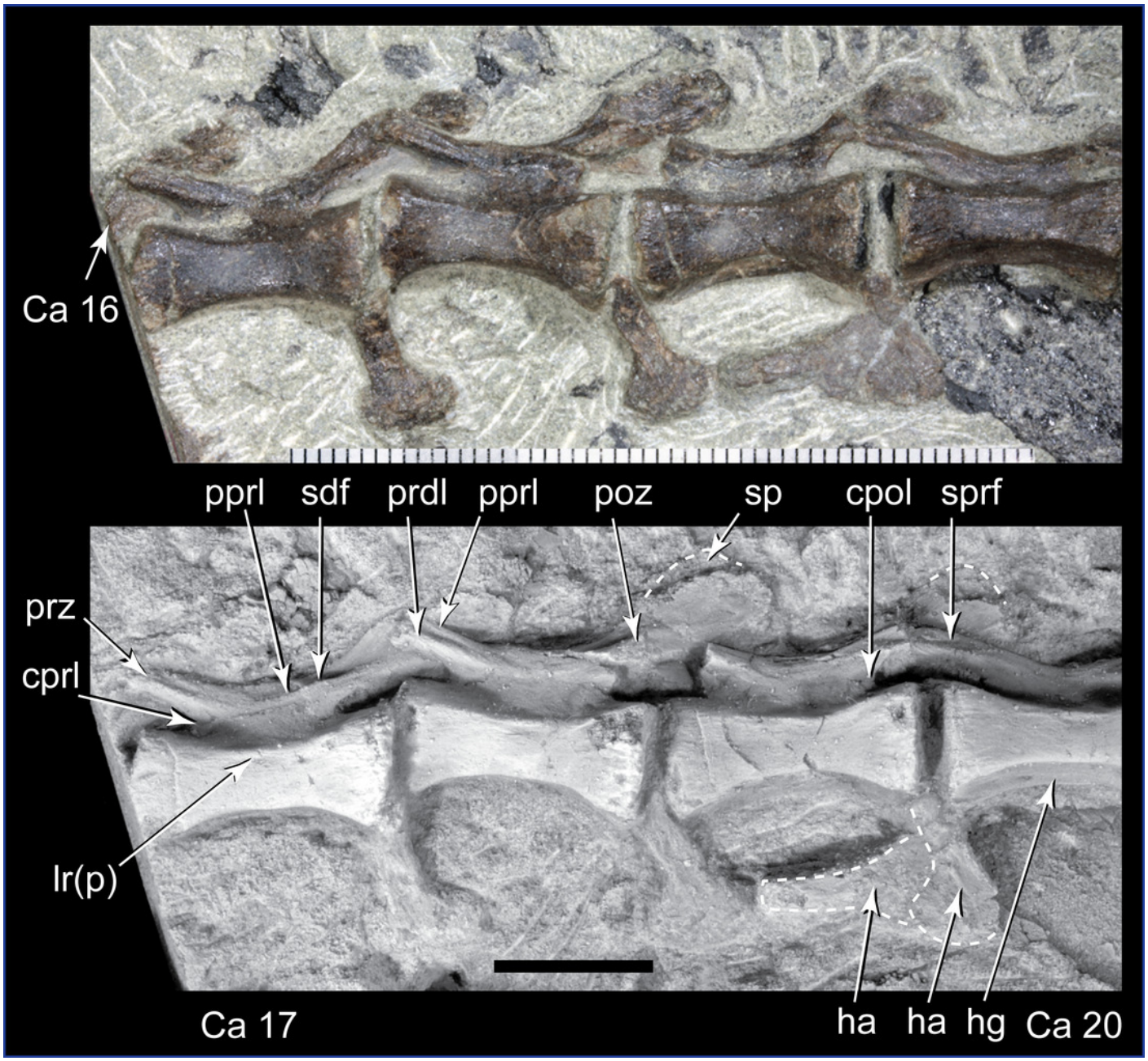
Ca 16
pprl
sdf
prdl
pprl
poz
sp
cpol
sprf
prz
cprl
lr(p)
Ca 17
ha
ha
hg
Ca 20

Figure 14

Middle to posterior caudal vertebrae, Ca 19–23, of the *Diluvicursor pickeringi* gen. et sp. nov. holotype (NMV P221080).

A–B: (A) left lateral/lateroventral; and (B) ventral views. Abbreviations: Ca #, caudal vertebra and position; ha, haemal arch/process; hg, haemal groove; prz, prezygapophysis; sp, spinal process. Specimen in A (lower image) NH_4Cl coated. Scale increments in A: top image, 1 mm; lower image, 1 cm.

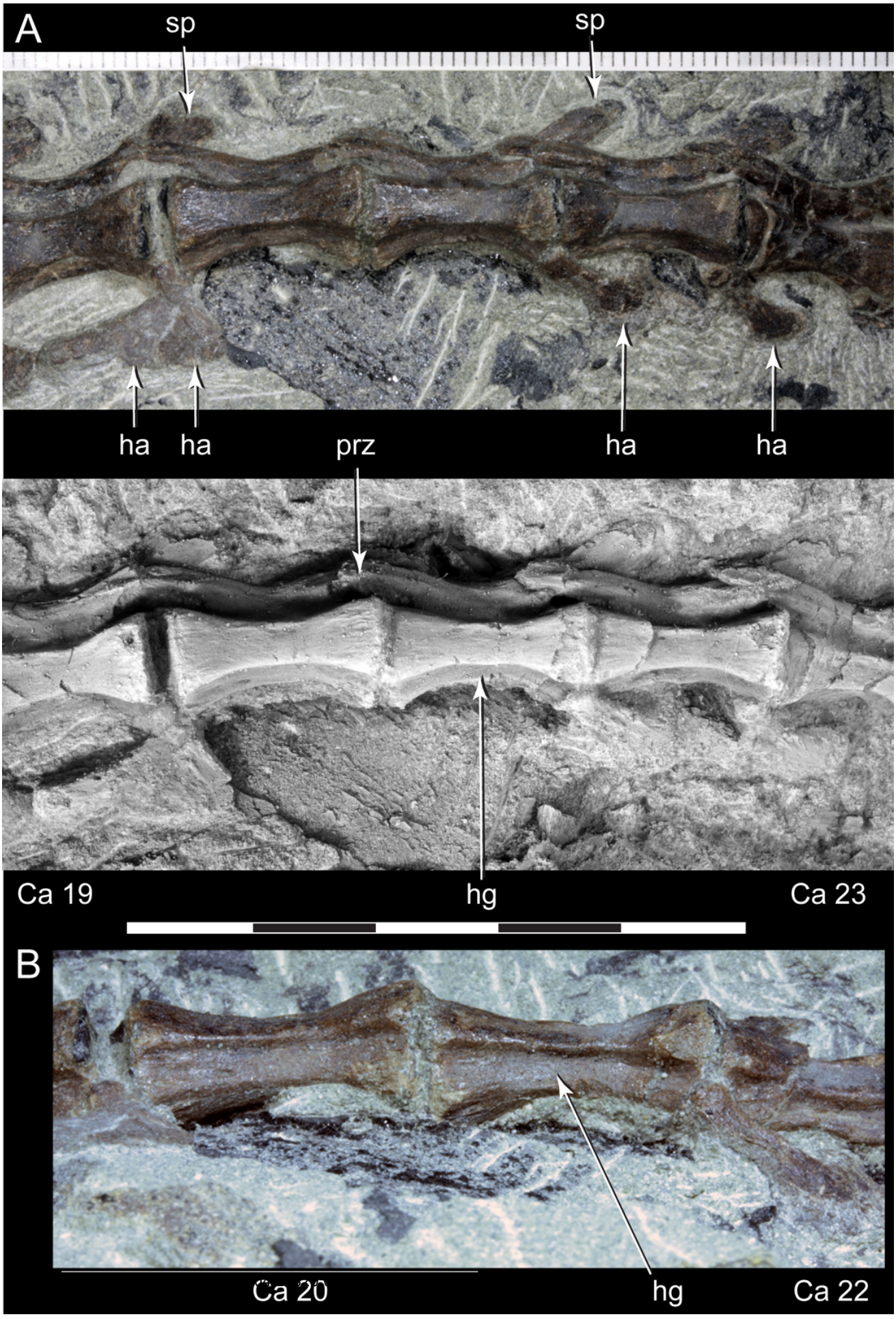
A
sp
sp
ha
ha
ha
ha
prz
Ca 19
hg
Ca 23
B
Ca 20
hg
Ca 22

Figure 15

Middle to posterior caudal vertebrae, Ca 21–25, of the *Diluvicursor pickeringi* gen. et sp. nov. holotype (NMV P221080), in left lateroventral view.

Dashed arrows indicate change in centrum shape from quadrangular (box-like), at Ca 22, to hexagonal, at Ca 23. Abbreviations: Ca #, caudal vertebra and position; ha, haemal arch/process; hg, haemal groove; lr(p), lateral ridge (and protuberance); prz, prezygapophysis; sp, spinal process; sul, sulcus on lateroventral fossa. Specimen NH_4Cl coated. Scale increments, 1 cm.

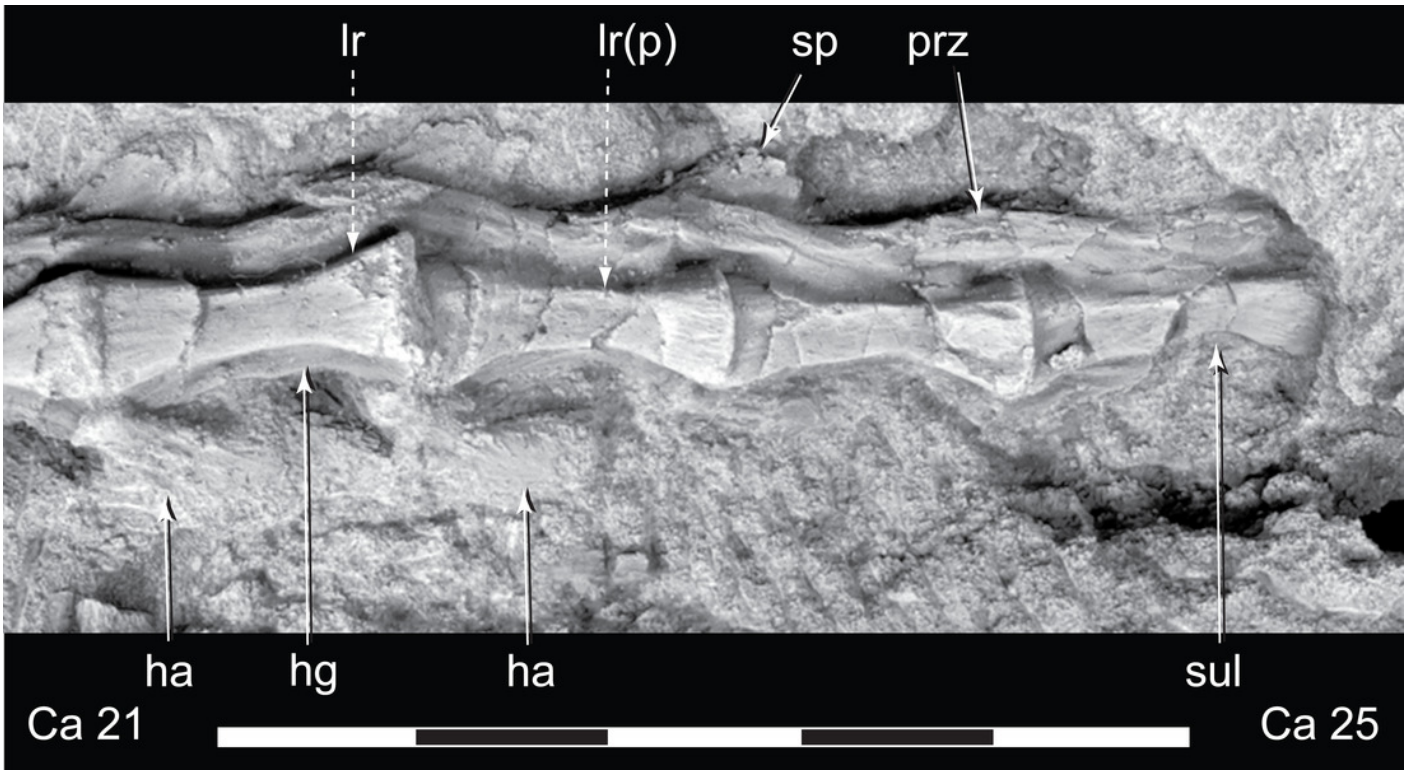

Figure 16

Posterior caudal vertebrae of the *Diluvicursor pickeringi* gen. et sp. nov. holotype (NMV P221080), in left lateral view.

(A) Ca 27–38. (B) Ca 27–30. (C) Ca 32–34. Specimen in A, NH_4Cl coated. Abbreviations: Ca #, caudal vertebra and position; cen, centrum; cprf, centroprezygapophyseal fossa; ha, haemal arch/process; lr, lateral ridge; na, neural arch; ncs, neurocentral suture or location; poz, postzygapophysis; pprl, postzygoprezygapophyseal lamina; prdl, prezygodiapophyseal lamina; prz, prezygapophysis (l-, left; r-, right); sp, spinal process; sprf, spinoprezygapophyseal fossa; sr, spinal ridge; sul, sulcus on lateroventral fossa. Breakage indicated by cross-hatching. Scale increments: A–B, 1 mm; C, 1 cm.

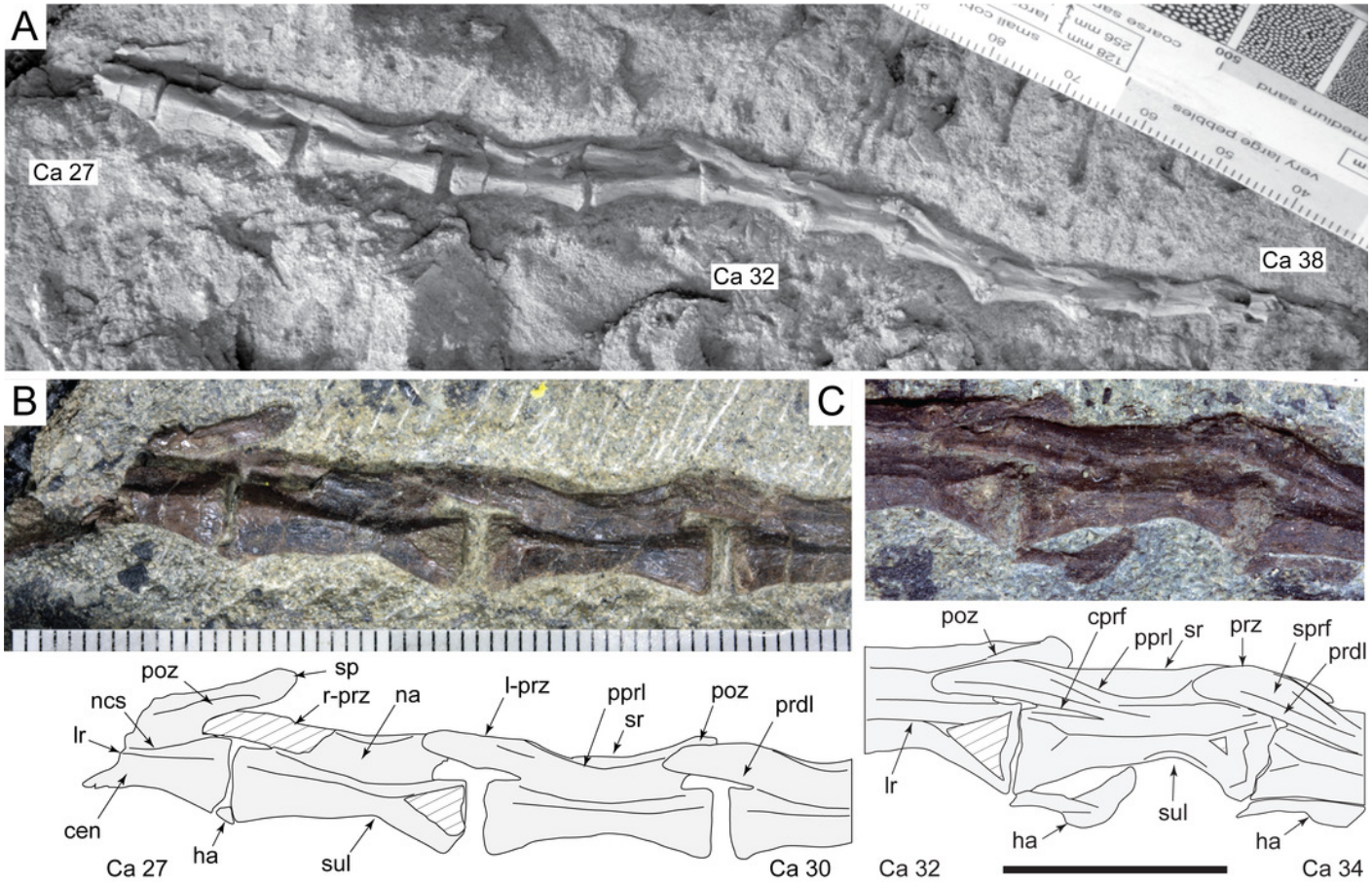

Figure 17

Posterior-most caudal vertebrae, Ca 34–38, of the *Diluvicursor pickeringi* gen. et sp. nov. holotype (NMV P221080).

A–C: (A) left lateral; (B) left lateral with schematic (lower); and (C) ventral views. Specimen in B, NH_4Cl coated. Abbreviations: Ca #, designated caudal vertebra and position; ha, haemal arch; hg, haemal groove; ivp, intervertebral processes; poz, postzygapophysis; pprl, postzygoprezygapophyseal lamina; prdl, prezygodiapophyseal lamina; prz, prezygapophysis; sr, spinal ridge; sp, spinal process; sul, sulcus on the lateroventral fossa. Scale bars, 1 cm.

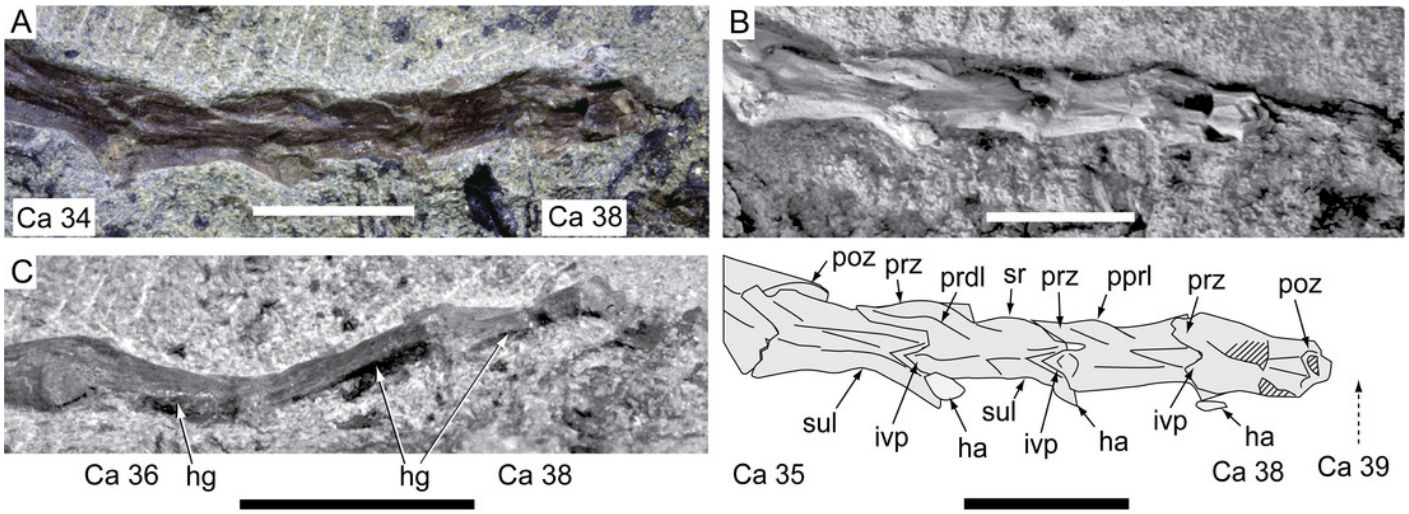

Figure 18

Referred caudal vertebra of *Diluvicursor pickeringi* gen. et sp. nov. (NMV P229456).

A–D: (A) left lateroventral; (B) left dorsolateral; (C) ventral; and (D) right lateral views. Abbreviations: cen, centrum; cprl(f), centroprezygapophyseal lamina (and fossa); hg, haemal groove; lr, lateral ridge; poz, postzygapophysis; pprl, postzygoprezygapophyseal lamina; prdl, prezygodiapophyseal lamina; prz, prezygapophysis; sr, spinal ridge; sul, sulcus on the lateroventral fossa. Scale bar, 1 cm.

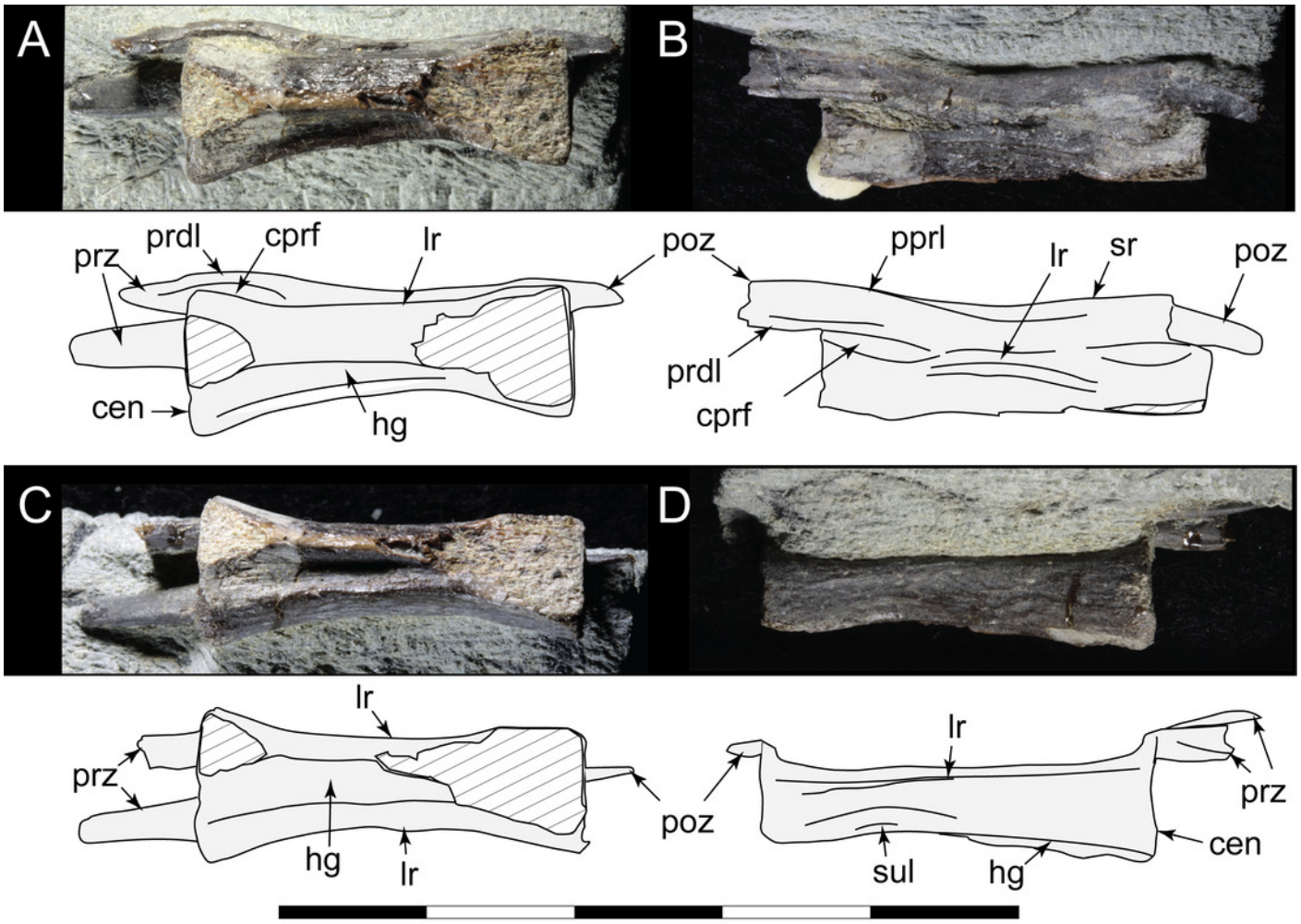

Figure 19

Distal right crus, tarsus and pes of the *Diluvicursor pickeringi* gen. et sp. nov. holotype (NMV P221080).

A–B: (A) anterior/plantomedial; and (B) anterior/plantar views. Abbreviations: as, astragalus; cal, calcaneum; fib, fibula; fos, fossa; ldt, lateral distal tarsal; mdt, medial distal tarsal; mt #, metatarsal position; pd #, pedal digit number and phalanx position; tib, tibia; tub, tuberosity. Specimen in lower images of A and B, NH_4Cl coated. Scale increments in: A (lower image), 1 mm; and B (lower image), 1 cm.

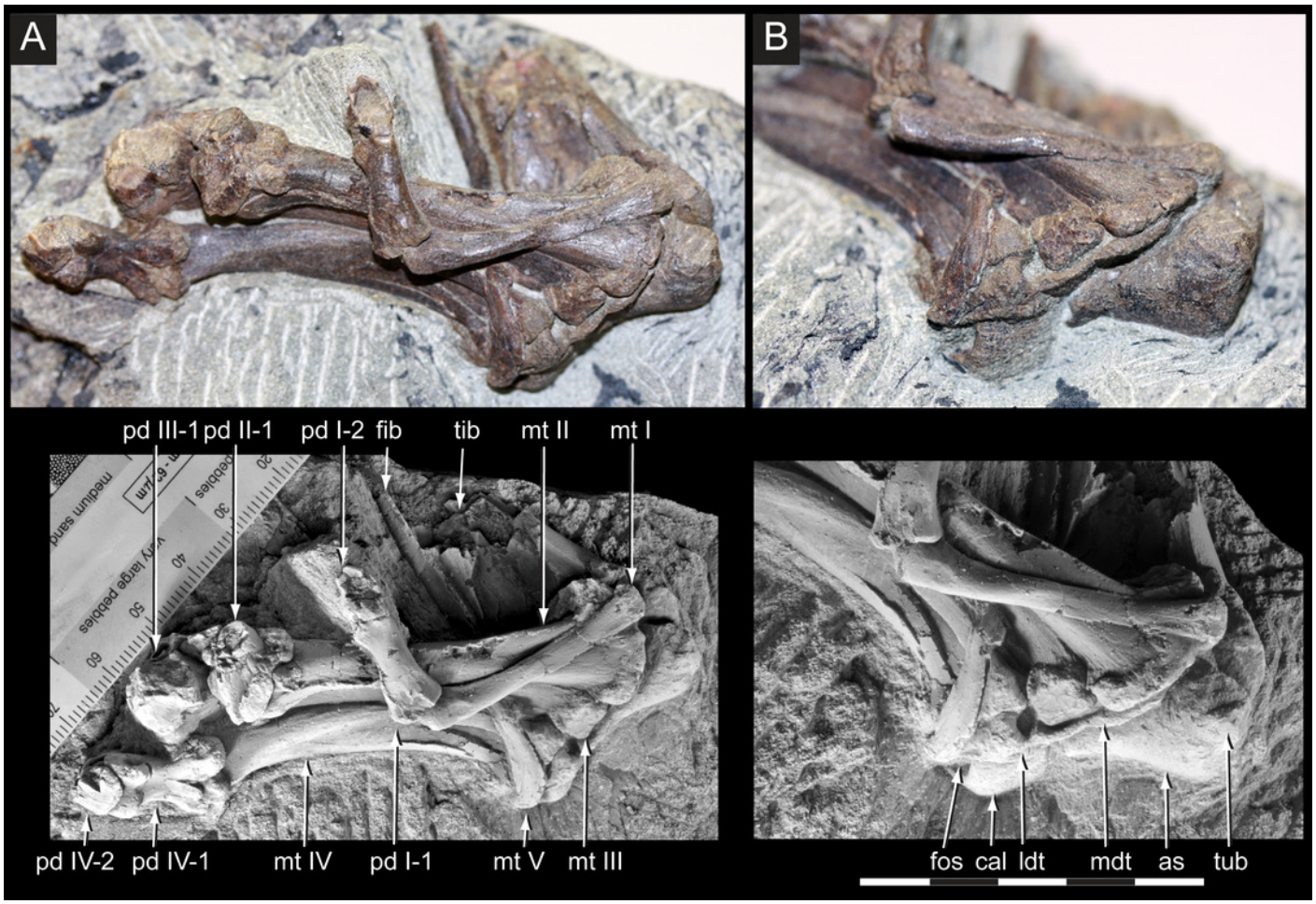

Figure 20

Virtual right distal crus, tarsus and pes of the *Diluvicursor pickeringi* gen. et sp. nov. holotype (NMV P221080).

A–B: (A) cranial/dorsal; and (B) plantar views. Abbreviations: as, astragalus; cal, calcaneum; fib, fibula; ldt, lateral distal tarsal; mdt, medial distal tarsal; pd #, pedal digit number and phalanx position; tib, tibia. Scale indicated in Figures 23, 25, 28.

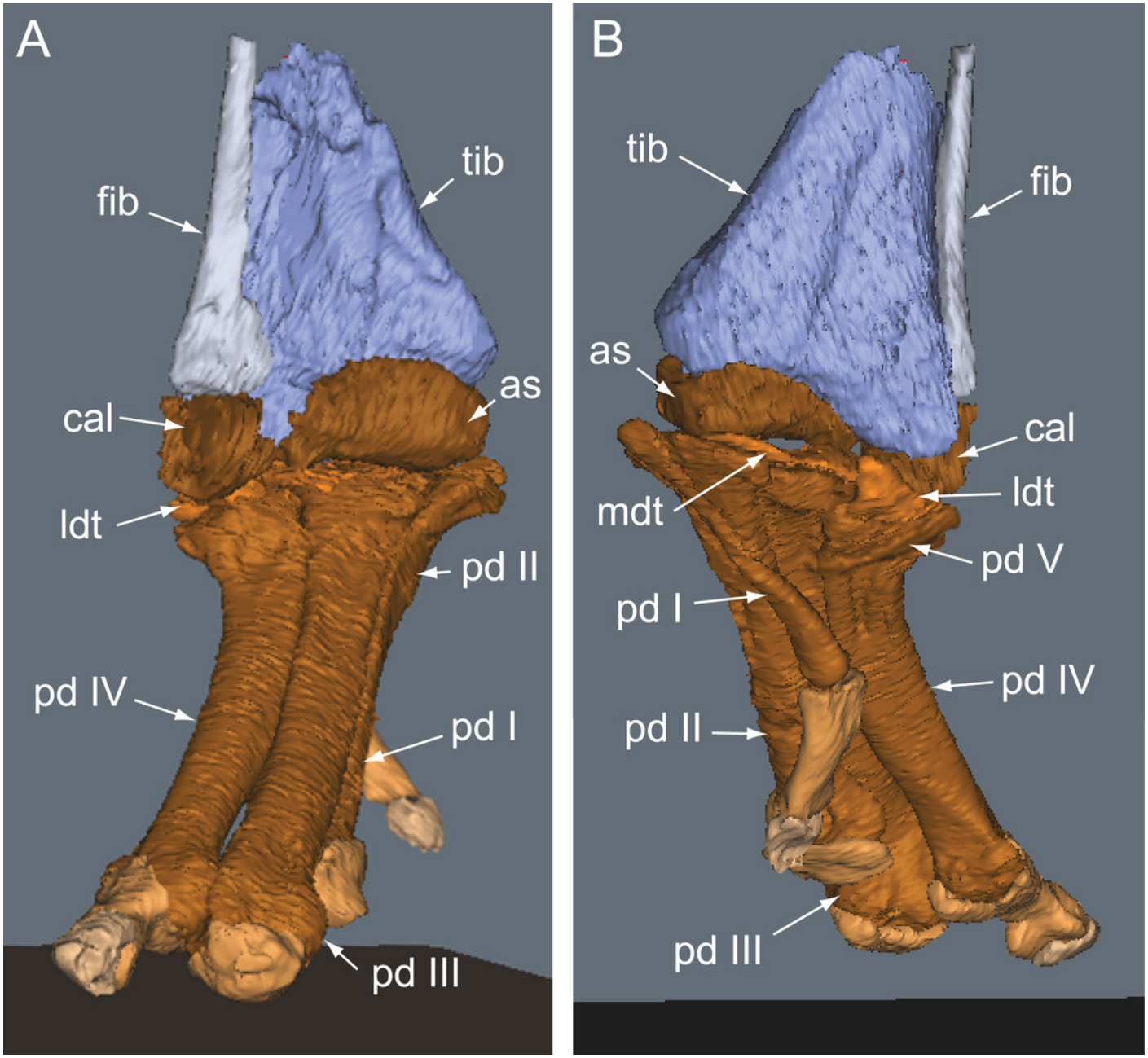

Figure 21

Virtual right distal crus and proximal tarsus of the *Diluvicursor pickeringi* gen. et sp. nov. holotype (NMV P221080).

A–G: (A) cranial; (B) caudal; (C) lateral; (D) medial; (E) distal, with proximal tarsus removed; (F) distal; and (G) proximal views. Abbreviations: as, astragalus; cal, calcaneum; cd, condyle; fib, fibula; imf, inter-malleolar fossa; lf, lateral fossa; lm, lateral malleolus; mm, medial malleolus; pmmr, posterior medial malleolar ridge; tib, tibia. Scale increments, 1 cm.

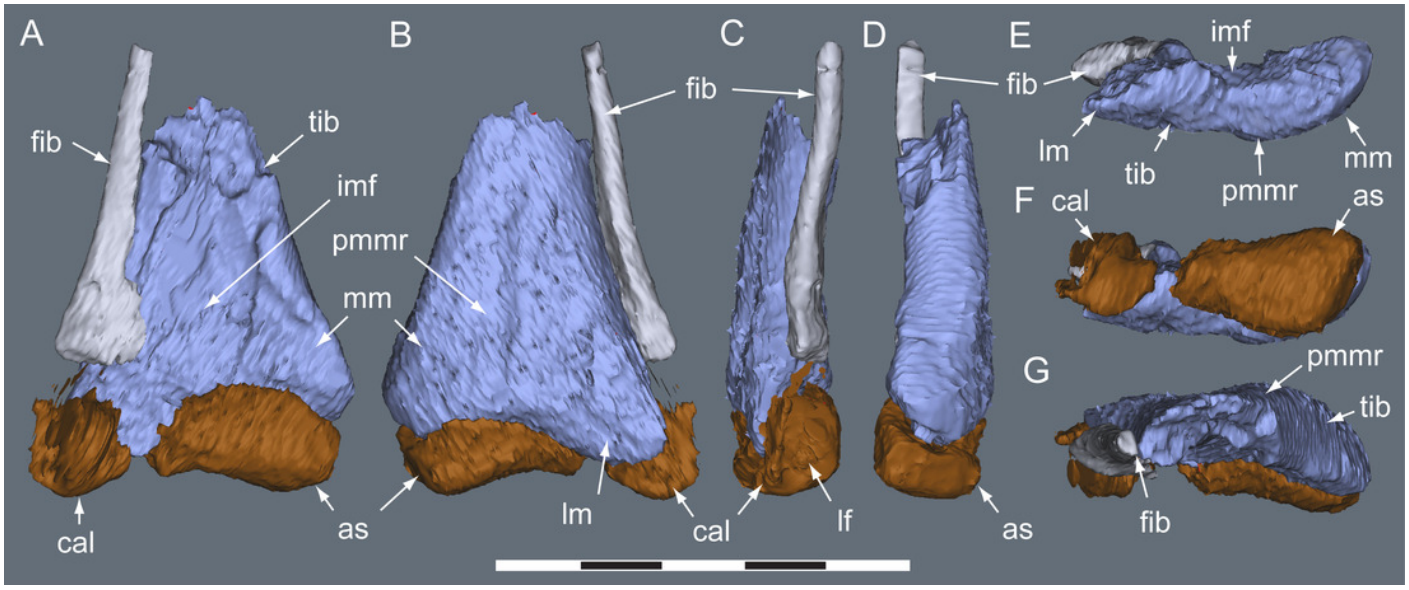

Figure 22

Virtual right tarsus of the *Diluvicursor pickeringi* gen. et sp. nov. holotype (NMV P221080).

A–D, proximal tarsus in: (A) anterior; (B) posterior; (C) proximal; and (D) distal views. E–H, distal tarsus in: (E) proximal; (F) distal; (G) plantar; and (H) dorsal views. (I) Virtual right distal tarsus in proximal view, with metatarsus *in situ*. Dashed arrows in A indicate anterior proximodistal distance on the astragalus discussed in-text. Dashed line in B indicates proximal margin of posterior ascending process. Abbreviations: as, astragalus; cal, calcaneum; aap, anterior ascending process; cal, calcaneum; fos, fossa; gv, groove; ldt, lateral distal tarsal; mdt, medial distal tarsal; mt #, metatarsal and position; mp, medial process; sul, sulcus; tub, tuberosity; pap, posterior ascending process. Scale increments, 1 cm.

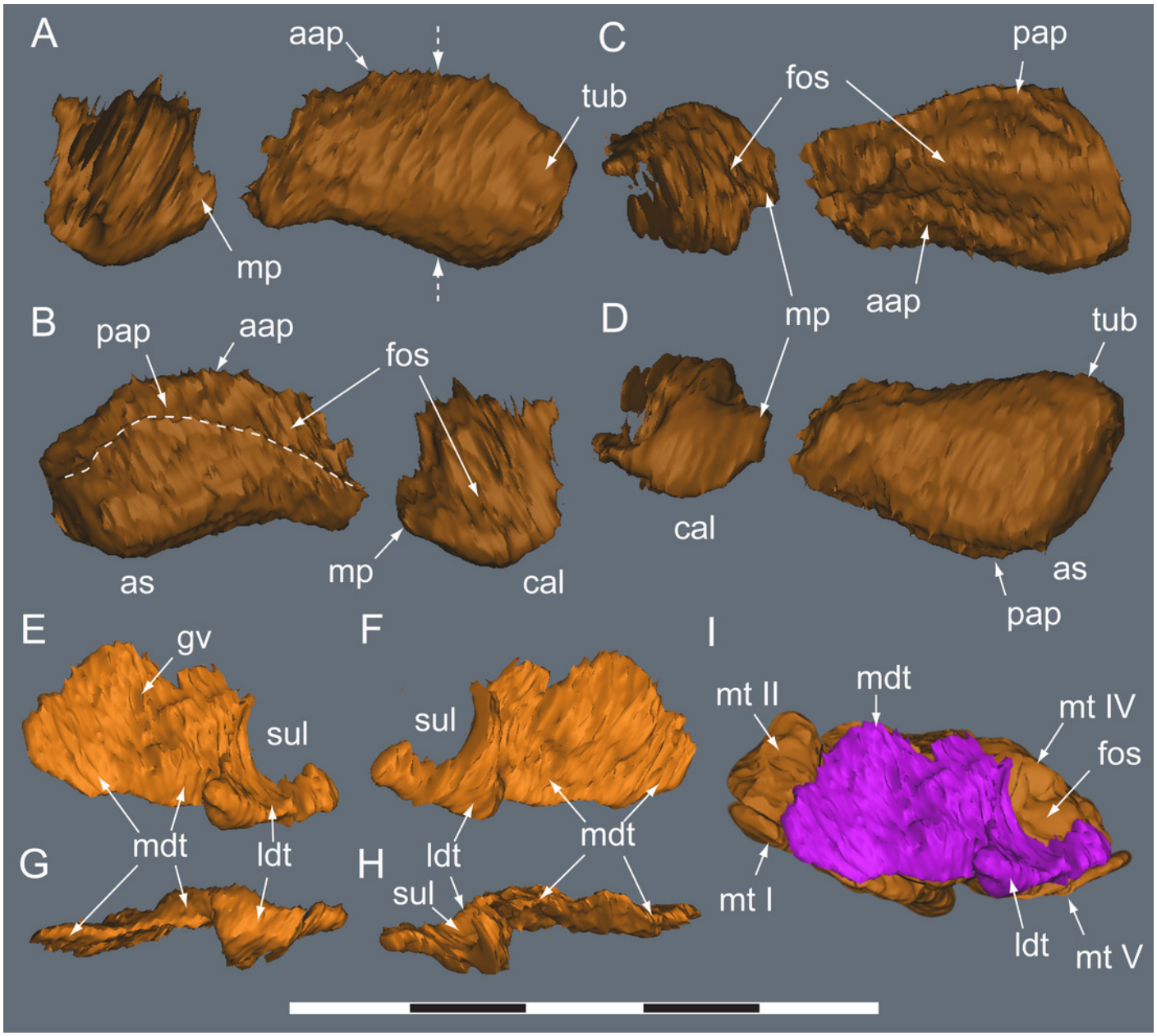
A
aap
tub
mp
C
fos
pap
mp
aap
B
pap
aap
fos
as
mp
cal
D
tub
cal
as
pap
E
gv
sul
mdt
ldt
G
F
sul
ldt
mdt
H
sul
I
mt II
mdt
mt IV
fos
mt I
ldt
mt V

Figure 23

Virtual right pes of the *Diluvicursor pickeringi* gen. et sp. nov. holotype (NMV P221080).

A–B, pes with pedal digits I and V removed in: (A) dorsal; and (B) plantar views. C–D, partial metatarsus in: (C) proximal; and (D) distal views. Abbreviations: fos, fossa; gv mt I, groove for mt I; mt #, metatarsal position; pd #, pedal digit number and phalanx position. Scale increments, 1 cm.

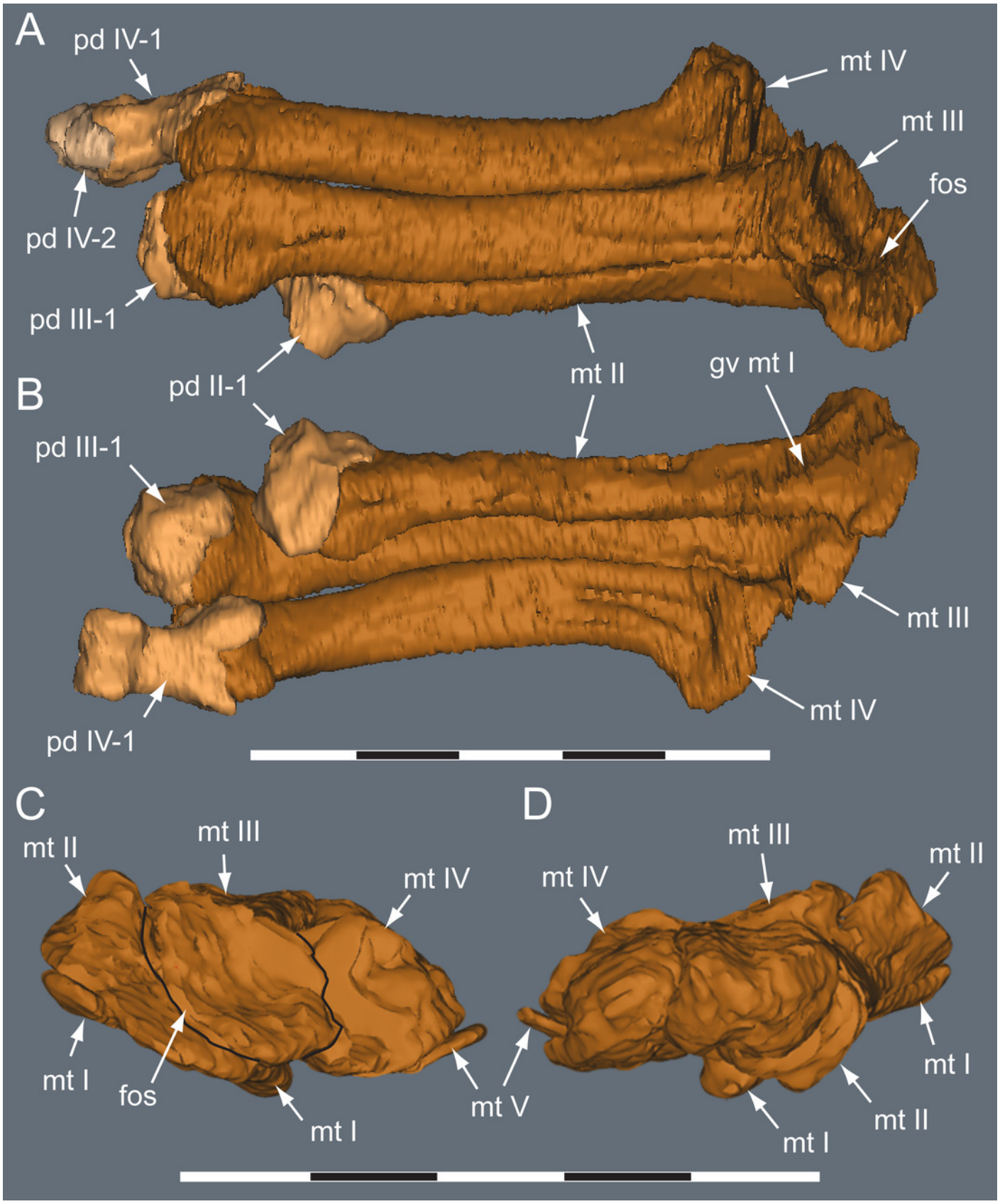
A
pd IV-1
mt IV
mt III
fos
pd IV-2
pd III-1
pd II-1
mt II
gv mt I
B
pd III-1
mt III
mt IV
pd IV-1
C
mt II
mt III
mt IV
mt I
fos
mt I
mt V
D
mt III
mt IV
mt II
mt I
mt II
mt I

Figure 24

Virtual right pedal digit I of the *Diluvicursor pickeringi* gen. et sp. nov. holotype (NMV P221080).

A–F, mt I in: (A) lateral; (B) plantar; (C) dorsal; (D) medial; (E) proximal; and (F) distal views. G–L, pd I-1 and pd I-2 in articulation in: (G) dorsal; (H) plantar; (I) medial; (J) lateral; (K) proximal; and (L) distal views. (M) pd I-1 in distal view. Abbreviations: abd, abductor surface/groove; add, adductor surface/groove; clg, collateral ligament groove/fossa; cot, cotyle; dia, diaphysis; ex, extensor groove or surface; fl, flexor groove or surface; pd #, pedal digit number and phalanx position; s mt II, surface for mt II. Scale increments, 1 cm.

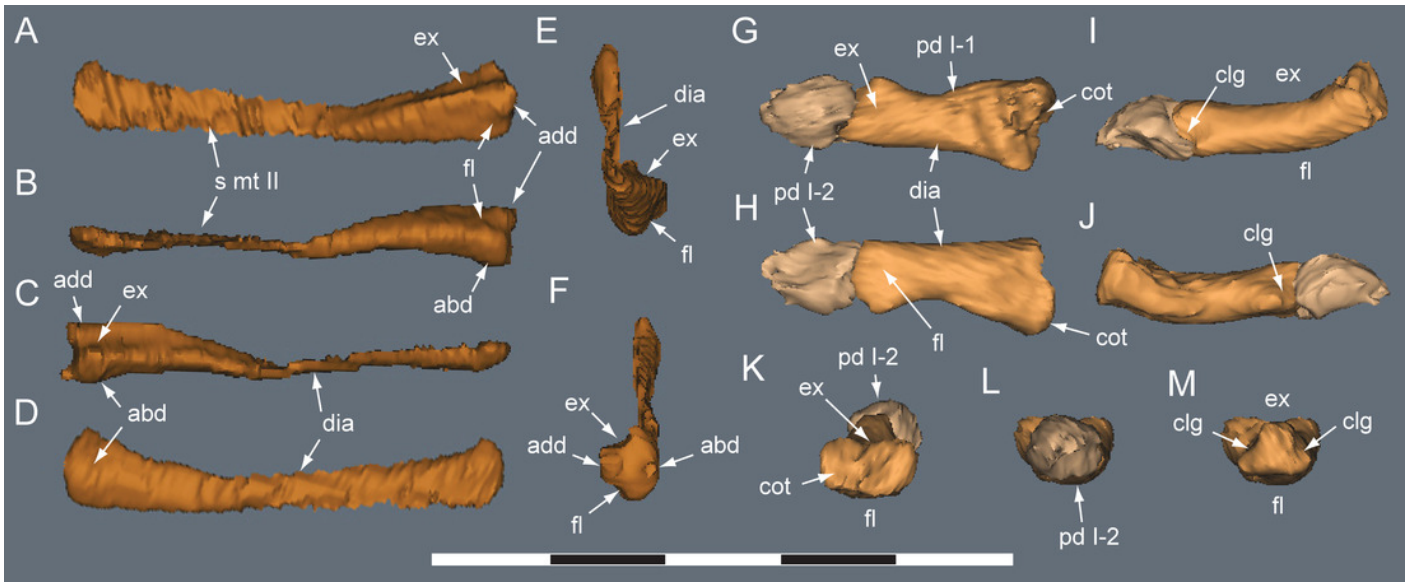

Figure 25

Virtual right metatarsals of the *Diluvicursor pickeringi* gen. et sp. nov. holotype (NMV P221080).

A–F, mt II in: (A) dorsal; (B) plantar; (C) lateral; (D) medial; (E) distal; and (F) proximal views. G–L, mt III in: (G) dorsal; (H) plantar; (I) lateral; (J) medial; (K) distal; and (L) proximal views. Abbreviations: abd, abductor surface/groove; add, adductor surface/groove; con, condyle; dia, diaphysis; ex, extensor groove or surface; fl, flexor groove or surface; fla, flange; fos, fossa; gv mt I, groove for metatarsal I; rid, ridge. Scale increments, 1 cm.

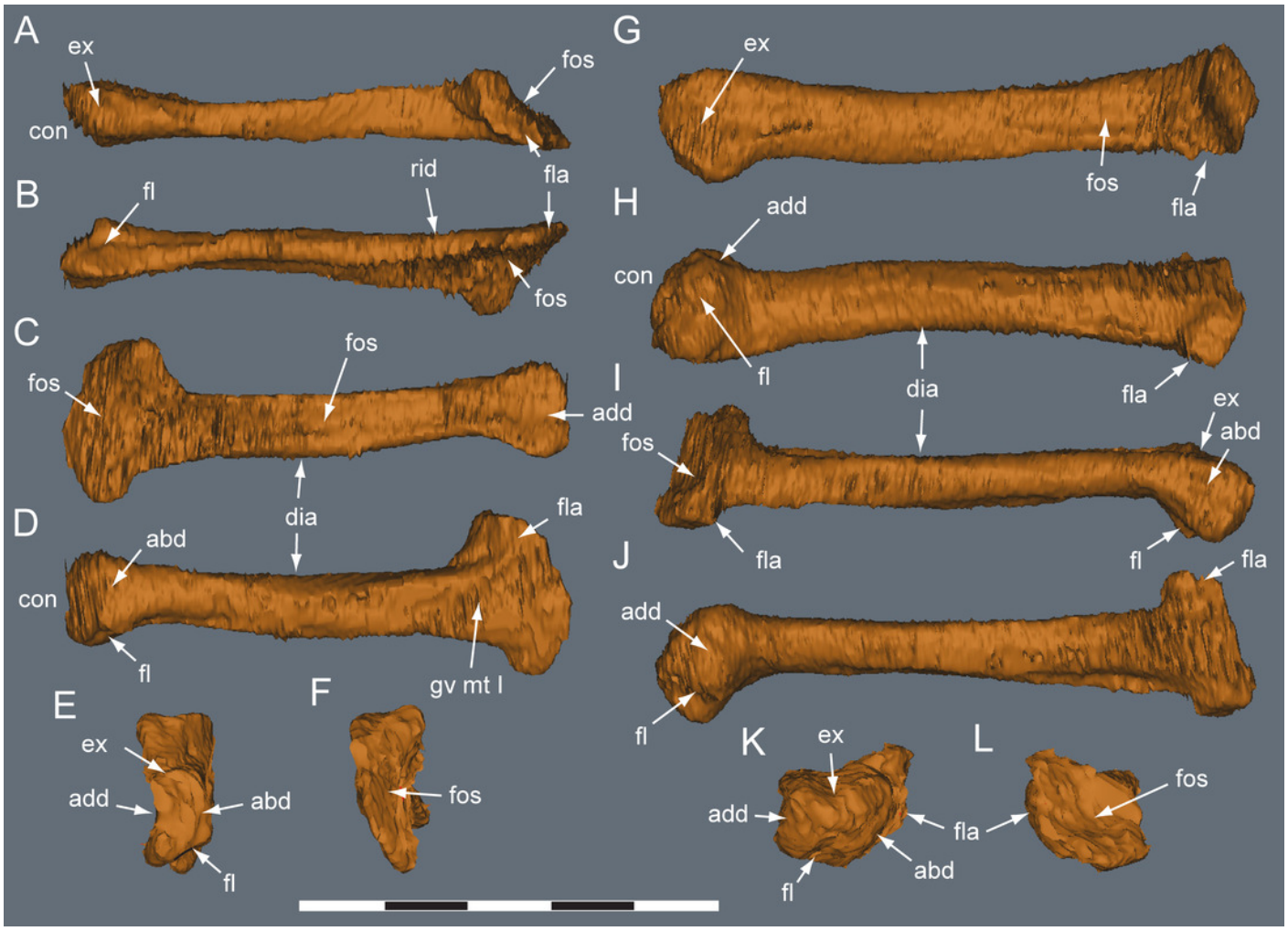

Figure 26

Virtual right pedal digit IV of the *Diluvicursor pickeringi* gen. et sp. nov. holotype (NMV P221080).

A–F, mt IV in: (A) dorsal; (B) plantar; (C) medial; (D) lateral; (E) proximal; and (F) distal views. G–L, pd IV-1 and pd IV-2 in: (G) dorsal; (H) plantar; (I) lateral; (J) medial; (K) distal; and (L) proximal views. Abbreviations: abd, abductor surface/groove; add, adductor surface/groove; clf, collateral ligament fossa; cot, cotyle; dia, diaphysis; dmc, dorsomedial condyle; ex, extensor groove or surface; fl, flexor groove or surface; fla, flange; fos, fossa; pd #, pedal digit number and phalanx position; plc, plantolateral condyle; rid, ridge. Scale increments, 1 cm.

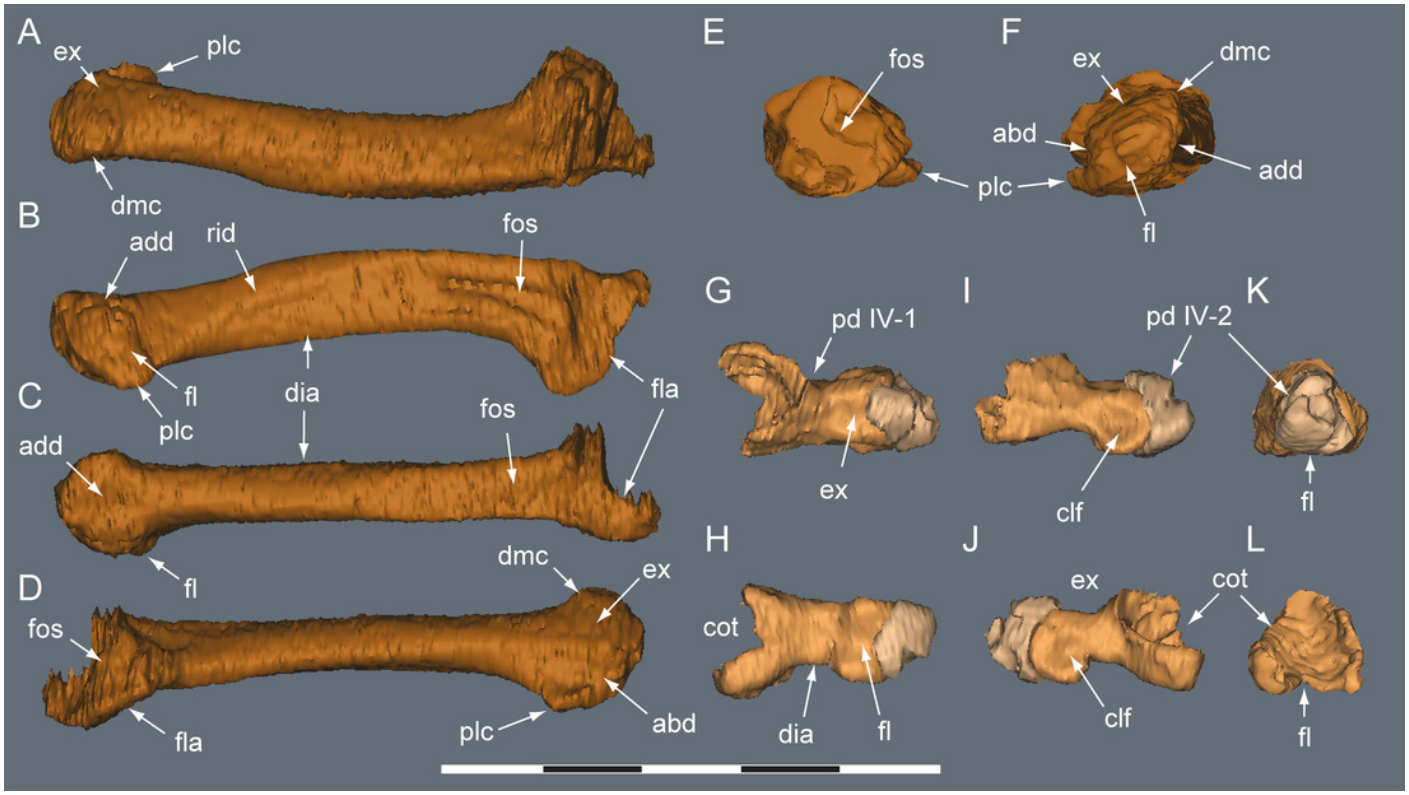

Figure 27

Virtual right mt V of the *Diluvicursor pickeringi* gen. et sp. nov. holotype (NMV P221080).

A–D: (A) plantar; (B) dorsal; (C) medial; and (D) lateral views. Abbreviations: dist, distal; prox, proximal. Scale bar, 1 cm.

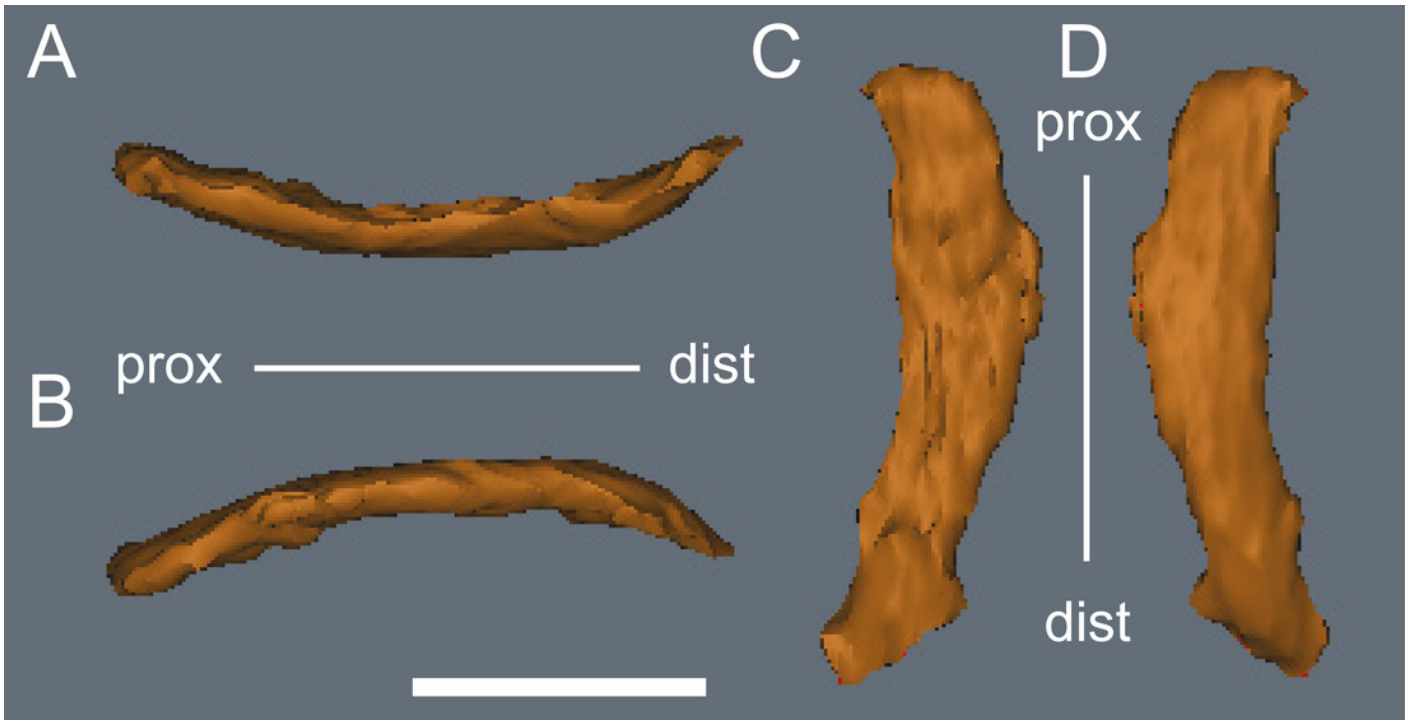

Figure 28

Dorsoventral vertebral proportions on the anterior caudal vertebrae of selected ornithopods.

(A) Neural arch height ‘a’ (=height from dorsal tip of the spinal process to top of the centrum, or centre of transverse process base) relative to vertebral height ‘b’ (=vertebral height without haemal arch). (B) Neural arch height ‘a’ relative to vertebral height ‘c’ (=vertebral height including haemal arch). Distances ‘a’, ‘b’ and ‘c’, shown in Figures 13 and 38. Tabulated data and vertebral positions indicated in Table S2

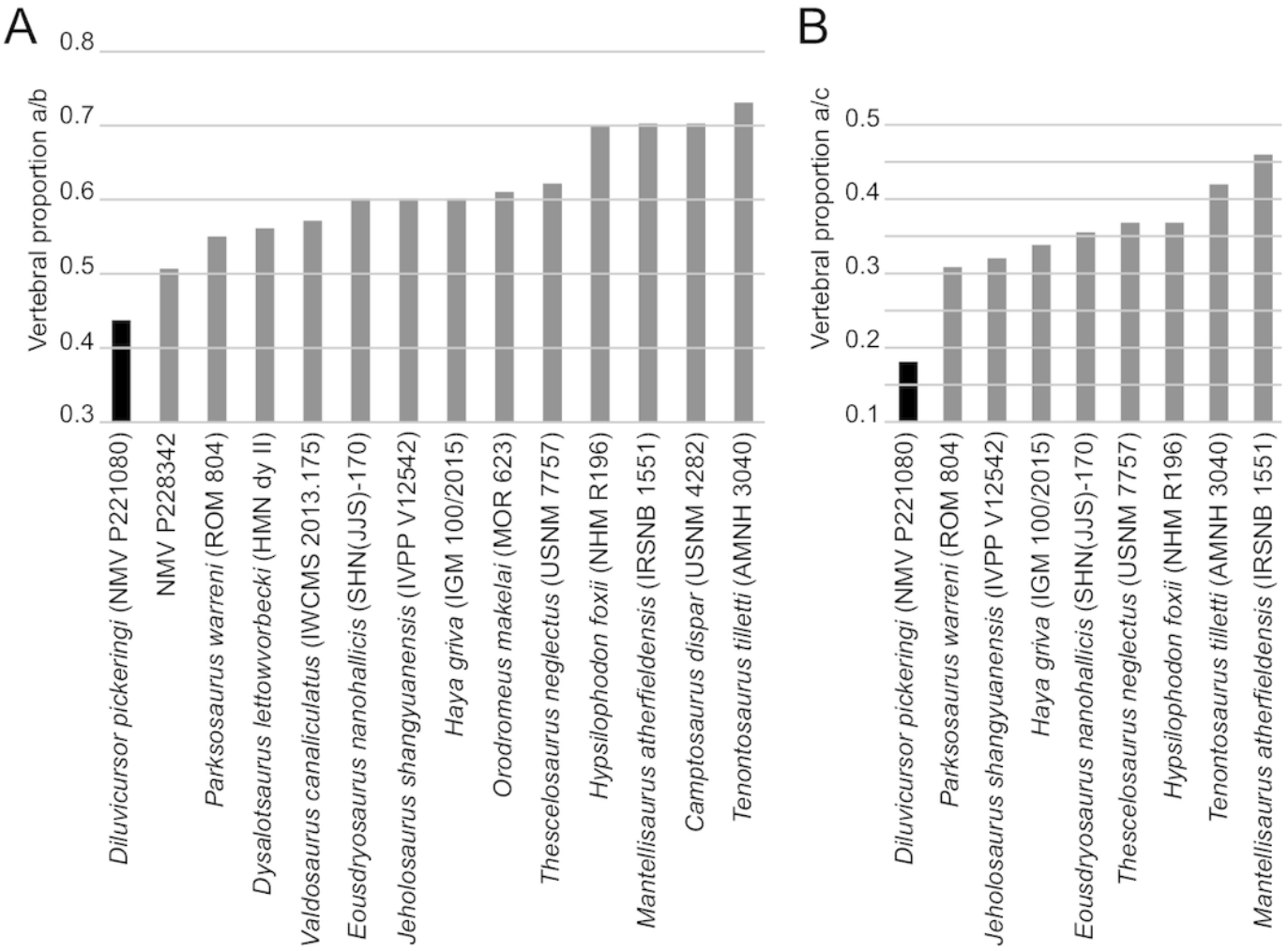

Figure 29

Middle caudal vertebral profiles for selected ornithopods in left lateral view.

A–G: (A) *Diluvicursor pickeringi* gen. et sp. nov. holotype (NMV P221080), ~Ca 14; (B) NMV P185992/NMV P185993, ~Ca 14; (C) *Gasparinisaura cincosaltensis*, anterior-most posterior caudal (MUCPv-212, Coria and Salgado 1996, fig. 4); (D) *Valdosaurus canaliculatus*, Ca 16 (Barrett, 2016, noting Ca 14 is transitional); (E) *Hypsilophodon foxii*, ~Ca 13 (MNHUK R196, based on Hulke, 1882, pl. 74, fig. 13; following vertebral positions reported in Galton, 1974, figs 28–29); (F) *Haya griva*, Ca 13 (following Makovicky et al., 2011, fig. 3, noting that caudal ribs persist along the entire vertebral series); (G) *Thescelosaurus* sp., Ca 13 (Sternberg, 1940, fig. 17). (H) Haemal process profile in NMV P186047, ~Ca 14. Vertebral scales normalised for centrum length (‘f’) at Ca 14 on NMV P221080, with distances ‘a’ and ‘e’ based on the same vertebra, where ‘a’ equals neural arch height and ‘e’ equals vertebral height from the neurocentral suture to the ventral tip of the haemal process (i.e., ‘a’ plus ‘e’ equals total vertebral height, ‘c’; Fig. 13). Abbreviations: cen, centrum; ha, haemal arch/process; sp, spinal process; tp, transverse process. Scale bars, 1 cm.

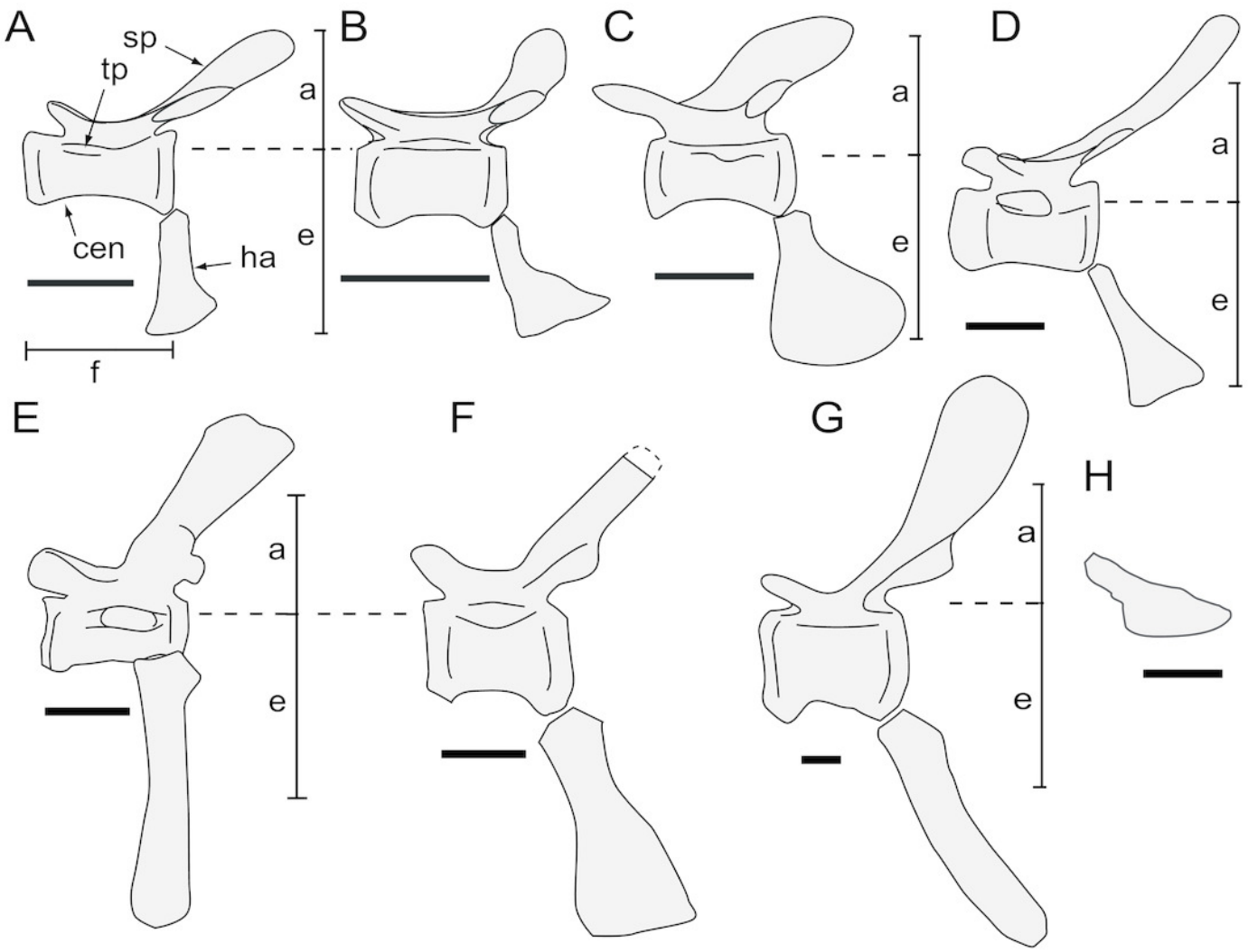
A
sp
tp
cen
ha
f
a
e
B
C
D
E
F
G
H

Figure 30

Distal crura and tarsi of Eumeralla Formation ornithopods.

A–B, right limb on the *Diluvicursor pickeringi* gen. et sp. nov. holotype (NMV P221080): (A) distal crus and proximal tarsus in anterior view; and (B) distal tarsus in proximal view. C–D, left limb of NMV P186047: (C, C’) distal crus and proximal tarsus in anterior view (schematic C is reflected); and (D, D’) distal tarsus in proximal view. Abbreviations: aap, anterior ascending process; as, astragalus; cal, calcaneum; dt?, uncertain distal tarsal; fib, fibula; fos, fossa; gv, groove; ldt, lateral distal tarsal; mdt, medial distal tarsal; mm, medial malleolus; mt #, metatarsal position; tib, tibia. Scale bars, 1 cm.

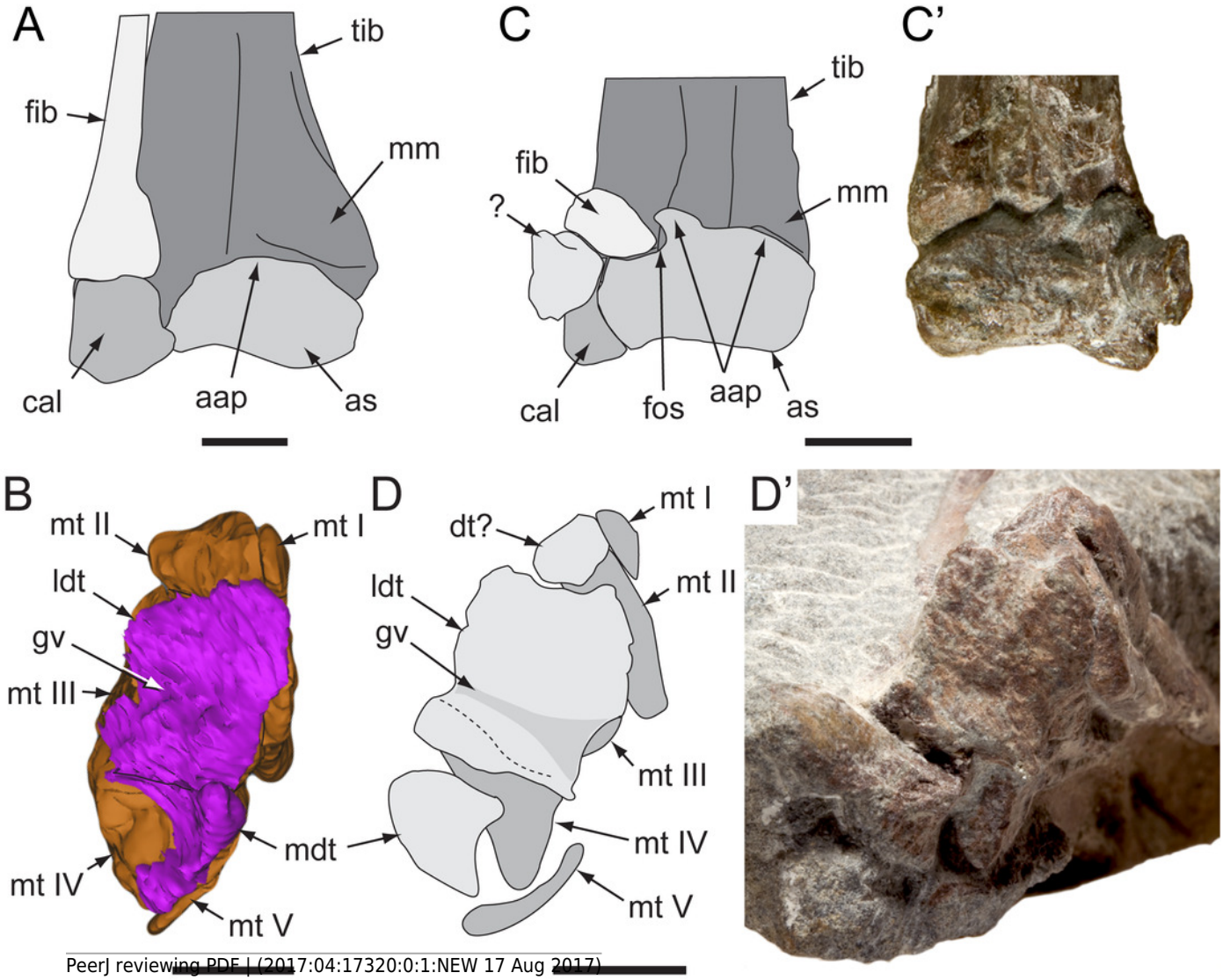

Figure 31

Pedes of Eumeralla Formation ornithopods in plantar view.

(A) Virtual right pedal digit I of the *Diluvicursor pickeringi* gen. et sp. nov. holotype (NMV P221080). (B) Right partial pes of NMV P185992/NMV P185993. (C) Left partial pes of NMV P186047. Dashed arrows in A and B indicate lateral flaring on the cotyle. Specimen in B, NH_4Cl coated. Abbreviations: fl, flexor groove; mdt, medial distal tarsal; mt #, metatarsal position; pd #, pedal digit number and phalanx position; tib, tibia. Scale increments, 1 cm.

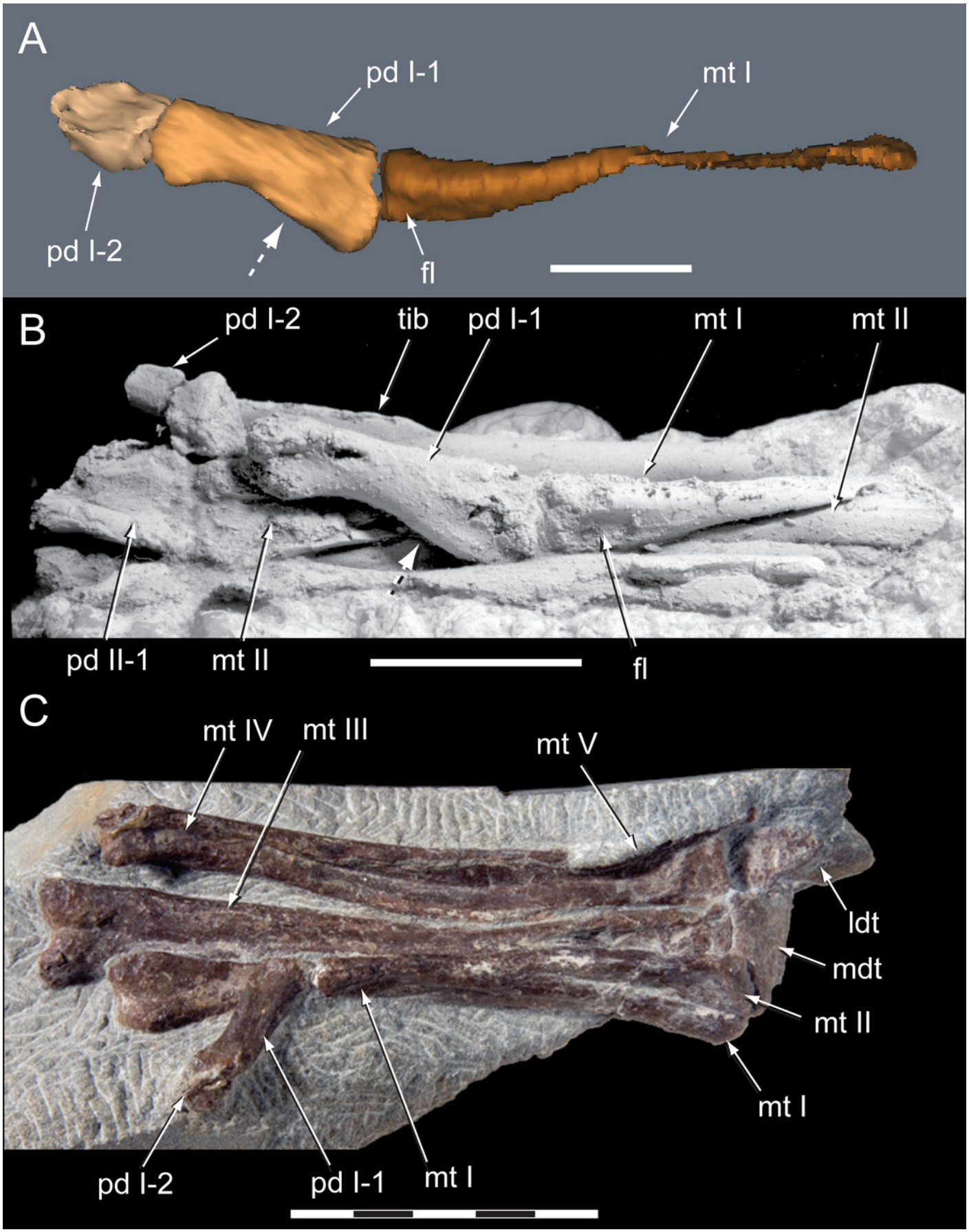
A
pd I-1
mt I
pd I-2
fl
B
pd I-2
tib
pd I-1
mt I
mt II
pd II-1
mt II
fl
C
mt IV
mt III
mt V
ldt
mdt
mt II
mt I
pd I-2
pd I-1
mt I

Figure 32

Right metatarsi of selected ornithopods, in proximal view.

Metatarsi normalised for dorsoplantar depth of metatarsal II (shaded black). Dashed lines indicate assumed or postulated surfaces/bones. Dashed lines indicate uncertain bone margins. ?, indicates expected/missing metatarsal(s). For data sources, see Table S1.

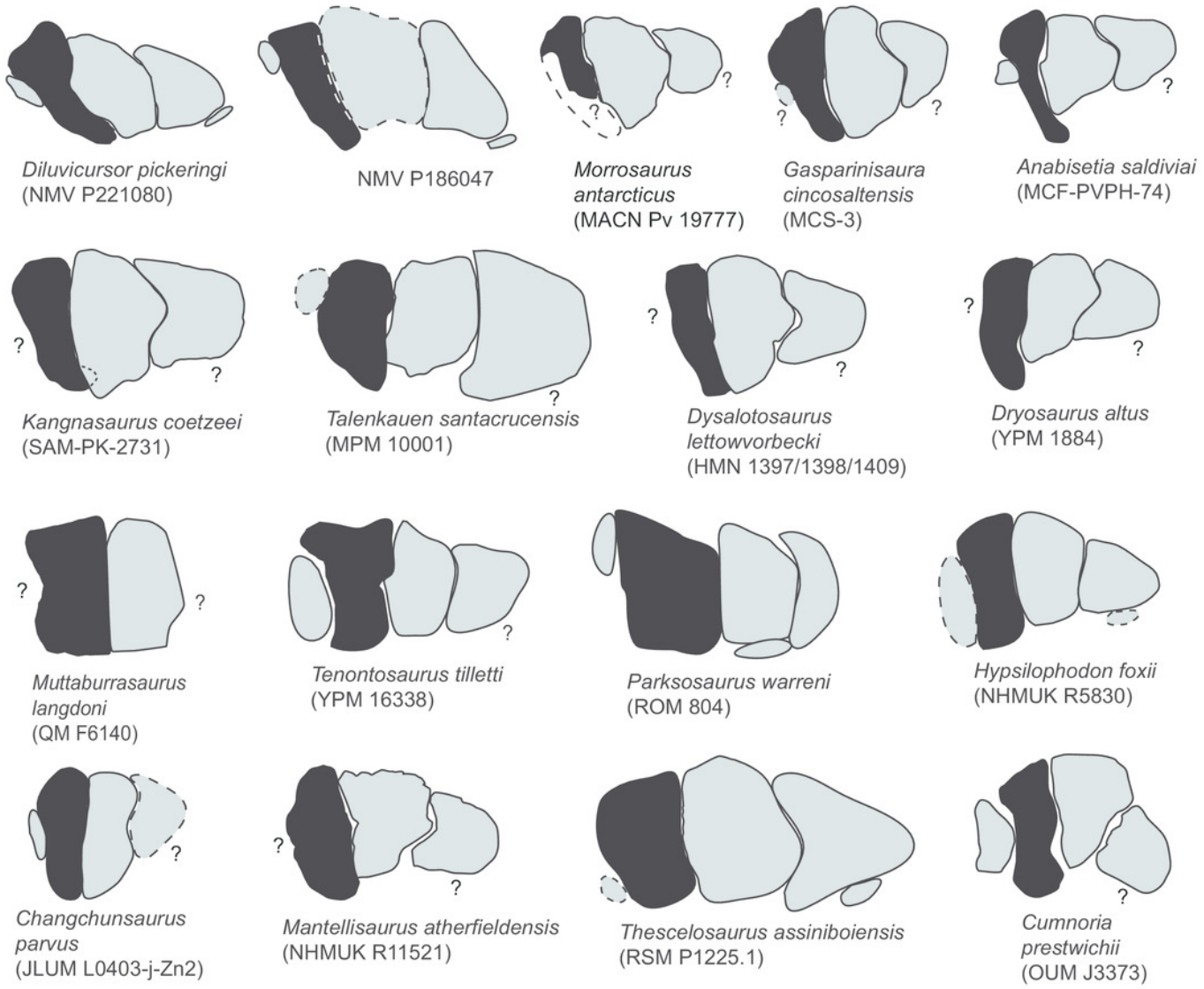

Figure 33

Virtual right pes of the *Diluvicursor pickeringi* gen. et sp. nov. holotype (NMV P221080) showing pathologies, with pedal digits I and V removed.

A–B: (A) dorsal; and (B) plantar views. Dashed lines indicate deflected axes of bones. Dashed arrows indicate regions of osteophytosis (see photographs, Fig. 23A). Dotted arrow indicates suggested trauma to the cotyle on pd IV-1. Abbreviations: mt #, metatarsal position; pd #, pedal digit number and phalanx position. Scale increments equal 1 cm.

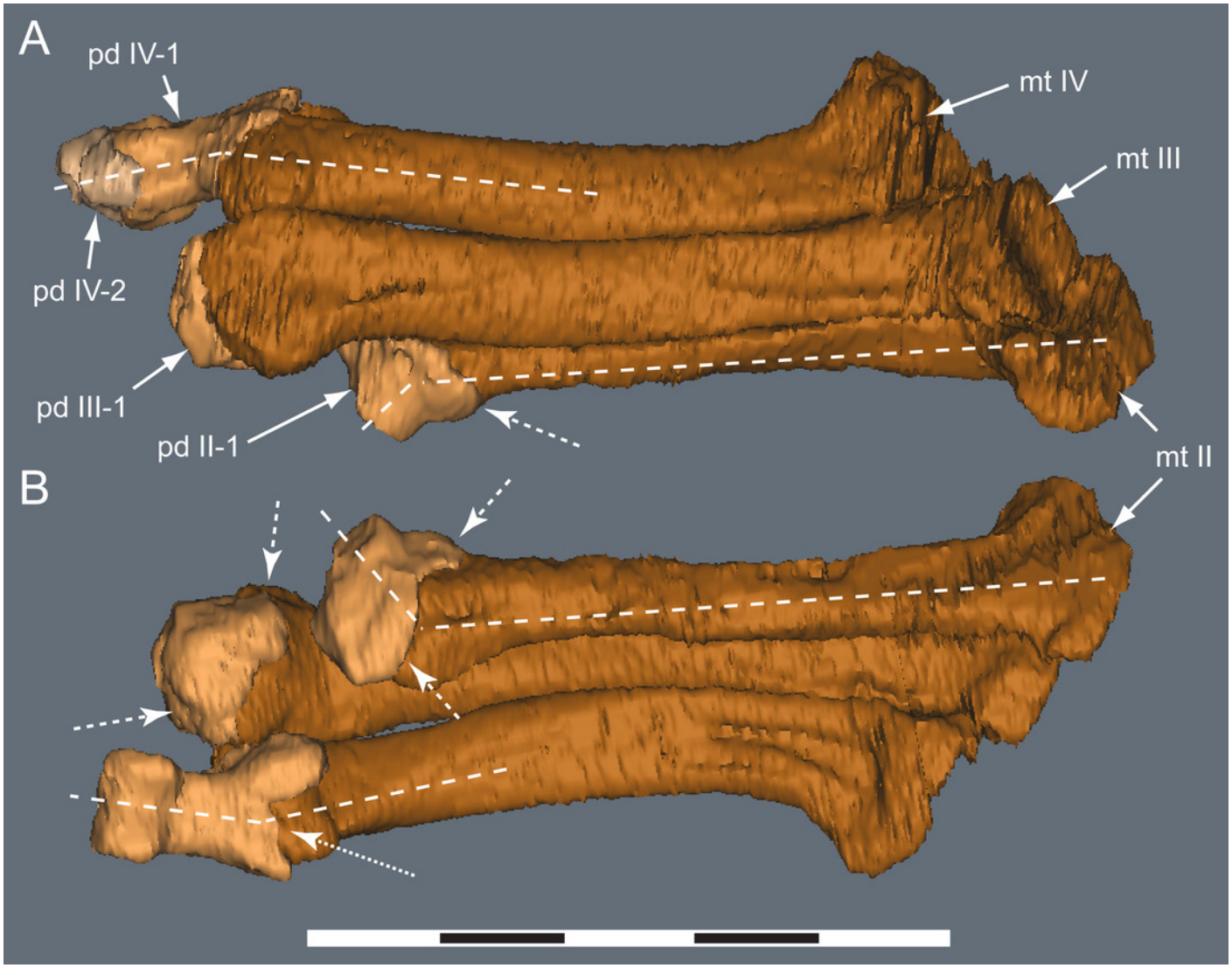

Figure 34

Anterior caudal vertebra (NMV P228342) of an indeterminate ornithischian from the ETRW Sandstone.

A–F: (A) left lateral; (B) posterior; (C, C’) right lateral; (D, D’) dorsal; (E) cranial; and (F) ventral views. Vertebral proportions (see also comparisons Fig. 32): ‘a’, distance from the dorsal tip of the spinal process to the centre of the transverse process base (i.e., neural arch height); and ‘b’, vertebral height without haemal arch. Specimen NH_4Cl coated. Abbreviations: acdl, anterior centrodiapophseal lamina; cen, centrum; cprl, centroprezygapophyseal lamina; dap, diapophysis; lcf, laterocentral fossa; m-spol, medial-spinopostzygapophyseal lamina; nc, neural canal; ncs, neurocentral suture; pcdl, posterior centrodiapophyseal lamina; posf, postspinal fossa; podl(p), postzygodiapophyseal lamina (and protuberance); poz, postzygapophysis; pprl, postzygoprezygapophyseal lamina; prdl, prezygodiapophyseal lamina; prsl(p), prespinal lamina (and protuberance); prz, prezygapophysis; sdf, spinodiapophyseal fossa; sp, spinal process; sprf, spinoprezygapophyseal fossa; sprl, spinoprezygapophyseal lamina; tp, transverse process; tprl, intraprezygapophyseal lamina; vb, vertebral body. Scale increments, 1 cm.

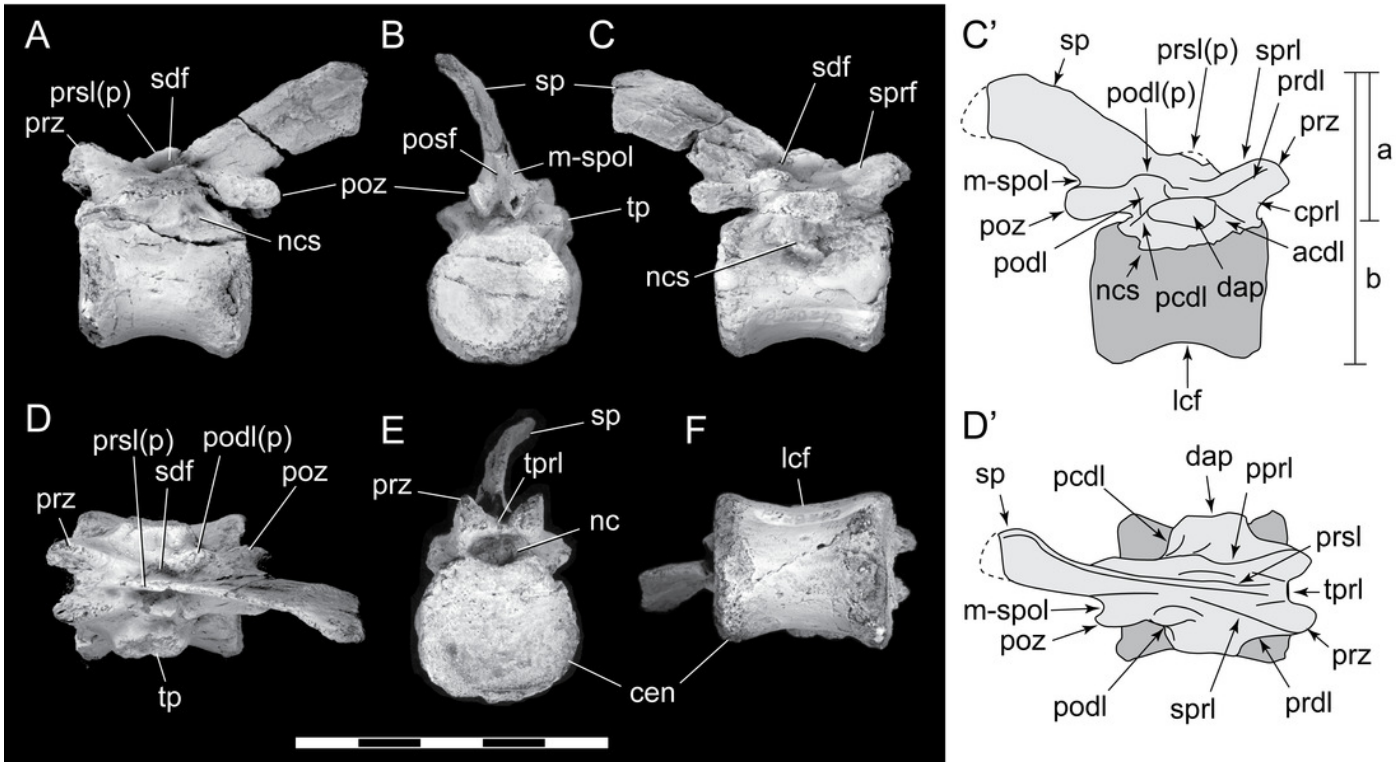
A
prsl(p)
sdf
prz
poz
ncs
B
sp
posf
m-spol
tp
C
sdf
sprf
ncs
C'
sp
prsl(p)
sprl
podl(p)
prdl
prz
a
m-spol
cprl
poz
acdl
podl
ncs
pcdl
dap
b
lcf
D
prsl(p)
podl(p)
sdf
poz
prz
tp
E
sp
tprl
prz
nc
cen
F
lcf
D'
sp
pcdl
dap
pprl
prsl
tprl
m-spol
poz
prz
podl
sprl
prdl

Figure 35

Schematic transverse section through the anterior epaxial and hypaxial muscular regions of the ornithopod tail.

(A) *Diluvicursor pickeringi* gen. et sp. nov. holotype (NMV P221080), designated Ca 3 (see also Fig. 13); and (B) *Hypsilophodon foxii*, Ca 4 (NHMUK R196; following Galton, 1974, figs 28–29). Sections normalised for total vertebral depth. Extent of viscera (brown shading) ventral to hypaxial musculature (dashed lines) not shown. Abbreviations: Ca #, caudal vertebra and position. Scale bars, 1 cm.

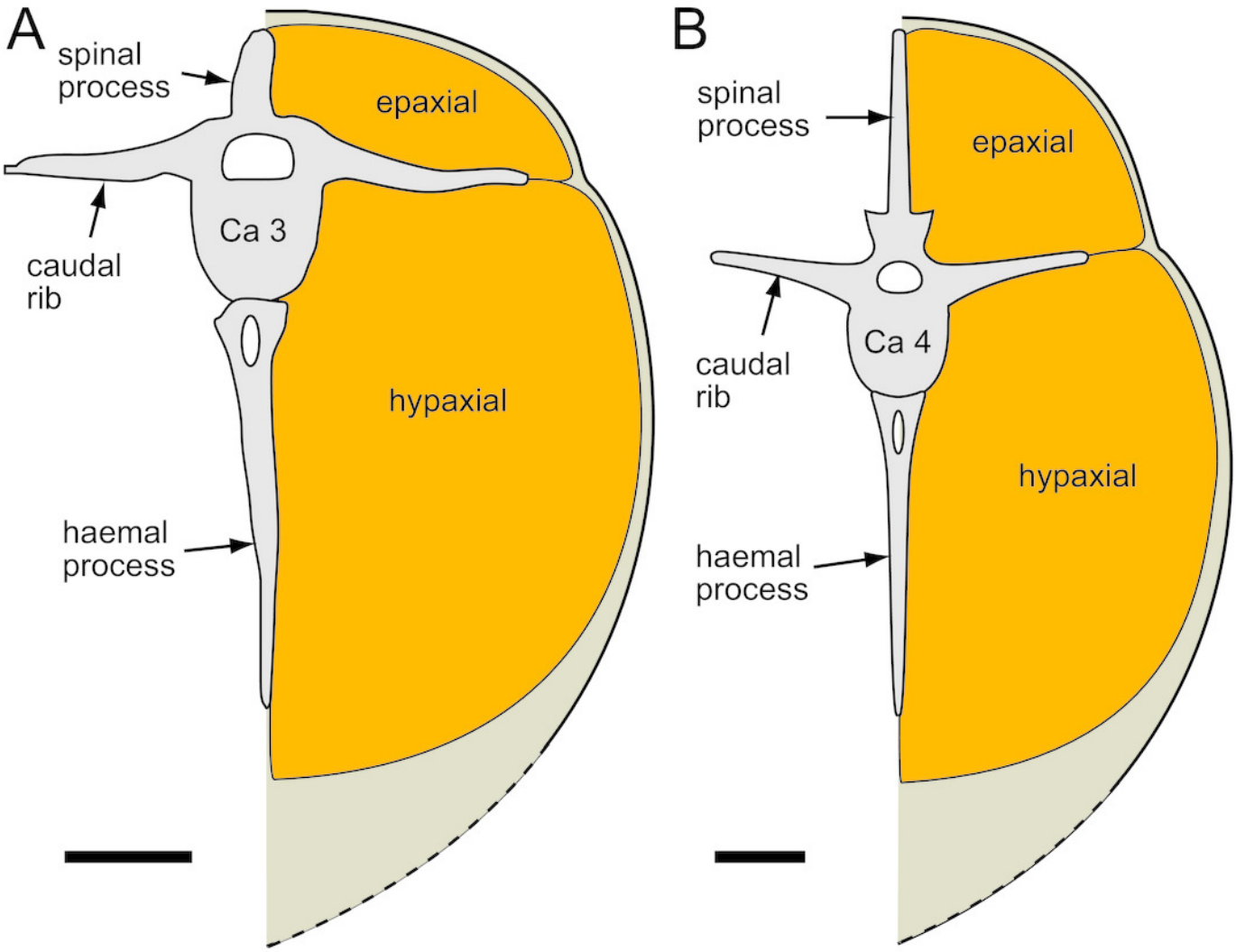

Table 1 (on next page)

Nomenclature of vertebral laminae and fossae.

1

Lamina/fossa	Abbreviation	Landmark 1/bounding margin*	Landmark 2/bounding margin*
anterior centrodiapophseal lamina	acdl	anteroventral margin of transverse process	dorsolateral margin of anterior centrum
centroprezygapophyseal fossa	cprf	ventral margin of prdl*	acdl or dorsolateral margin of anterior centrum*
centroprezygapophyseal lamina	cprl	ventral margin of prezygapophysis	dorsolateral margin of anterior centrum
intraprezygapophyseal lamina	tprl	left prezygapophysis	right prezygapophysis
medial spinopostzygapophyseal lamina	m-spol	posterior margin of spinal process	medial margin of postzygapophysis
posterior centrodiapophyseal lamina	pcdl	posteroventral margin of transverse process	dorsolateral margin of posterior centrum
postspinal fossa	posf	medial spinopostzygapophyseal lamina*	medial spinopostzygapophyseal lamina*
postzygodiapophyseal lamina	podl	dorsoanterior margin of postzygapophysis	dorsal surface of transverse process
postzygoprezygapophyseal lamina	pprl	postzygapophysis	prezygapophysis
prespinal lamina	prsl	medial margin of tprl	anterior base of spinal process
prezygodiapophyseal lamina	prdl	lateral margin of prezygapophysis	anterodorsal surface of transverse process
spinal ridge	sr	medial margin of tprl	medial margin of paired postzygapophyses
spinodiapophyseal fossa	sdf	lateral surface of spinal process*	medial surface of podl and or transverse process*
spinoprezygapophyseal fossa	sprf	sprl*	prdl*
spinoprezygapophyseal lamina	sprl	spinal process	prezygapophysis

2

Table 2 (on next page)

Diluvicursor pickeringi gen. et sp. nov., holotype (NMV P221080), dimensions of caudal vertebrae.

Dimensions in mm. Abbreviations: a, anterior end; APL, anteroposterior length; Ca #, caudal vertebra and position; DVH, dorsoventral height; e, estimated; inc, incomplete; p, posterior end; and TW, transverse width. Caudal vertebral sequence based on the first preserved haemal arch at the position designated Ca 1.

1

Vertebra	Centrum APL	Centrum DVH	Centrum TW	Caudal ribs, total TW	Vertebral DVH (excluding haemal arch)	Haemal arch DVH
Ca 1	missing	–	–	–	–	21.7 inc
Ca 2	missing	–	–	–	–	30.3
Ca 3	15.0 inc	10.0 a 10.0 p	9.6 a 10.0 p	41.5	19.5	23.3 inc
Ca 4	15.2	10.2 a 9.4 p	9.5 a 9.5 p	39.0	20.5	28.0
Ca 5	15.0	10.0 a 9.4 p	10.0 a 10.0 p	33.0	–	–
Ca 6	10.5 inc	9.3 a	10.0 a	27.5 e	–	–
Ca 7	9 inc	–	–	–	–	20.0
Ca 8	14.0	–	9.0 a 9.0 p	–	–	–
Ca 9	14.6	–	9.0 a 8.6 p	–	–	21.0
Ca 10	15.0	–	9.2 a 9.0 p	–	–	18.0
Ca 11	12.5 inc	–	–	–	–	–
Ca 12	missing	–	–	–	–	–
Ca 13	13 inc	–	–	16.0 e	18.0	–
Ca 14	14.3	8.0 a 9.2 p	12.0 e	–	20.0	13.0

Ca 15	15.2	8.2 a 8.2 p	10.8 e	–	20.0	8.5
Ca 16	13 inc	8.5 a 8.2 p	9.6 e	–	18.0	–
Ca 17	17.0	8.0 a	10.4 e	–	15.2 inc	10.1
Ca 18	16.6	8.1 a 8.0 p	10.4 e	–	16.0	11.1
Ca 19	17.0	8.2 a 7.0 p	–	–	14.5	9.7
Ca 20	17.0	7.0 a 6.0 p	–	–	–	–
Ca 21	16.2	6.0 a 6.5 p	7.6 p	–	14.1	9.5
Ca 22	16.0	6.0 a 6.3 p	7.0 p	–	13.2	9.0
Ca 23	15.5	7.2 p	7.5 p	–	13.5	–
Ca 24	15.8	7.0 p	7.0 p	–	13.5	–
Ca 25	15.9	7.2 p	–	–	–	–
Ca 26	Un-prepared	–	–	–	–	–
Ca 27	16.0	4.6 p	–	–	10.0	–
Ca 28	16.0	4.8 a 4.8 p	–	–	9.5	–
Ca 29	15.5	5.0 a 4.8 p	–	–	9.0	–

Ca 30	15.5	4.8 a 4.7 p	–	–	–	–
Ca 31	12.8	4.5 a 4.0 p	–	–	–	–
Ca 32	13.0	4.6 a 4.5 p	–	–	7.8	5.8
Ca 33	11.9	3.5 a 3.0 p	–	–	6.0	5.8
Ca 34	11.5	3.5 a 3.5 p	–	–	6.0	–
Ca 35	11.5	3.0 a 3.5 p	–	–	6.1	–
Ca 36	9.0	2.5 a 2.5 p	–	–	5.8	–
Ca 37	8.0	2.5 a 2.5 p	–	–	4.5	–
Ca 38	8.0 inc	2.5 a	–	–	3.5 inc	–

Table 3 (on next page)

Diluvicursor pickeringi gen. et sp. nov., holotype (NMV P221080), dimensions of the right crus.

Dimensions in mm. Abbreviations: DAPW, distal anteroposterior width; DTW, distal transverse width; NAPWD, narrowest anteroposterior width of diaphysis; and NTWD, narrowest transverse width of diaphysis.

Element	DTW	DAPW	NTWD	NAPWD
Tibia	34.5	15.0	16.0	10.0
Fibula	10.0	5.0	2.5	4.0

Table 4(on next page)

Diluvicursor pickeringi gen. et sp. nov., holotype (NMV P221080), dimensions of right tarsus.

Dimensions in mm. Abbreviations: GAPW, greatest anteroposterior width; GPDH, greatest proximodistal height; GTW, greatest transverse width; NAPW, narrowest anterioposterior width.

Element	GTW	GAPW	NAPW	GPDH
Astragalus	27.0	16.0	10.0 (medial edge)	16.5
Calcaneum	13.0	10.5	4.5 (medial process)	14.0
Lateral distal tarsal	19.3	13.3		8.0
Medial distal tarsal	19.0	14.6		4.0

Table 5 (on next page)

Diluvicursor pickeringi gen. et sp. nov., holotype (NMV P221080), dimensions of right pes.

Dimensions in mm. Abbreviations: d, dorsal; DDPH, distal dorsoplantar height; DTW, distal transverse width; inc, incomplete; mt #, metatarsal position; p, plantar; pd #, pedal digit number and phalanx position; PDL, proximodistal length; PDPH, proximal dorsoplantar height; and PTW, proximal transverse width.

Element	PDL	PDPH	DDPH	PTW	DTW
mt I	38.0	5.0	5.0	2.0	4.8
mt II	58.5	20.0	10.5	8.5 d/4.0 p	8.0
mt III	66.0	15.0	11.6	14.0 d/7.0 p	13.0
mt IV	56.0	11.2	11.0	12.0	8.4
mt V	21.5	3.9	–	1.9	–
pd I-1	17.7	5.3	5.0	8.5	5.6
pd I-2	8.0 inc	5.5	–	–	–
pd II-1	–	10.5	–	8.5	–
pd III-1	inc	–	–	–	–
pd IV-1	17.1	–	–	11.2	7.9
pd IV-2	inc	–	–	8.0	–